

People's Democratic Republic of Algeria
Ministry of Higher Education and Scientific Research

UNIVERSITY OF RELIZANE
Faculty of Science and Technology
Department of Mechanical Engineering



DOCTORAL THESIS LMD 3rd cycle

Field: Mechanical Engineering

Specialization: Materials Engineering

Presented By

Sif Eddine BELALIA

Thesis title

Numerical and Parametric study of FSW process using a pneumatic source

Fr : Etude numérique et paramétrique du procédé FSW par source pneumatique

Defended on: 29/04/2024.

Before the jury composed of:

President	Adda HADJ MOSTEFA	MCA	Univ.of Relizane
Thesis Director	Mohamed SERIER	Pr	Univ.of Ain Temouchent
Thesis Co-Director	Affaf TABETI	MCA	Univ. of Relizane
Examiner	Maamar DJILALI BEIDA	MCA	Univ.of Relizane
Examiner	Khadidja YACHBA	MCA	Univ.of ESE Oran
Examiner	Taieb NEHARI	MCA	Univ.of Ain Temouchent

Academic Year: 2023/2024

Dedication

I dedicate this thesis to:

My Dear parents,

My wife and daughter,

The Palestinian heroes,

To my family and friends,

And to anyone who supported me on this journey.

Sif Eddine BELALIA

ACKNOWLEDGMENTS

First and foremost, I offer my deepest gratitude to Allah, the Most Merciful and Compassionate, for guiding me through this challenging journey of doctoral research. It is through His infinite wisdom and grace that I have found strength, perseverance, and clarity of purpose in pursuit of knowledge.

Throughout this endeavor, I have relied solely on the guidance and blessings bestowed upon me by Allah. His divine wisdom has illuminated my path, provided solace in times of uncertainty, and inspired me to strive for excellence in all aspects of my academic pursuit.

While my journey may have been solitary in human terms, I have never felt alone, for Allah's presence has been a constant source of comfort and support. His divine assistance has enabled me to overcome obstacles, navigate complexities, and achieve milestones that seemed insurmountable.

I am deeply grateful to Allah for granting me the opportunity to embark on this scholarly journey, for bestowing upon me the intellectual capacity to pursue knowledge, and for blessing me with unwavering faith and resilience in the face of challenges.

In acknowledging Allah's infinite mercy and benevolence, I am reminded of the profound truth that all achievements are ultimately His blessings. Therefore, I dedicate this thesis to His divine guidance and seek His pleasure in all my endeavors.

Furthermore, I extend my heartfelt appreciation to all those who have supported and encouraged me throughout this journey, whether from near or far. I pray that Allah, the All Merciful, guides, protects, and blesses them abundantly for their kindness and assistance.

ملخص

تستكشف هذه الرسالة تحسين عمليات اللحام بالاحتكاك الدوراني (FSW)، مع التركيز الأساسي على استعمال مصدر الهواء المضغوط كمصدر طاقة، وتقليل استهلاك الطاقة، وتمكين العمل في البيئات الخطرة، وتعزيز الكفاءة. تنقسم الدراسة إلى أربعة فصول، حيث تهدف إلى تحديد المحرك الهوائي (أو الأداة الدوارة الهوائية) الأكثر ملاءمة لعملية FSW الهوائية، باستخدام قوة خوارزميات التعلم الآلي والـ Metaheuristics .

يقدم الفصل الأول استكشافاً حول أساسيات FSW ويؤكد الدور المحوري لمصادر الهواء المضغوط في هذه التقنية للحامية. تؤكد المناقشة على الفوائد الكامنة المقدمة من قبل مصادر الهواء المضغوط، خاصة فيما يتعلق بقابلية التنقل وكفاءة الطاقة.

في الفصل التالي، يُحدد منهج الدراسة، الذي يشمل مختلف تقنيات الذكاء الاصطناعي مثل الشبكات العصبية الاصطناعية، وخوارزميات الغابات العشوائية، والانحدار الجبري. تكمل هذه الطرق بأساليب SHAPLEY الإضافية للتفسير وخوارزمية التحسين لطائر البجع، المصممة خصيصاً لتحليل وتحسين خصائص FSW مع مصادر الهواء المضغوط.

تتقدم الرسالة بعد ذلك إلى تطوير نماذج التنبؤية لخصائص FSW في الفصل الثالث. من خلال إجراءات تحقق صارمة، يتم تقييم أداء هذه النماذج للوصول إلى R^2 بنسبة 99.60٪ و MAPE بنسبة 4.54٪، مما يوفر رؤى حول تحسين الخصائص.

في الفصل الأخير، يُقترح نهج مختلط، يجمع بين النماذج المطورة مع خوارزمية تحسين طائر البجع. يهدف هذا النهج الجديد إلى تحديد مجموعة مناسبة من الخصائص، بما في ذلك شكل هندسي مناسب لأداة اللحام الدوراني، وسرعة اللحام، وسرعة الدوران، وزاوية الإمالة، والعزم، واستهلاك طاقة منخفض، مخصصة خصيصاً لعمليات FSW المدفوعة بالهواء المضغوط. وبالتالي، يسهل هذا اختيار المحركات الهوائية أو الأدوات الدوارة المناسبة، جنباً إلى جنب مع أبعاد أدوات اللحام المناسبة، لتبسيط وتعزيز عمليات FSW.

ABSTRACT

This thesis explores the optimization of friction stir welding (FSW) processes, with a primary emphasis on harnessing pneumatic sources to introduce portability, minimize power consumption, enable workability in hazardous environments, and enhance efficiency. Structured into four chapters, the study is dedicated to identifying the pneumatic motor (or rotary hand tool) best suited for the pneumatic FSW process, leveraging the power of machine learning and metaheuristic algorithms.

The initial chapter provides a comprehensive exploration of FSW fundamentals and emphasizes the pivotal role of pneumatic sources in this welding technique. The discussion underscores the potential advantages offered by pneumatic sources, particularly in terms of portability and energy efficiency.

In the subsequent chapter, the methodology of the study is delineated, encompassing various artificial intelligence techniques such as artificial neural networks, random forest algorithms, and polynomial regression. Complementing these methods are the SHAPLEY additive explanation and Pelican optimization algorithm, tailored specifically to analyze and optimize FSW parameters with pneumatic sources.

The thesis then progresses to the development and validation of predictive models for FSW parameters in the third chapter. Through rigorous validation procedures, the performance of these models is assessed to reach an R^2 of 99.60% and a MAPE of 4.54%, providing insights into the optimization of parameters.

In the final chapter, a hybrid approach is proposed, synthesizing the developed models with the Pelican optimization algorithm. This novel approach aims to identify an optimum set of parameters, including tool geometry, welding speed, rotational speed, tilt angle, torque, and minimal power consumption, specifically tailored for pneumatic-driven FSW processes. Consequently, this facilitates the selection of suitable pneumatic motors or rotary hand tools, alongside appropriate tool geometries, to further streamline and enhance FSW operations.

RESUME

Cette thèse explore l'optimisation des processus de soudage par friction-malaxage (FSW), en mettant principalement l'accent sur l'utilisation de sources pneumatiques pour introduire la portabilité, minimiser la consommation d'énergie, permettre le travail dans des environnements dangereux et améliorer l'efficacité. Structurée en quatre chapitres, l'étude est dédiée à l'identification du moteur pneumatique (ou outil rotatif) le mieux adapté au processus de FSW pneumatique, en tirant parti de la puissance des algorithmes d'apprentissage automatique et métaheuristiques.

Le premier chapitre offre une exploration complète des fondamentaux du FSW et met l'accent sur le rôle central des sources pneumatiques dans cette technique de soudage. La discussion souligne les avantages potentiels offerts par les sources pneumatiques, notamment en termes de portabilité et d'efficacité énergétique.

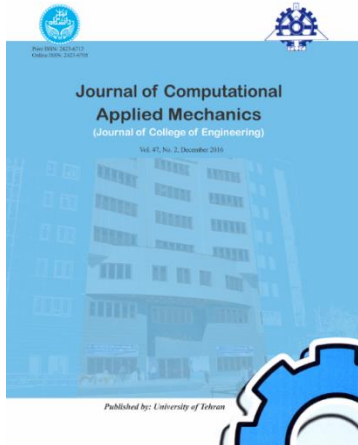
Dans le chapitre suivant, la méthodologie de l'étude est décrite, englobant diverses techniques d'intelligence artificielle telles que les réseaux de neurones artificiels, les algorithmes de forêt aléatoire et la régression polynomiale. Ces méthodes sont complétées par l'explication additive SHAPLEY et l'algorithme d'optimisation Pelican, spécialement conçus pour analyser et optimiser les paramètres du FSW avec des sources pneumatiques.

La thèse progresse ensuite vers le développement et la validation de modèles prédictifs pour les paramètres du FSW dans le troisième chapitre. À travers des procédures de validation rigoureuses, les performances de ces modèles sont évaluées pour atteindre un R^2 de 99,60% et un MAPE de 4,54%, fournissant des insights sur l'optimisation des paramètres.

Dans le dernier chapitre, une approche hybride est proposée, synthétisant les modèles développés avec l'algorithme d'optimisation Pelican. Cette approche novatrice vise à identifier un ensemble optimum de paramètres, comprenant la géométrie de l'outil, la vitesse de soudage, la vitesse de rotation, l'angle d'inclinaison, le couple et la consommation minimale d'énergie, spécifiquement adaptés aux processus de FSW pneumatique. En conséquence, cela facilite la sélection de moteurs pneumatiques ou d'outils rotatifs adaptés, ainsi que de géométries d'outil appropriées, pour rationaliser et améliorer davantage les opérations de FSW.

SCIENTIFIC WORK

SCIENTIFIC ARTICLES



[Sif Eddine Belalia](#); Mohamed Serier; Raheem Al-Sabur. "Parametric Analysis for Torque Prediction in Friction Stir Welding Using Machine Learning and Shapley Additive Explanations". *Journal of Computational Applied Mechanics*, 55, 1, 2024, 113-124. doi: 10.22059/jcamech.2024.370055.924

SCIENTIFIC COMMUNICATIONS

[S. Belalia](#), M. Serier, "Optimization of FSW process by studying the effect of different tool geometries". 1st National Conference of Thermal Engineering on Renewable and Conventional Processes NCTE'22", Batna (Algeria). 25th-26th October 2022.

[S. Belalia](#), B. Ghoul, M. Serier, M. Khorchef, "Predicting the tensile strength of Friction stir welded joint of dissimilar aluminium alloy plates AA2024 and AA7075". the First Seminar on Engineering Materials and Energy Technologies FNCOMET'23", Relizane (Algeria). 4th July 2023.

[S. Belalia](#), M. Khorchef, M. Serier, B. Ghoul, "Impact of axial force on the FSW of AA6061 T6". the First Seminar on Engineering Materials and Energy Technologies FNCOMET'23", Relizane (Algeria). 4th July 2023.

B. Ghoul, [S. Belalia](#), Y. Benyssaad, Y. Meddahi, "Minimization of energy consumption of 6-dof drones with a PID controller adjusted by GWO". the First Seminar on Engineering Materials and Energy Technologies FNCOMET'23", Relizane (Algeria). 4th July 2023.

M. Khorchef, M. Serier, A. Benariba, [S. Belalia](#), "Parametric study on thermal performance of earth-to-air heat exchanger used for cooling of buildings". the First Seminar on Engineering Materials and Energy Technologies FNCOMET'23, Relizane (Algeria). 4th July 2023.

[S. Belalia](#), M. Khorchef, "Optimizing the tensile strength of friction stir welded joints using pelican optimization algorithm". First National Conference in Computer Science Research and its Applications RIA'23", Relizane (Algeria). 10th May, 2023.

M. A. Khorchef, A. Benariba, A. Fidjah, [S. Belalia](#) "OPTIMIZING COOLING CAPABILITIES OF EARTH-TO-AIR HEAT EXCHANGER USING GEOTHERMAL ENERGY". VI. HAGIA SOPHIA INTERNATIONAL CONFERENCE ON MULTIDISCIPLINARY SCIENTIFIC STUDIES, Istanbul, (Türkiye). 2nd June, 2023

TABLE OF CONTENTS

ACKNOWLEDGMENTS	I
ملخص	II
ABSTRACT.....	III
RESUME	IV
SCIENTIFIC WORK.....	V
TABLE OF CONTENTS.....	VI
NOMENCLATURES.....	VIII
LIST OF TABLES.....	IX
LIST OF FIGURES	X
GENERAL INTRODUCTION.....	1
Chapter I - FSW fundamentals and the concept of a pneumatic source	3
I.1. Introduction	3
I.2. Overview of FSW and it's principles.....	3
I.2.1 Introduction to Friction Stir Welding	3
I.2.2 FSW welding zones	6
I.2.3 Application of FSW process	8
I.2.4 Friction Stir Welding Tool	10
I.2.5 Joint Design of the Friction Stir Welding Process.....	17
I.2.6 Advantages and limitations of FSW	18
I.3. Parameters of FSW	20
I.4. Torque in FSW.....	22
I.5. conventional FSW machines and power source	23
I.5.1 FSW machines.....	23
I.5.2 Electricity as a main power source	29
I.6. The concept of Pneumatic source in FSW.....	30
I.6.1 potential advantages of a pneumatic source in FSW	32
I.7. Conclusion.....	33
Chapter II - METHODOLOGY.....	36
II.1. Introduction.....	36
II.2. Background of study methodology	37
II.2.1 Deep learning	37

II.3. Methodology specifics	48
II.3.1 Artificial Neural Network.....	48
II.3.2 Random Forest Algorithm.....	49
II.3.3 Polynomial regression.....	51
II.3.4 Shapley Additive Explanations (SHAP): Understanding Model Predictions	52
II.3.5 Pelican Optimization Algorithm (POA): Harnessing Nature's Wisdom for Optimization	54
II.4. Some applications of Machine Learning, Deep Learning, and metaheuristics in FSW	57
II.5. Conclusion.....	63
Chapter III - Modeling and parametric importance Analysis of torque in FSW	65
III.1. Introduction.....	65
III.2. Materials and Methods.....	65
III.2.1 Experimental studies.....	65
III.2.2 Methodology	66
III.3. Results and discussion	70
III.3.1 ANN model	70
III.3.2 Random Forest Algorithm.....	71
III.3.3 Polynomial regression.....	74
III.3.4 Artificial Shapley Additive exPlanations (SHAP)	78
III.4. Conclusion	82
Chapter IV - A hybrid Artificial intelligence approach for Tool and Motor Selection in a Pneumatic FSW setup	85
IV.1. Introduction.....	85
IV.2. Materials and Methods.....	85
IV.2.1 Materials.....	85
IV.2.2 Methodology	86
IV.3. Results and discussion.....	88
IV.3.1 POA-ANN.....	88
IV.3.2 POA-RF.....	89
IV.3.3 Pneumatic motor selection	90
IV.4. Conclusion.....	93
GENERAL CONCLUSION	96
REFERENCES.....	99

NOMENCLATURES

Symbol	Signification Abbreviation	Unit
FSW	Friction Stir Welding	
MAE	Mean Absolute Error	
MAPE	Mean absolute Percentage Error	
RMSE	Root Mean Square Error	
ANN	Artificial Neural Network	
MSE	Mean Square Error	
SHAP	Shapley Additive exPlanations	
SSE	Sum Square Error	
RS	Rotational Speed	rpm
WS	Welding Speed (advancing speed)	mm/min
AS TS	Advancing Side Tensile Strength	MPa
RS TS	Retreating Side Tensile Strength	MPa
L0	Plate Thickness	mm
L1	Pin Length	mm
R1	Shoulder Radius	mm
R2	Pin base Radius	mm
R3	Pin tip Radius	mm
Alpha	Tilt angle	
T	Torque	N.m
RF	Random Forest Algorithm	
POA	Pelican Optimization Algorithm	
RF-POA	A Hybrid algorithm of Random Forrest and Pelican Optimization Algorithm	
ANN-POA	A Hybrid algorithm of Artificial Neural Network and Pelican Optimization	
PR-POA	A Hybrid algorithm of Polynomial Regression and Pelican Optimization	
P_{Tool}	Power associated with the moving tool	

LIST OF TABLES

TABLE I-1 - A SELECTION OF TOOLS DESIGNED AT TWI [8].....	14
TABLE I-2 - TOOL MATERIALS AND SUITABLE WELD METALS [11].	16
TABLE I-3 - MATERIALS JOINED BY FRICTION STIR WELDING USING WC TOOL MATERIAL [11]	17
TABLE I-4 - FSW PROCESS PARAMETERS [2]	21
TABLE I-5 - MAIN PROCESS PARAMETERS IN FRICTION STIR WELDING [10] [24].	22
TABLE I-6 - MAIN EXPERIMENTAL TORQUE STUDIES IN FSW.....	23
TABLE I-7 - MAIN TORQUE MODELS FOR FSW REPORTED IN THE LITERATURE.	23
TABLE I-8 - FSW EQUIPMENT FEATURES [54].....	29
TABLE II-1 - DIFFERENCE BETWEEN MACHINE LEARNING AND DEEP LEARNING [63].....	40
TABLE II-2 - A FEW RECENT METAHEURISTIC ALGORITHMS	45
TABLE II-3 - SOME OF THE DEEP LEARNING & METAHEURISTICS USED WITH FSW TECHNOLOGY [118].....	58
TABLE III-1 - WELDING CONFIGURATIONS OF THE EXAMINED STUDIES [167].....	66
TABLE III-2 - STATISTICS OF THE DATASET USED IN THIS STUDY [167]	68
TABLE III-3: COMPARING RESULTS OF POLYNOMIAL REGRESSION, ANN MODEL, AND THE RF MODEL.....	78
TABLE III-4 - ABSOLUTE MEAN SHAP VALUES FOR THE IMPACT OF EACH PARAMETES ON THE MODEL'S OUTPUT	81
TABLE IV-1 - ANN-POA OPTIMAL PARAMETERS FOR SELECTION OF PNEUMATIC FSW MOTOR (HAND TOOL) AND FSW TOOL GEOMETRY	92
TABLE IV-2 - RF-POA OPTIMUM PARAMETERS FOR SELECTION OF PNEUMATIC FSW MOTOR (HAND TOOL) AND FSW TOOL GEOMETRY	92

LIST OF FIGURES

FIG. I-1: SCHEMATIC OF THE FSW AND THE ACTING FORCES [54].	4
FIG. I-2 – MODIFIED MILLING MACHINE [182]	5
FIG. I-3 - CLAMPING SYSTEM [183].	5
FIG. I-4 - FSW STEPS: 1) TOOL PLUNGING, 2) DWELLING, 3) WELDING, 4) TOOL WITHDRAWAL [4].	6
FIG. I-5 - VARIOUS ZONES GENERATED IN THE FSW PROCESS [184].	7
FIG. I-6 - VARIOUS ZONES OF FSW JOINT [185]	7
FIG. I-7 - MATERIAL FLOW DURING FSW [5].	8
FIG. I-8 - FSW USED IN AUTOMOTIVE, AEROSPACE AND SHIPBUILDING INDUSTRY [6].	9
FIG. I-9 - FSW TOOL TYPES (A) FIXED, (B) ADJUSTABLE AND (C) BOBBIN [8].	11
FIG. I-10 - SHOULDER OUTER SURFACES, THE BOTTOM END SURFACES, AND THE END FEATURES [8].	12
FIG. I-11 - SOME PIN SHAPES AND THEIR MAIN FEATURES [8].	13
FIG. I-12 - JOINT CONFIGURATIONS UTILIZED IN FRICTION STIR WELDING: (A) SQUARE BUTT, (B) EDGE BUTT, (C) T BUTT JOINT, (D) LAP JOINT, (E) MULTIPLE LAP JOINT, (F) T LAP JOINT, AND (G) FILLET JOINT.	18
FIG. I-13 - DEDICATED FSW MACHINE - FSW LEGIO™ [54].	26
FIG. I-14 - ROBOTIC FSW OF A MULTI WELDING PART [186].	27
FIG. I-15 - ARTICULATED ARM ROBOT PERFORMING FSW AT THE UNIVERSITY OF COIMBRA [54].	28
FIG. I-16 - PNEUMATIC FSW SETUP [57].	31
FIG. II-1 - GRAPHICAL REPRESENTATION OF NEURAL NETWORKS [187].	38
FIG. II-2 - GRAPHICAL REPRESENTATION OF DEEP BELIEF NETWORK [63].	39
FIG. II-3 - MH ALGORITHMS WORKING PROCESS.	42
FIG. III-1 - ARCHITECTURE OF THE ANN MODEL [167]	67
FIG. III-2 - PREDICTED VALUES OF TORQUE LOSS FOR TRAINING AND VALIDATION DATASETS [167]	70
FIG. III-3 – ANN PREDICTED AND EXPERIMENTAL TORQUE COMPARISON.	70
FIG. III-4 - LOCAL AND GLOBAL MODELS PREDICTION OF RF VS TRUE VALUES	71
FIG. III-5 - RF PREDICTED AND EXPERIMENTAL TORQUE COMPARISON.	72
FIG. III-6 - METRICS OF THE RF MODELS (GLOBAL AND LOCAL).	73
FIG. III-7 - LOCAL AND GLOBAL MODELS PREDICTION OF PR VS TRUE VALUES	75
FIG. III-8 - PR PREDICTED AND EXPERIMENTAL TORQUE COMPARISON.	76
FIG. III-9 - METRICS OF THE PR MODELS (GLOBAL AND LOCAL)	77
FIG. III-10 - MEAN ABSOLUTE SHAP VALUES FOR ANN.	79
FIG. III-11 - SHAP VALUES FOR THE PREDICTIVE ANN TORQUE MODEL	79
FIG. III-12 - SHAP VALUES FOR THE PREDICTIVE RF TORQUE MODEL.	80
FIG. III-13 - MEAN ABSOLUTE SHAP VALUES FOR RF.	80
FIG. IV-1 - POWER LEVEL DURING THE ITERATIONS OF THE ANN-POA MODEL	89
FIG. IV-2 - POWER LEVEL DURING ITERATIONS OF RF-POA	91

GENERAL INTRODUCTION

GENERAL INTRODUCTION

Friction Stir Welding (FSW) stands as a transformative welding technique, revolutionizing the landscape of material joining in various industries. Its inherent ability to create high-strength, defect-free welds without melting the material has garnered significant attention. Yet, within this promising field, the integration of a pneumatic source of power represents an unexplored frontier, offering potential advancements and innovation.

The conventional power source -electric power- utilized in FSW have laid the groundwork for its success, but the introduction of a pneumatic source introduces a paradigm shift. This thesis embarks on an exploration of this novel avenue, delving into the uncharted territory of FSW enhanced by pneumatic source of power, aiming to unearth its promises and advancements.

Machine learning, a powerful tool in today's technological era, serves as the guiding force in this endeavor. Its ability to decipher complex patterns and predict outcomes holds immense potential in optimizing FSW processes, especially when applied in conjunction with a novel source of power such as the pneumatic one.

This thesis aims to bridge the gap between traditional FSW source of power and the untapped potential offered by the pneumatic source. By harnessing the capabilities of machine learning and integrating them into the FSW domain As this study uses previously conducted experimental results from different researches and fit them to the service of pneumatic FSW, the objective is to unlock new insights, enhance predictive capabilities, and pave the way for a future where pneumatic FSW stands as a pinnacle of efficiency and precision by opening the door to use light weight and portable equipment as well as it introduces more safety in use at environments where the electric power might impose a risk like in the underwater environment.

Through a comprehensive exploration of machine learning models, particularly neural networks and Random Forest in conjunction with innovative optimization techniques like the Pelican Optimization Algorithm, this research aspires to propel FSW technology into uncharted realms, offering a glimpse into its unprecedented possibilities.

The scope of this thesis encompasses an in-depth analysis of the theoretical fundamentals, methodological intricacies, and forward-looking implications of integrating machine learning with the revolutionary concept of pneumatic FSW.

CHAPTER I

Chapter I - FSW fundamentals and the concept of a pneumatic source

I.1. Introduction

Our initial focus revolves around establishing a comprehensive understanding of FSW fundamentals. We begin by unpacking the process itself, highlighting the role of the dedicated tool, joint design considerations, and a meticulous analysis of the inherent advantages and limitations compared to other joining methods. Subsequently, we navigate the intricacies of FSW parameters, scrutinizing their individual and combined influence on the welding process and the final joint quality.

To gain a deeper understanding of the practical aspects, we explore the landscape of conventional FSW machines and their dedicated power sources. This section analyzes their design configurations, operational characteristics, and potential limitations. However, the chapter also ventures into the burgeoning realm of pneumatic power sources, exploring their untapped potential to revolutionize the FSW landscape. By examining the theoretical and practical advantages of pneumatic technology, we pave the way for future research and development in this dynamic field.

This chapter aspires to demonstrate a robust understanding of FSW, serving as a valuable primer for further exploration. By methodically dissecting the process, its parameters, equipment, and potential advancements, we aim to demystify this transformative technology and explore the necessary knowledge to navigate its intricacies and leverage its potential across diverse applications.

I.2. Overview of FSW and it's principles

I.2.1 Introduction to Friction Stir Welding

Friction Stir Welding (FSW) is acknowledged as a solid-state joining process where the generated heat does not surpass the melting temperature of the materials being joined. Developed in 1991 at The Welding Institute (TWI) in the UK [1]. It addresses the challenge of welding materials traditionally considered non-weldable, such as dissimilar materials, magnesium alloys, certain aluminum alloys, copper, titanium, etc. These materials often exhibit poor solidification microstructure, porosity in the fusion zone, and significant loss of mechanical properties through conventional welding methods [1].

In the FSW process (illustrated in Fig. I-1), a non-consumable cylindrical tool with a shoulder and pin serves as a stirrer. The tool, fixed to a milling machine chuck, undergoes rotation along its longitudinal axis (as shown in Fig. I-2, depicting a modified milling machine). Workpieces slated for welding can be butted up or overlapped, then clamped to remain stationary and withstand substantial applied forces (as seen in the clamping system of Fig. I-3). Clamping effectively prevents workpiece spreading.

Initiating the FSW process involves inserting the rotating tool pin into the joint of the workpiece, with the shoulder making contact with the workpiece surface. Friction between the workpiece surface and the tool shoulder induces heating of the material being joined. Transversely moving the tool along the joint combines friction heating with pin stirring, softening and integrating the material into a weld. Crucially, the process is meticulously managed to keep the temperature below the melting point of the base materials [2] [3]. Upon reaching the end of the joint, the tool is retracted from the workpiece. The four distinct steps of the FSW process are outlined in Fig. I-4.

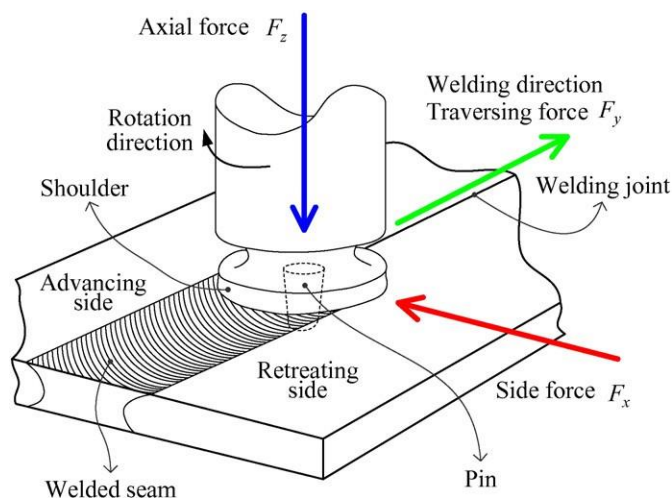


Fig. I-1: Schematic of the FSW and the acting forces [54].

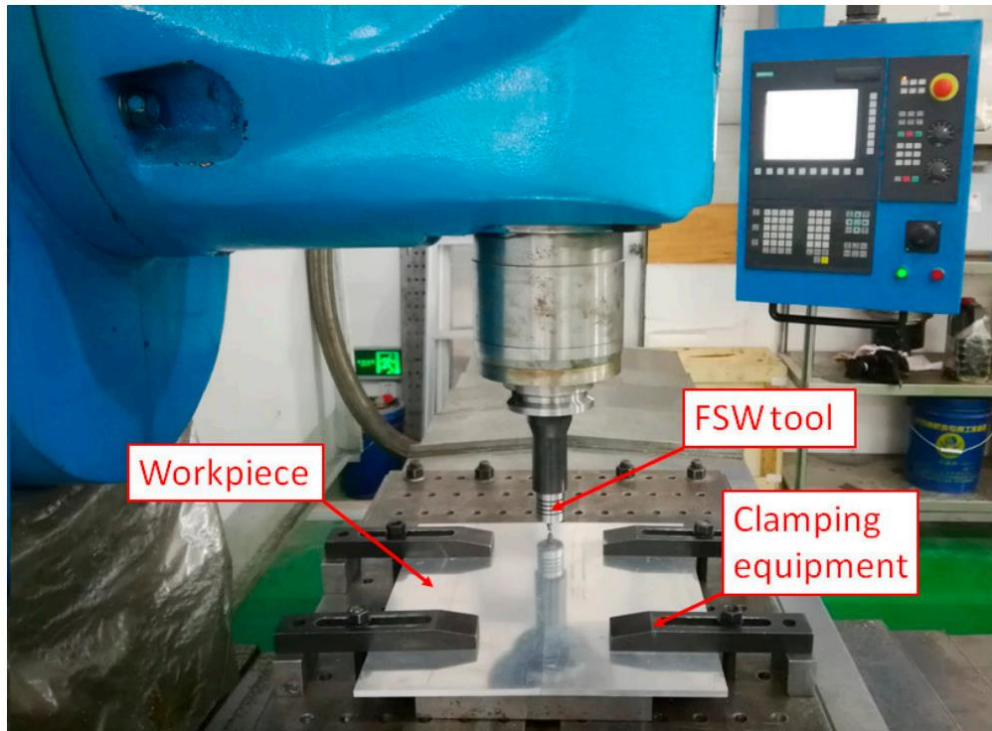


Fig. I-2 – Modified milling machine [182]

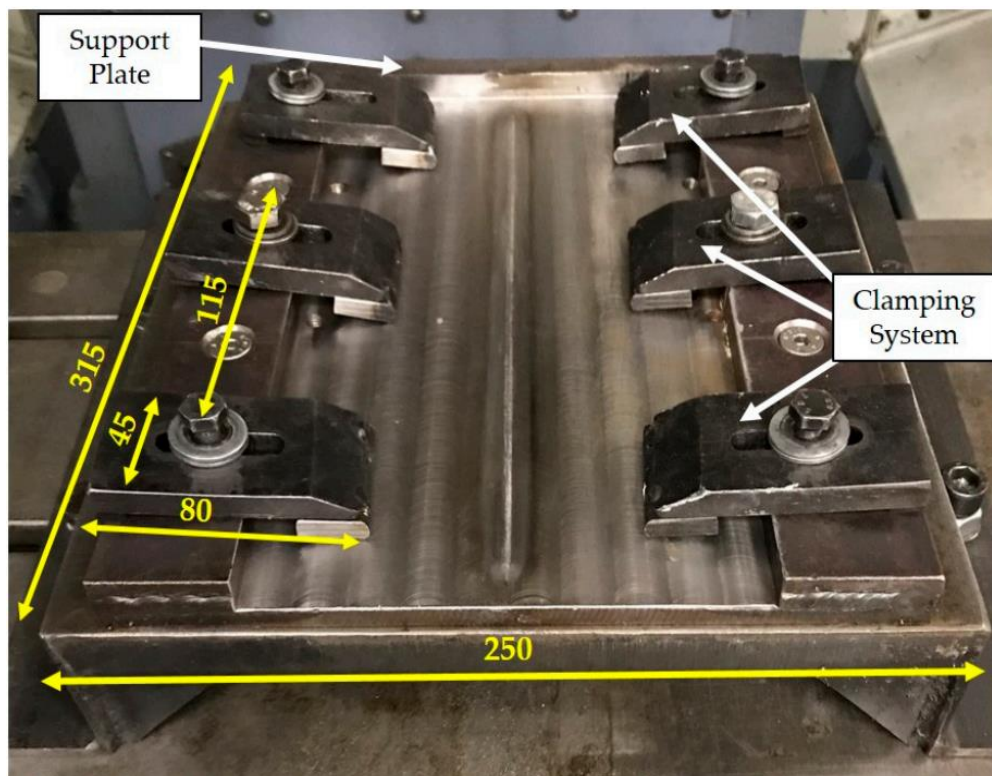


Fig. I-3 - Clamping system [183].

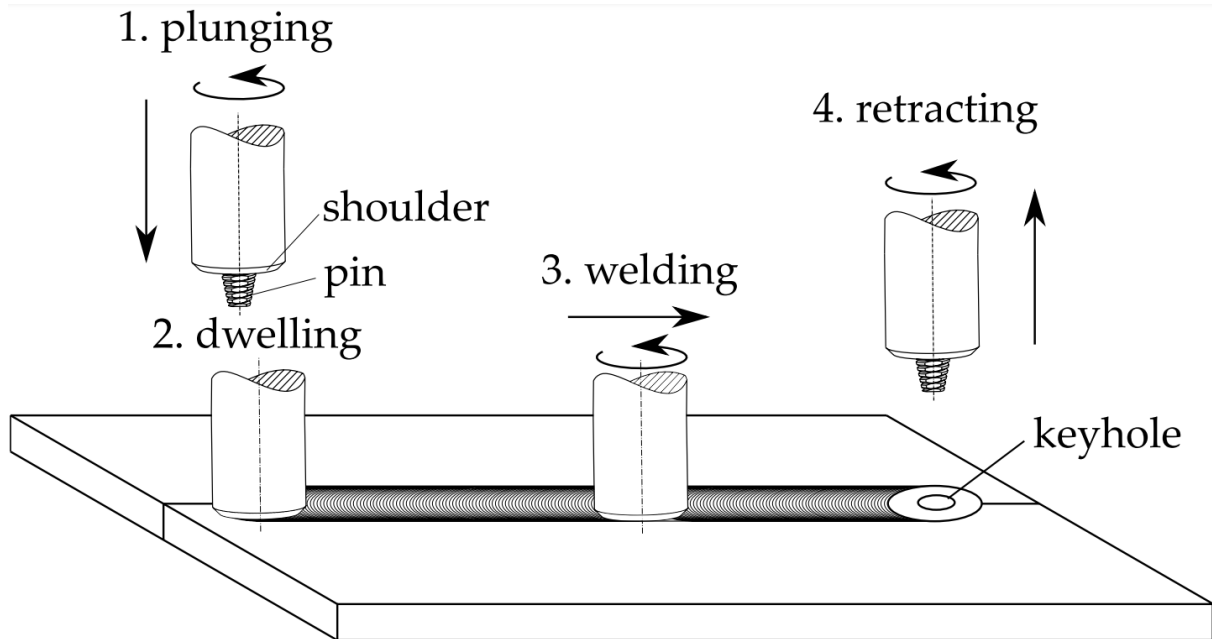


Fig. I-4 - FSW steps: 1) tool plunging, 2) Dwelling, 3) Welding, 4) tool withdrawal [4]

I.2.2 FSW welding zones

FSW operation creates different zones in the welded plates due to them affected by heat and mechanical work (see Fig. I-5). We can categorize the zones to [2]:

I.2.2.1 Parent metal/base metal (PM/BM):

In regions where the material remains undeformed, it may also undergo thermal cycles without experiencing any microstructural or mechanical alterations.

I.2.2.2 Heat affected zone (HAZ):

Within this zone, the metal undergoes a thermal cycle that induces alterations in microstructure and mechanical properties. Importantly, there is an absence of plastic deformation or dynamic recrystallization, preserving the same grain structure as that of the parent metal.

I.2.2.3 Thermo-mechanical affected zone (TMAZ):

In this zone, both thermal cycling and plastic deformation occur, leading to a highly deformed microstructure. The grains originating from the parent metal undergo deformation and elongation, forming an upward-flowing pattern around the stirred zone. Due to insufficient plastic strain, dynamic recrystallization does not take place, and only plastic deformation is observed.

I.2.2.4 Stir zone (SZ):

Dynamic recrystallization has undergone complete occurrence. The presence of fine grain sizes is attributed to severe deformation at elevated temperatures. These diminutive grain sizes contribute to heightened strength and hardness in the welded metal.

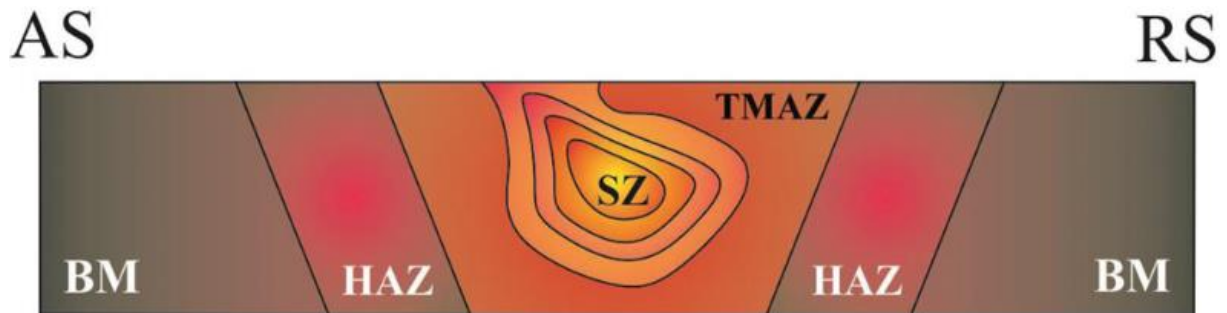


Fig. I-5 - Various zones generated in the FSW process [184]

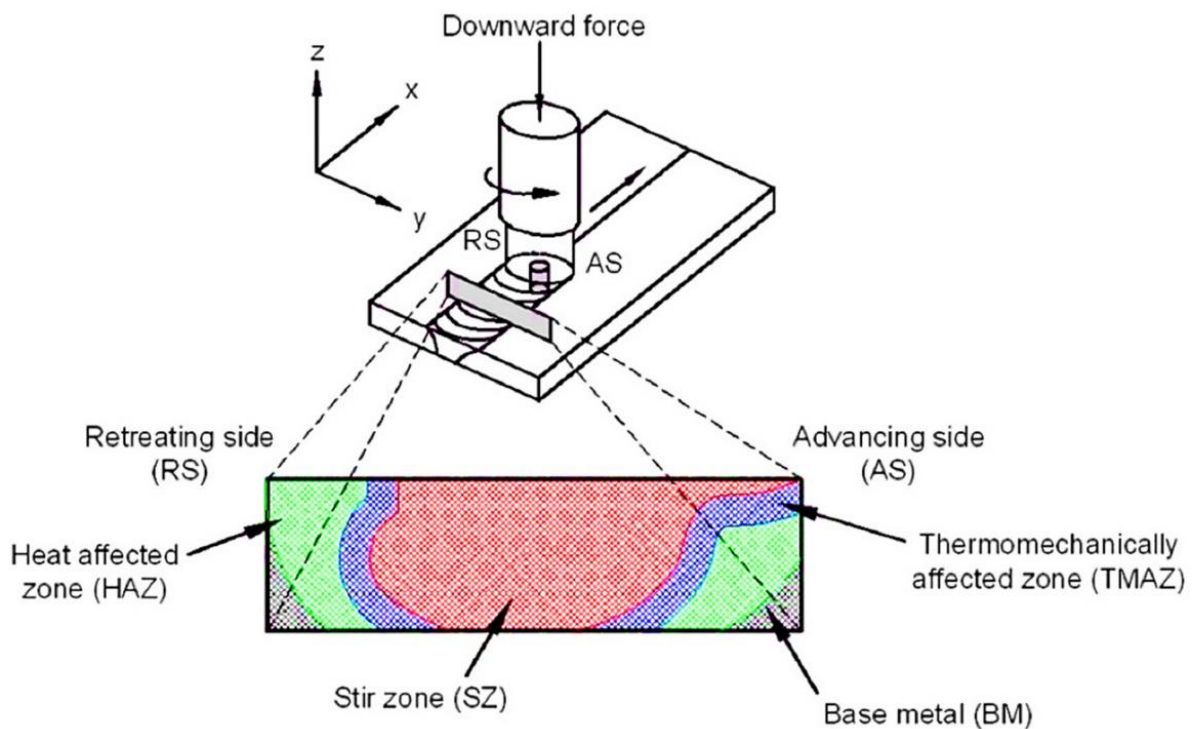


Fig. I-6 - Various zones of FSW joint [185]

The material flow and dynamics within Friction Stir Welding (FSW) can exhibit considerable complexity (Fig. I-7). The region surrounding the tool undergoes heating through two primary mechanisms: frictional heating occurring between the tool, particularly the shoulder, and the

workpiece, and the plastic deformation associated with the movement of the workpiece material, commonly referred to as stirring. This localized heating effectively softens the material proximate to the tool. The combined rotational and translational motion of the tool along the joint leads to the displacement of material from the front to the rear of the pin [2]. Numerous studies have explored material flow using markers and etching techniques, with findings indicating that the design of the tool significantly influences material flow patterns [2].

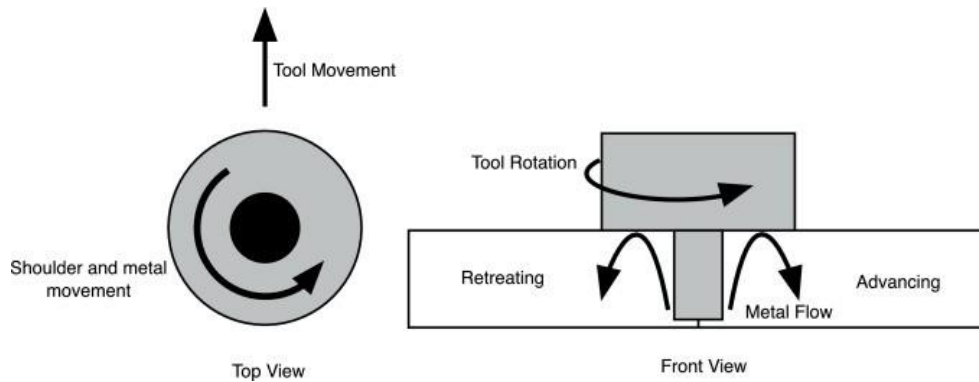


Fig. I-7 - material flow during FSW [5].

I.2.3 Application of FSW process

There Friction Stir Welding (FSW) finds applications across various industries (Fig. I-8), and the following list provides a representative snapshot, acknowledging that new applications continue to emerge [1] [2] [5] [6].

Aerospace:

- Wings
- Fuselages
- Floor panels
- Aircraft landing gear doors
- Fuel tanks
- SpaceX Falcon 1 and Falcon 9 rockets
- NASA Space Shuttle external tanks

Automotive (Fig. I-8):

- Trailer beds
- Door panels

- Center console (smooth design)

Military: Joining Armor Aluminum Alloys, particularly in Advanced Amphibious Armored Vehicles (AAAVs)

Railway: Roof and side panels, Bodies

Shipbuilding (Fig. I-8) and Offshore:

- Panels for decks, sides, bulkheads, floors, hulls
- Superstructures, helipads
- Offshore accommodations
- Masts, booms

Computers: iMac in 2012, specifically in joining front and back panels

Construction: Aluminum bridges, Window frames, Aluminum pipelines and heat exchangers, Oil and Gas pipelines



Fig. I-8 - FSW used in automotive, aerospace and shipbuilding industry [6].

I.2.4 Friction Stir Welding Tool

The friction stir welding tool stands as a pivotal component in this welding technique, exerting a profound influence on the quality of the welding zone. Enhanced tool properties contribute to improved welding outcomes. Comprising three integral parts -shank, shoulder, and pin (i.e., probe)- the friction stir welding tool serves various functions. The shoulder plays a multifaceted role, applying pressure on the workpieces and confining the plasticized material around the pin. As the shoulder encounters friction with the upper workpiece's surface, it generates heat, leading to plastic deformation.

The primary function of the pin is to soften, plasticize, and stir the materials within the stir zone (SZ). Employing friction stir welding with specialized tool designs, shapes, dimensions, and materials yields significant improvements in various mechanical and physical properties. These enhancements encompass creep resistance, ductility, strength, fatigue performance, elimination of casting defects, manipulation of grain microstructure, corrosion resistance, and formability [7] [8].

1. Tool Types of the Friction Stir Welding Process

The primary functions of the friction stir welding tool encompass heating the workpieces, achieved through the friction between the pin and shoulder with the workpieces, inducing plastic deformation of the workpiece metal, and facilitating the flow of material while constraining the heat beneath the shoulder. There exist three distinct types of friction stir welding tools: fixed, adjustable, and self-reacting, also known as the bobbin tool.

The fixed pin tool is a singular piece that integrates both the shoulder and the pin. Its applicability is limited to welding metals of specific thicknesses due to the fixed pin length. Additionally, a backing anvil is required to secure the workpieces. In case of pin breakage or wear, the entire tool needs replacement.

The adjustable tool, in contrast, consists of two independent components—the shoulder and the pin. This tool permits the alteration of pin length during the friction stir welding process, simplifying pin replacement in case of damage. While the pin and shoulder can be made from different materials, the tool's strength may be compromised compared to when both components are of the same material. The adjustable tool is versatile, accommodating different thicknesses of workpieces, but it also necessitates a backing anvil.

The self-reacting tool, or bobbin tool, is constructed from three distinct pieces: top shoulder, bottom shoulder, and pin. This tool's versatility allows it to handle joints with varying

thicknesses, as the pin length can be adjusted between the two shoulders. Unlike the fixed and adjustable tools, the bobbin tool can work perpendicular to surfaces, eliminating the need for a backing anvil. However, it lacks the capability to be tilted at a specific angle, a feature present in fixed and adjustable tools, providing control over the appearance of the welding zone [9] [10] [11] [12]. (Fig. I-9) below illustrates the three types of tools.

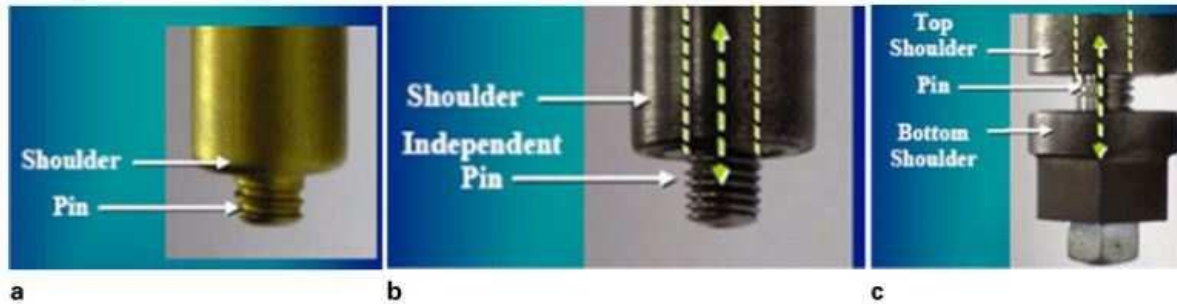


Fig. I-9 - FSW tool types (a) fixed, (b) adjustable and (c) bobbin [8].

1.2.4.1 Shoulder Shapes of Friction Stir Welding

The design of tool shoulders holds a crucial role in heating the upper surface of workpieces through frictional forces. The shoulder contributes a downward forging pressure, vital for welding integration and constraining heated material beneath the bottom surface. While the outer surface of the shoulder commonly adopts a cylindrical shape, occasionally a conical shape is employed. The choice between cylindrical and conical shapes has minimal impact on welding quality due to the shallow plunge depth of the shoulder, typically ranging from 1-5% of the sheet's thickness.

A straightforward shoulder design, termed flat, lacks effectiveness in trapping flowing materials underneath, resulting in excessive material flash due to flat end shoulder surfaces. In contrast, the other end surface adopts a concave design, widely favored in friction stir welding. The concave angle, ranging between 6-10°, facilitates material flow control, ease of machining, and high-quality welding. This concave shoulder serves as a reservoir for the material stirred by the rotating pin. Tilting the tool during the friction stir welding process, typically between 1-3° against the tool's travel direction, optimizes the advantages of the concave shoulder design. This includes the application of compressive forging force on the welding zone, maintaining continuity in material storage, hydrostatic pressures, enhancing nugget zone integrity, and stirring material around the pin.

Another shoulder design, convex, successfully pushes material away from the pin, maintaining contact along the shoulder's end surface. While the smooth surface lacks the ability to prevent material displacement, it controls differences in thickness between joined workpieces. The characteristics of shear and plastic deformation on shoulder end surfaces enhance material mixing, weld quality, and friction. Various shoulder end styles, including scrolls, concentric circles, ridges, knurling, grooves, and flat (smooth or featureless), are utilized during the friction stir welding process. The scrolled shoulder, featuring a spiral channel, aids material flow from the shoulder's edge to the center. Combining the concave design with a scrolled feature reduces tool lifting, removes undercut defects, decreases flash, and increases frictional heat. Further advantages arise from combining the convex shoulder with a scroll, providing greater flexibility, improved mismatch tolerance, and the ability to weld complex curvatures and metals with different thicknesses [2] [8] [9] [10] [11] [12]. (Fig. I-10) below illustrates the various types of shoulders.

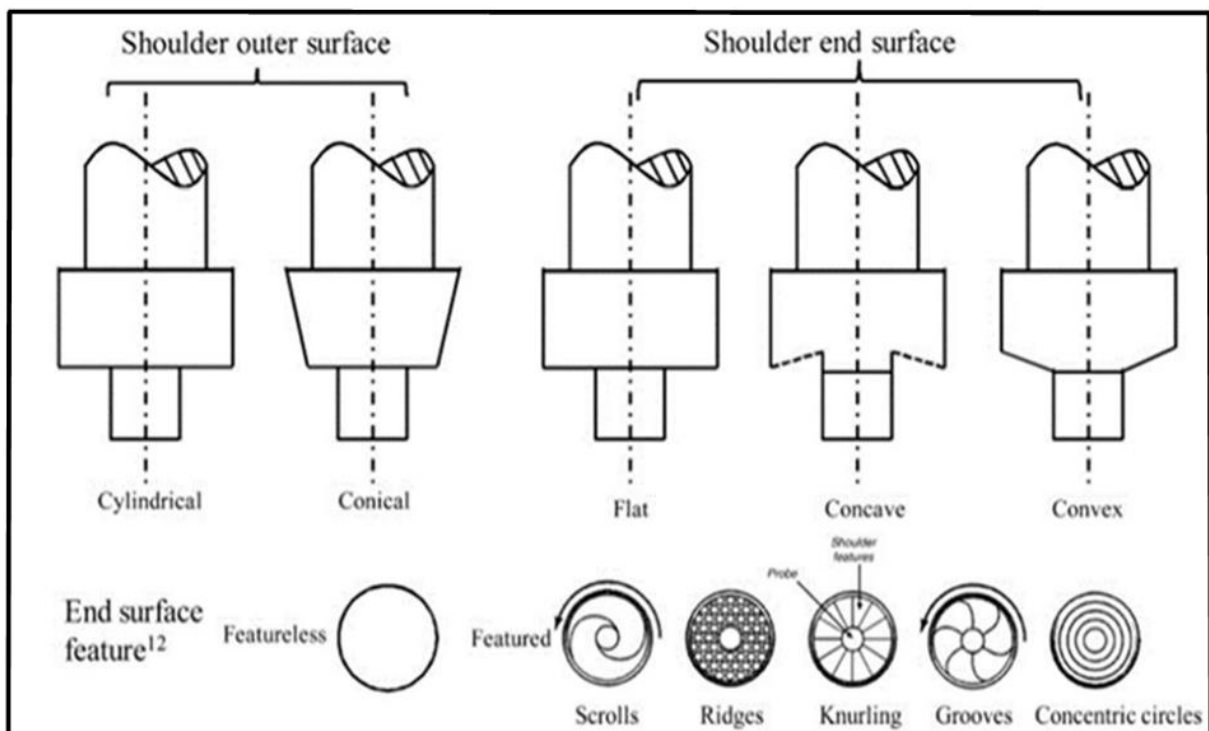


Fig. I-10 - shoulder outer surfaces, the bottom end surfaces, and the end features [8].

1.2.4.2 Pin Shapes of Friction Stir Welding

The pin in the friction stir welding process serves several key functions, including frictional heating and deformation, cutting materials in front of the tool, damaging workpiece edges, and stirring and mixing materials behind the tool. Two distinct end shapes of the pin are

commonly utilized: flat and domed (see Fig. 7). The flat design, being easy to manufacture, is the most prevalent in friction stir welding. It can provide high forge force during the plunging step, reducing overall forge force and tool wear. On the other hand, the domed design enhances the joint root at the bottom of the pin and extends tool life by minimizing stress concentration in the joint zone. The benefits of the domed design are maximized when the dome radius at the pin end is equal to 75% of the pin diameter.

In the case of cylindrical pins, they prove useful for joining different metals until the thickness reaches 12 mm. Thicker metals require the welding process to operate with high rotational and low travel speeds to maintain weld integrity. Tapered pins, generating frictional heat, enhance plastic deformation due to their substantial contact area with the workpieces. They also produce high hydrostatic pressure in the joint region, crucial for improving nugget integrity and materials stirring. However, the features of tapered pins can lead to sharp tool wear.

The outer surface of the pin may have different shapes and features, including threads, flat surfaces, or flutes. Although threaded pins are more susceptible to corrosion, they are frequently used in the friction stir welding process. Improved void closure, materials stirring, and oxide layer breakdown can be achieved through two factors: the material circulating twice around the pin before depositing and the threaded pin rotating the materials clockwise, drawing them down along the pin surface (see Fig. I-11) [9] [12] [13] [14] [15].

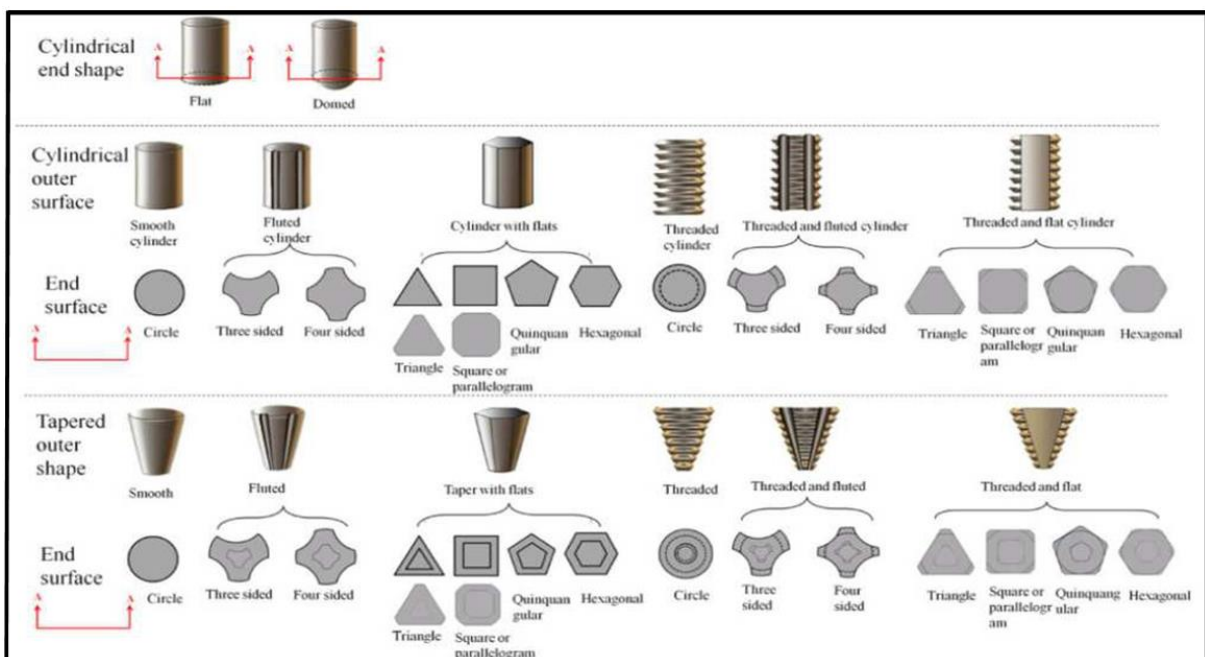








Fig. I-11 - some pin shapes and their main features [8].

Tapered pin designs in friction stir welding come in three variants: non-threaded, threaded, and threaded with flats. Threaded and threaded with flats pins yield fully consolidated welds, while the non-threaded design may result in voids in the welding zone. The presence of flats restricts and releases material, enhancing mixing. Increasing the number of flats can raise temperature and nugget zone width. Flat-shaped pins can act like cutting edges. Typically, cylindrical threaded pins are employed for aluminum alloys with thicknesses exceeding 12 mm in butt joints. However, for thicker workpieces, additional features are beneficial to enhance material flow and mixing, as well as to reduce friction stir welding loads.

Critical to the friction stir welding process is the tool design. Tools with high swept rates, developed by welding institutes such as Whorl and MX Triflute, play a significant role in reducing voids, increasing material stirring and mixing, and dispersing the oxide layer in the nugget zone. These tool types, including straight cylindrical, threaded cylindrical, tapered cylindrical, and triangular, can achieve a volume reduction of approximately 60-70% (see Table I-1). The geometry of the tool is paramount in the friction stir welding process, especially in governing material flow and determining the travel rate.

Table I-1 - a selection of tools designed at TWI [8].

Tool	Cylindrical	Whorl™	MX triflute™	Flared triflute™	A-skew™	Re-stir™
Schematics						
Tool pin shape	Cylindrical with threads	Tapered with threads	Threaded, tapered with three flutes	Tri-flute with flute ends flared out	Inclined cylindrical with threads	Tapered with threads
Ratio of pin volume to cylindrical pin volume	1	0.4	0.3	0.3	1	0.4
Swept volume to pin volume ratio	1.1	1.8	2.6	2.6	depends on pin angle	1.8
Rotary reversal	No	No	No	No	No	Yes
Application	Butt welding; fails in lap welding	Butt welding with lower welding torque	Butt welding with further lower welding torque	Lap welding with lower thinning of upper plate	Lap welding with lower thinning of upper plate	When minimum asymmetry in weld property is desired

I.2.4.3 Tool Dimensions of Friction Stir Welding

The dimensions of the tool play a crucial role in the friction stir welding process, exerting a significant influence on the outcomes and mechanical properties. As a general guideline, the diameter of the tool pin should match the thickness of the workpiece, and the height of the pin should be slightly less than the thickness. Additionally, the shoulder diameter is typically maintained between 3-5 times the diameter of the pin.

The heat input during the friction stir welding process is influenced by the shoulder radius to the third power. This heat input linearly depends on both the rotational speed and the downward forge force. In essence, the energy input in the friction stir welding process is contingent on the dimensions of the shoulder. The equation below encapsulates these considerations, emphasizing that the Z axis of the downward force is a function of the shoulder radius.

$$Q_0 = \frac{4}{3} \pi^2 \mu k P \omega R^3 \quad (I-1)$$

$$F_f = \mu k F_n \quad (I-2)$$

In the given equation, Q_0 symbolizes the net power (unit unspecified), $\frac{4}{3} \pi^2$ represents a constant, μ denotes the dimensionless friction coefficient between the pin, shoulder, and workpieces, P stands for pressure measured in megapascals (MPa), R signifies the shoulder radius measured in millimeters (mm), ω indicates the rotational speed measured in revolutions per minute (rev/min), F_f represents the frictional force measured in Newtons, and F_n corresponds to the normal force measured in Newtons. The shoulder diameter is considered a function of the plate's thickness or the pin diameter. This relationship implies that an increase in sheet thickness necessitates a greater amount of energy. Consequently, a larger shoulder diameter is required to generate the necessary heat.

I.2.4.4 Tool Materials of Friction Stir Welding

The selection of the tool material for the friction stir welding (FSW) process is a critical consideration, as it significantly influences the quality of the welding joint. Several factors contribute to the decision-making process, including the workpiece material, user experience,

performance expectations, and tool life. Consequently, the chosen tool material must possess specific properties to ensure optimal performance in the FSW process.

Key properties that a suitable tool material for FSW should exhibit include high strength, creep resistance, and dimensional stability. The compressive yield strength at the operating temperature should surpass the stresses generated by the forces applied on the tool. Thermal fatigue strength is crucial, as it should withstand repeated heating and cooling cycles. Additionally, the tool material should not undergo harmful reactions with the workpiece material, and its fracture toughness should be high to resist damage during the plunging and dwelling process. A low thermal expansion coefficient between the pin and shoulder materials helps reduce thermal stresses. The application of a thermal barrier coating can prevent heat from moving into the shank part of the tungsten carbide tool. Machinability is essential for ease of manufacturing different shapes for each shoulder and pin, and cost-effectiveness is a practical consideration.

Various materials can be used to manufacture FSW tools, each with its own set of advantages and disadvantages based on the type of material being welded. Steel tools like H13 are suitable for welding soft materials such as aluminum. Tungsten carbide with cobalt and polycrystalline cubic boron nitride (PCBN) are preferred for hard materials like titanium and its alloys.

Tungsten carbide, in particular, is widely used as a tool material in FSW due to its excellent mechanical properties. It offers exceptional toughness and wear resistance at ambient temperature, excellent fracture toughness, high hardness reaching 1650 HV, insensitivity to sudden changes in temperature and loading, and minimal deformation owing to its chemical inertness.

While tools have been well-developed for materials with low strength like aluminum alloys, a cost-effective and long-lasting tool for abrasive materials and high-strength materials such as titanium, nickel, and steels remains a challenge. The choice of tool material has a profound impact on various joint properties, including microstructure, heat generation, thermal conductivity, and thermal stresses of workpieces [2] [9] [10] [11] [12] [15] [16].

Table I-2 - Tool materials and suitable weld metals [11].

Tool Material	Suitable weld material
Tool steels	Al alloys, aluminum metal matrix composites (AMCs) and copper alloys

WC –Co	Aluminum alloys, mild steel
Ni-Alloys	Copper alloys
WC composite	Aluminum alloys, low alloy steel and magnesium alloys, Ti-alloys
W-alloys	Titanium alloys, stainless steel and copper alloys
PCBN	Copper alloys, stainless steels and nickel alloys

Table I-3 - Materials joined by friction stir welding using WC tool material [11]

No	Materials used
1	A3003-H112 Al alloy 15 mm thick & SUS304 (SS) 12 mm thick.
2	Al. alloy 1060 and titanium alloy Ti–6Al–4V plates 3 mm thick
3	Plates of SK4 high carbon steel alloy (0.95% C). 2 mm thick
4	Hyper-eutectoid steel (0.85mass% C, AISI-1080), 1.6 mm thick
5	SAF 2205 duplex stainless steel. 2mm thick
6	High carbon steel S70C (0.72 wt. % C). 1.6 mm thick
7	Carbon steels IF steel, S12C and S35C 1.6 mm thick plates

I.2.5 Joint Design of the Friction Stir Welding Process

During the friction stir welding (FSW) process, butt and lap joints are the most suitable types of joints employed. Lap joints, in particular, pose specific challenges and advantages in comparison to butt joints. The inherent hardness of lap joints during FSW is attributed to several factors. Wider welds are required to bear the loads, and avoiding hooking defects is crucial to maximize fatigue strength. Additionally, disrupting the oxides at the workpiece interface in lap joints is more challenging.

Butt joints involve clamping two plates together firmly to prevent any movement of the joint. These plates have identical thickness and are positioned on the backing plate. Care must be taken to ensure the plates do not shift when the tool is inserted into the butt joint. The tool pin plunges and rotates within the butt joint, traveling along the joint line. The direct contact of the shoulder with the upper surface of the plates results in the formation of a long welded butt joint.

In lap joints, two plates are clamped onto the backing plate, and the tool is rotated vertically while traveling along the appropriate direction. Special surface preparation is not required for each butt and lap joint in the FSW process. Metals can be joined without concerns about the condition of the surfaces. Fig. I-12 provides an illustration of different types of joints in the FSW process [2].

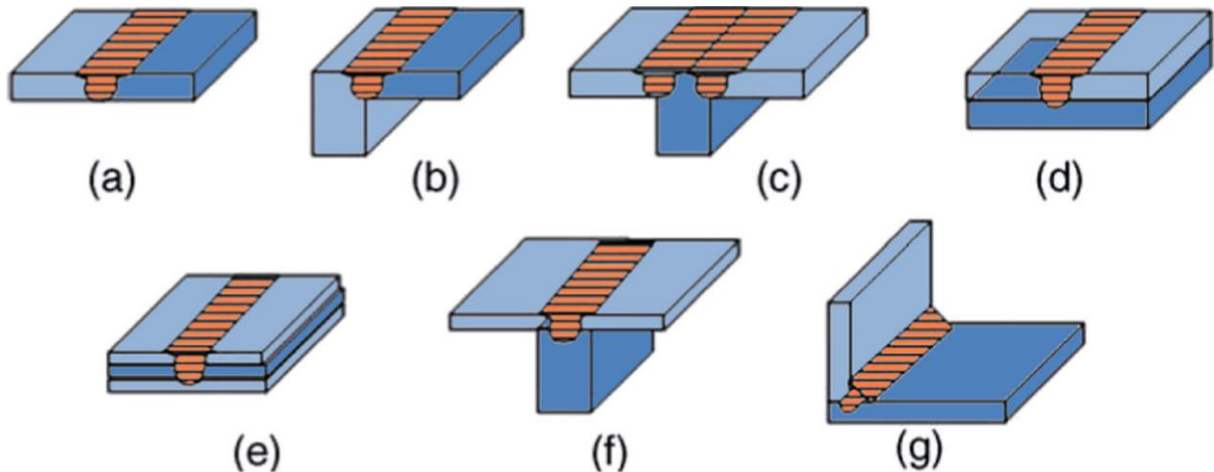


Fig. I-12 - joint configurations utilized in friction stir welding: (a) square butt, (b) edge butt, (c) T butt joint, (d) lap joint, (e) multiple lap joint, (f) T lap joint, and (g) fillet joint.

I.2.6 Advantages and limitations of FSW

FSW, like other welding technologies, presents both advantages and limitations. Some of the key advantages are outlined below:

I.2.6.1 Advantages

1. **Improved Microstructure:** FSW enhances the microstructure by generating fine grains, resulting in excellent mechanical properties in the welding zone, including enhanced strength, bending, tensile, and fatigue properties compared to other welding processes. Joint efficiency can range from 70-96%, and in some cases, it can even reach 100% with shorter joint zones.
2. **Solid-State Joining:** FSW enables the joining of similar or dissimilar materials without melting, producing a joint in a solid state. This minimizes or eliminates typical defects encountered in traditional welding processes, such as porosity, cracking, shrinkage, and solidification.
3. **No Need for Shielding Gases or Filler Materials:** The FSW process eliminates the need for shielding gases, avoiding issues like porosity, spatter, arcs, or fumes. Additionally, no filler materials are required, streamlining the welding process.

4. Elimination of Solidification Defects and Weld Distortion: FSW can completely eliminate common issues like solidification defects and weld distortion, contributing to the overall quality of the welded joints.

5. Low Power Requirement: FSW requires relatively low power, necessitating only enough energy to rotate the tool and apply the force that generates friction heat.

6. Cost and Time Efficiency: FSW offers cost and time savings, is environmentally-friendly, minimizes material wastage, and is energy-efficient. The process is characterized by good properties, is pollution-free, and can weld both similar and dissimilar materials that are challenging to fusion weld.

These advantages make friction stir welding an attractive option for various applications, especially where the avoidance of melting and the achievement of superior mechanical properties are critical considerations [17] [18] [19].

I.2.6.2 Limitations:

1. Joint Type Limitations: Friction stir welding (FSW) has limited flexibility in the types of joints that can be welded.

2. Tool Wear: Welding harder materials can lead to excessive wear on the FSW tool, making tool replacement an expensive aspect of the process.

3. Equipment Weight: FSW machines are typically heavy equipment, limiting their mobility and ease of transportation.

4. Lack of Mobility: FSW equipment lacks mobility, making it challenging to use outside of controlled environments that require tight fixation, precision, and temperature control.

5. Clamping Requirements: The necessity for clamping workpieces to prevent joint movement and the application of force limits FSW applications to joints with specific geometries.

6. Undesired Hole Formation: At the end of the welding process, lifting the tool may result in an undesired hole, which is undesirable in many applications.

7. Temperature Sensitivity: High traverse speeds or low rotation speeds can lead to insufficient weld temperatures, preventing materials from accommodating extensive deformation during the welding process.

8. Welding Parameter Sensitivity: Welding parameters such as low forging pressure, short friction time, and low friction pressure can result in weak joints with voids.

9. Kissing Bond Defect: When two workpieces are lightly contacted, forming a "kissing bond," defects may occur that are challenging to detect using non-destructive methods.

10. Lack of Penetration Defect: Insufficient penetration may occur at the bottom of the weld joint if the pin is not long enough.

11. Hole Initiation: Increased travel speed can lead to hole initiation near the bottom of the weld joint due to insufficient material flow.

12. Processing Temperature: The processing temperature for FSW of different materials varies; for example, titanium alloys may require temperatures between 700 to 950 °C, while for steel, it's 600 to 875 °C.

13. Limited Formability: Studying the stability of both the formability and microstructure of FSW joints is rare, making forming FSW welds challenging due to limited formability [20] [21] [22] [23].

I.3. Parameters of FSW

The Friction Stir Welding (FSW) process is a complex physical phenomenon influenced by various interconnected variables that directly or indirectly impact weld quality and performance (Table I-4). These variables fall into categories such as tool-related parameters, joint design factors, machine (welding) parameters, and other miscellaneous factors. Tool-related parameters encompass tool geometry and the material type used. Joint design involves considerations such as the type of joint, including butt, lap, or fillet joints. Machine parameters include tool rotation speed (ω , rpm), transverse speed (V , mm/min), axial force (insertion depth), tool tilt (angle of the spindle), and the offset from the center of the joint. Additional factors influencing weld quality include the initial material temperature (pre-heat or cooling) and the cooling rate.

As previously mentioned, the FSW tool serves the dual purposes of heating the workpiece and facilitating material movement. The tool's geometry significantly affects heat generation, plastic flow, and the uniformity of the weld joint. The shoulder, responsible for generating heat through friction, also prevents plasticized material from escaping the workpiece. Key considerations for the tool include wear resistance, high fracture toughness, and machinability. The shoulder's design, particularly whether it is flat, concave, or convex, and its diameter, plays a crucial role. A concave surface tends to create moderate flash and some defects, while a convex surface minimizes flash and defects. The pin's critical role in FSW lies in material flow and, consequently, welding speeds. Factors influencing the pin include probe length, probe shape (tapered, cylindrical, square, triangular, tri-sided, threaded) [2].

Table I-4 - FSW Process Parameters [2]

Process Parameters
Rotational speed (RPM)
Welding (traverse) speed (mm/min)
Pin length (mm)
Tool shoulder diameter (mm)
Axial force (kN)
Tilt Angle
Pin diameter (mm)
Shoulder diameter (mm)
D/d Ratio of Tool
Tool materials
Tool profile

Several parameters play a crucial role in the friction stir welding process, influencing the quality of the weld (Table I-5). These include:

1. Rotational Speed (ω , rpm): Direction: Clockwise or counterclockwise.
2. Travel Speed (v , mm/min): Measured along the line of the welding joint.
3. Tilt Angle:
 - Ensures the tool shoulder holds the material by the threaded pin from front to back.
 - Influences weld appearance and thinning.
 - Optimal tilt angle is typically between 1 and 3°.

4. Downward Axial Force: Applied by the machine, the force of the tool shoulder on the workpiece.

Achieving optimal welding in friction stir welding is challenging due to the dependence on controlling these four factors. Researchers emphasize the importance of balancing these parameters. For instance, low rotational speeds with high axial pressure result in a high rate of deformation and shorter weld times. Conversely, high rotational speeds with low axial pressure lead to a relatively low rate of deformation. The ideal friction time for welding two sheets depends on factors like dimensions, material composition, rotational speed, and friction pressure. Inadequate friction time can result in irregular heating distribution and weak bond strength, while excessive friction time reduces productivity and promotes coarse grain structure [21].

Table I-5 - Main process parameters in friction stir welding [10] [24].

Parameters	Effects
Rotational speed	Friction heat, “stirring,” oxide layer breaking and mixing of materials
Tilting angle	The appearance of the weld, thinning
Welding speed	Appearance, heat control
Down force	Friction heat, maintaining contact conditions.

I.4. Torque in FSW

Torque plays a crucial role in FSW process, influencing temperature in the stir zone, material state, weld quality, and is fundamental for process control and tool design, along with axial force. Researchers have established a strong correlation between torque and temperature, emphasizing its significance in understanding the FSW process. Torque is considered in equipment selection and process control, and its behavior is instrumental in detecting different phases of FSW.

Several experimental studies have explored torque during FSW (Table I-6), investigating its behavior and the influence of key process variables. The primary factors affecting torque include welding and rotational speeds, tool geometry, plunging depth, and material properties. Observations indicate that torque decreases with higher rotational speeds and increases with higher welding speeds. The rotational speed tends to have a more significant impact on torque than welding speed. While the influence of welding speed is relatively smaller, the interaction of both speeds affects torque behavior. Tool geometry also exhibits a strong influence on torque, as evidenced by various experimental studies.

Various models have been developed to describe torque behavior in the FSW process (Table I-7). Khandkar et al. [25] described torque as a function of the interfaces between the tool and material, using it to predict temperature distribution. Schmidt et al. [26] considered different contact conditions in the tool-material interface to describe torque, incorporating sticking, sliding, and partial sticking/sliding conditions. Pew et al. [27] utilized statistical models to describe torque behavior for specific aluminum alloys, incorporating tool depth and rotational and welding speeds as variables.

Table I-6 - Main experimental torque studies in FSW.

Year	Authors	Sheet material	Tool material	Welding speed (mm/min)	Rotational speed (rpm)
2005	Yan et al. [28]	AA2524-T351	-	126.6	150 – 800
2007	Long et al. [29]	AA5083-O AA2219-T87 AA7050-T751	H13	102	Variable, with increment rate: 1.4 rpm/mm
2007	Pew et al. [27]	AA7075-T7351 AA5083-H32 AA2024-T3	H13	127 – 279 127 – 279 51 – 152	200 – 800 200 – 700 175 – 350
2010	Upadhyay et al. [30]	AA7050-T7451	Shoulder: H13 Pin: MP-159	102 – 612	150 – 1000
2010	Cui et al. [31]	AA356	H13	28 – 450	63 – 1400
2012	Leitao et al. [32]	AA5083-H111	–	50 – 700	300 – 1100
2012	Kumar et al. [33]	AA6082-T6 AA5083-H112	H13	80, 120	420, 500
2013	Su et al. [34]	AA2024	–	40 – 120	600 – 1000
2017	Quintana and Silveira [35]	AA5052-H34	H13	100 – 300	600 – 1500

Table I-7 - Main torque models for FSW reported in the literature.

Year	Author	Sheet material	Tool material	Model type
2003	Khandkar et al. [25]	AA6061-T651	–	Analytical
2004	Schmidt et al. [26]	AA2024-T3	Steel	Analytical
2007	Pew et al. [27]	AA7075-T7351 AA5083-H32 AA2024-T3	H13	Experimental
2009	Arora et al. [36]	AA2524	–	Numerical
2010	Cui et al. [31]	AA356	H13	Experimental
2014	Zhang et al. [37]	AA6061-T6	–	Numerical

I.5. conventional FSW machines and power source

I.5.1 FSW machines

Three types of machines are identified in the literature as viable for performing Friction Stir Welding (FSW). These include:

1. Conventional Machine Tools: This category encompasses machines typically used for milling operations [38] [39]. They are adapted or repurposed for FSW processes.

2. Dedicated FSW Machines or Custom-Built Machines: Specifically designed machines tailored for FSW purposes fall into this category [40]. These machines are constructed with the sole intention of facilitating the FSW process efficiently.

3. Industrial Robots: The use of industrial robots for FSW has been explored, providing an automated and flexible approach to welding [41] [42] [43]. Industrial robots are adapted or configured to execute FSW operations, offering versatility in handling various joint configurations.

These machine types cater to different needs and preferences, providing options based on the specific requirements of the FSW application.

1.5.1.1 Conventional machine tools

The Friction Stir Welding (FSW) process shares fundamental operational principles with other technological manufacturing processes such as machining, deburring, grinding, and drilling. Essentially, these processes involve moving a rotating tool through a workpiece, resulting in material displacement within the workpiece. While conventional machine tools like milling machines can be adapted for FSW, it's crucial to consider the increased loads generated during the FSW process compared to other manufacturing operations [44]. The higher loads necessitate strengthening conventional machine tools to enhance their load-bearing capacity and stiffness [45] [46].

Modifications to conventional machine tools for FSW can occur on various levels, including structural, flexibility, decision-making, and sensing aspects [60]. Structural modifications involve reinforcing the equipment, such as replacing components like ways, guides, rails, motors, and spindles to make it more robust. Flexibility can be increased by integrating additional motors that provide extra degrees of freedom to the equipment. Given the substantial loads in FSW, many solutions implement force control to prevent equipment damage, ensure human safety, and achieve high-quality welds. Decision-making capabilities can be enhanced to enable simultaneous movement in multiple directions, and the machine can be equipped with various sensors to collect data for embedded control solutions.

Conventional machine tools modified for FSW find popularity due to their widespread use in industries for machining purposes, making them readily available and well-understood. These modified machines are recommended for prototyping, small series production of various workpiece sizes and thicknesses, applications requiring high stiffness, and single- or multi-axis

applications. While these machines offer versatility, it's essential to note that they may exhibit lower production performance. An example of a modified milling machine for FSW is illustrated in Fig. I-2.

I.5.1.2 Dedicated FSW machines

Dedicated FSW machines are known for their superior load capacity, stiffness, accuracy, and availability compared to other types of FSW equipment [40]. These machines come in various configurations, offering different levels of flexibility. Custom-built machines, a subset of dedicated FSW machines, are designed specifically to meet unique product requirements, such as the fabrication of ship deck components. Requalifying these machines for different applications can be challenging in many cases, and their relative cost tends to increase with added flexibility. While dedicated FSW machines are relatively expensive, they are well-suited for high-series production of identical parts, including long or small workpieces, thick or thin workpieces, and applications demanding high stiffness or involving single- or multi-axis movements. Custom-built machines may be considered when alternative solutions are unavailable or prohibitively expensive. Fig. I-13 provides an example of a dedicated FSW machine.

For welding high-temperature materials like steel, stainless steel, titanium, nickel alloys, etc., dedicated FSW machines are particularly recommended due to their robustness and structural stiffness, providing the necessary load support.

There is a growing interest in the development of portable FSW machines, offering the potential for applications in remote locations, in-situ repairs, and component additions to large structures. Research on FSW tools, mechanisms, and loads has been conducted to facilitate the development of portable machines. The main challenges to portability include reducing the loads required for FSW and minimizing equipment weight. While there have been studies on portable FSW, as of now, there are no commercially available systems. The increasing popularity of mobile robots in recent years may contribute to the development of effective portable FSW solutions [47] [48].

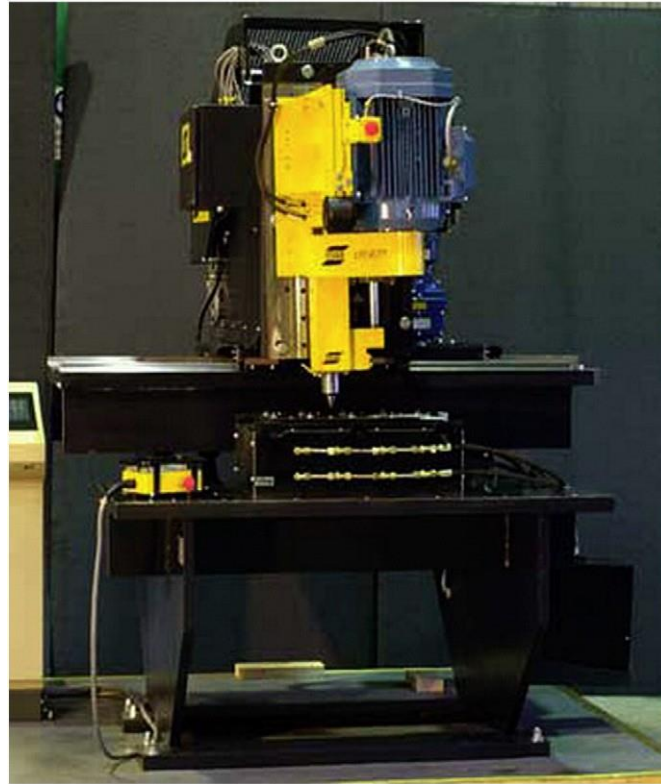


Fig. I-13 - dedicated FSW machine - FSW Legio™ [54]

I.5.1.3 Robotic FSW machines

A third category of machines introduced in FSW for metals involves robotic machines, specifically industrial robots. For several years, the limitations of low load capability (payload) and low stiffness in industrial robots hindered their use in FSW applications. However, recent advancements have resulted in the development and release of robotic equipment with high payloads, capable of performing FSW on materials with thin-to-moderate thickness. Robotic machines offer flexibility and process automation, leading to significant improvements in productivity. For example, in a workpiece requiring welds on multiple sides, a robotic solution allows welding on various sides in a single setup, reducing non-value-added materials handling and improving productivity, thereby lowering welding costs. Applications involving 3D welding paths have become more attractive and feasible with the use of robotic systems for FSW. Many such applications only require an industrial robot with five degrees of freedom (DOF), making the use of industrial robots more appealing, as most common robots in the market possess five or six DOF.

Robotic-based solutions are available in two main categories:

- Articulated arm robots [41] [42] [49]

- Parallel-kinematic robots [50]

Articulated arm robots exhibit high repeatability and flexibility but lower accuracy, especially under high loads. When compared to dedicated FSW machines, articulated robots generally offer higher flexibility and decision-making capabilities at a significantly lower cost. However, they have relatively low stiffness and moderate load capacity, limiting their application. Despite their flexibility and cost-effectiveness, they may have a restricted range of materials for FSW due to the high loads required for welding certain materials. As a general guideline, the most robust robots can weld up to 6 mm thick aluminum material, with their capability in higher-melting-point materials being somewhat reduced. Drawbacks include high compliance, leading to process stability issues [49] [51] [52].

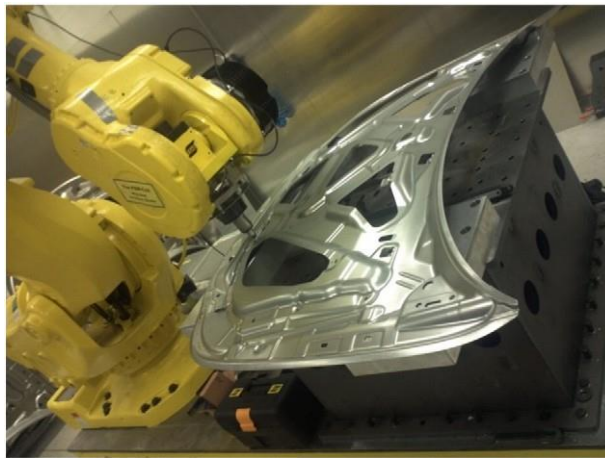


Fig. I-14 - robotic FSW of a multi welding part [186].

The use of articulated arm robots is recommended for various applications, including:

- Relatively thin materials
- Applications requiring multiple welds that would otherwise need multiple setups
- Dissimilar-thickness butt welds (tailor-welded blanks), which require both a travel angle and a work angle, making robots ideal for flexibility
- Applications where multi-axis capability is required, involving different tool orientations
- Higher work volume applications where productivity is crucial.

Marcotte and Abeele [49] successfully developed a robotic FSW system based on an articulated arm robot, reporting the production of aluminum welds with 1D, 2D, and 3D welding paths Fig. I-15 illustrates an articulated arm robot capable of performing FSW with 1D, 2D, and 3D

welding paths. Additionally, the use of articulated arm robots for friction stir spot welding (FSSW), a variant process of FSW, has been reported as feasible and appealing [53].

The other basic robotic configuration is the parallel-kinematic robot. This type of robot supports higher loads and exhibits significantly higher stiffness than articulated arm robots. However, they can be notably more expensive, and their work volume is considerably smaller than that of articulated arm robots, along with a restricted range of orientation. A typical example of this family of robots is the Tricept [54] [55]. Parallel-kinematic robots are suitable for applications where:

- The work volume of the workpieces is relatively small
- The workpiece can be welded near or close to the horizontal plane
- There are higher load or stiffness requirements.

Welding small, thin, high-temperature materials is also possible with this type of robot. Shi et al. [56] developed a 3-PRS (Prismatic, Revolute, and Spherical joint) parallel mechanism to perform FSW with 3D welding paths. Table 3 provides a comparative analysis among the different machines.

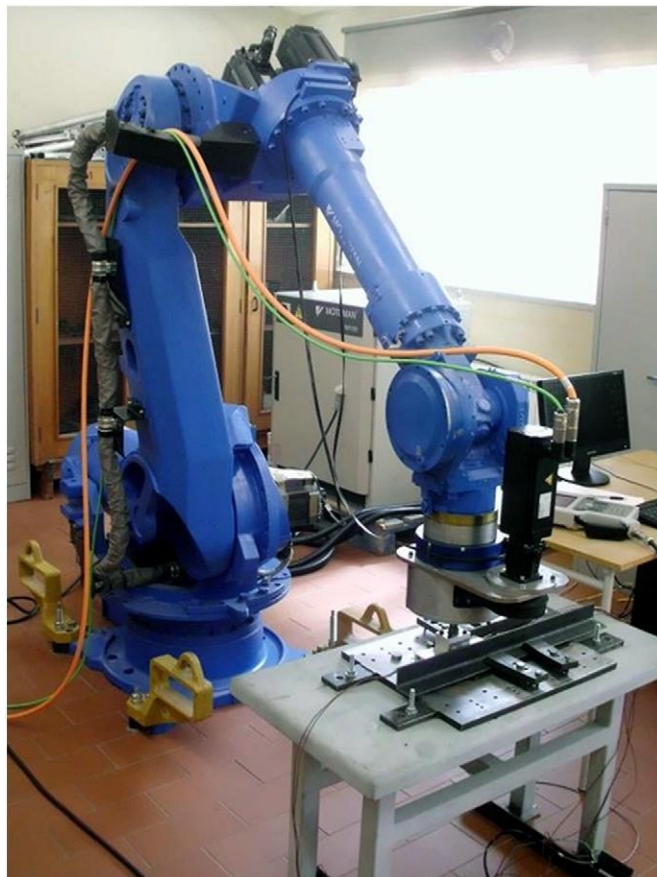


Fig. I-15 - articulated arm robot performing FSW at the university of Coimbra [54].

Table I-8 bellow presents a comparison between the different types of FSW equipment.

Table I-8 - FSW equipment features [54].

Characteristics Equipment				
↓	Milling machine	FSW machine	Parallel robot	Articulated robot
Flexibility	Low	Low/medium	High	High
Cost	Medium	High	High	Low
Stiffness	High	High	High	Low
Work volume	Medium	Medium	Low	High
Setup time	Low	High	Medium	Medium
Number of programming options	Low	Medium	High	High
Capacity to produce complex welds	Low	Medium	High	High
Control type	Motion	Motion/force	Motion	Motion

I.5.2 Electricity as a main power source

The machines examined in this section of the thesis, dedicated to Friction Stir Welding (FSW), encompass a spectrum of technologies catering to diverse welding requirements. Amidst this diversity, a unifying factor across all these machines is their reliance on various forms of electrical power as a fundamental energy source. This reliance on electrical power is not merely a coincidental attribute; it reflects a deliberate design choice and is deeply embedded in the operational principles of each machine.

In the realm of FSW, the adaptation of conventional machine tools involves the modification of milling machines, which inherently rely on electric motors for their rotary and linear motions. These modifications include structural enhancements, such as replacing components like motors, spindles, guides, and rails, all of which are crucial electrical elements contributing to the robustness and efficiency of the machine. Flexibility improvements, achieved by integrating additional electric motors for extra degrees of freedom, further emphasize the centrality of electrical power in tailoring conventional machines for FSW applications.

Dedicated FSW machines, renowned for their load capacity and stiffness, are custom-built to exact specifications, often involving advanced control systems powered by electrical energy. The structural and operational enhancements that make these machines superior are intricately tied to the use of electrically driven components, ensuring precision and efficiency in executing FSW. The reliance on electrical power is particularly evident when these machines are employed for welding high-temperature materials like steel, stainless steel, titanium, and nickel alloys, where robustness and structural stiffness are essential for withstanding the high loads encountered during the process.

Robotic FSW machines, a cutting-edge category, further underscore the pervasive use of electrical power in this domain. Whether articulated arm robots with high repeatability but lower accuracy, or parallel-kinematic robots with increased load-bearing capabilities, both configurations rely heavily on sophisticated electrical systems. These robots, equipped with electric motors for movement across multiple axes, showcase the integral role of electrical power in achieving the precision and flexibility demanded by FSW processes. The ability to execute 3D welding paths and perform automated, complex welding tasks is facilitated by the intricate interplay of electrical components within these robotic systems.

In essence, the omnipresence of electrical power as the primary energy source for these FSW machines is a testament to the technological landscape's electrification and the inherent advantages offered by electrically driven systems. The efficiency, precision, and adaptability afforded by electrical power contribute significantly to the advancement and success of Friction Stir Welding technologies. As research and development in FSW continue, this reliance on electrical power is likely to persist, reflecting a broader trend in the industrial landscape towards electrification and automation for enhanced performance and efficiency.

I.6. The concept of Pneumatic source in FSW

Friction stir welding (FSW) machines, whether dedicated, robotic, or milling machines, traditionally utilize electrical motors to drive the movement of the FSW tool. These machines, categorized as heavy and stationary equipment, contribute to one of the inherent limitations of FSW – its lack of portability. Recognizing this drawback, researchers have been fervently

exploring solutions to develop a portable FSW machine over the years, as evidenced by various studies. Despite these efforts, historical conceptions of portable FSW machines predominantly relied on electrical power sources.

A notable departure from this trend emerged in the recent work by Al-Sabur et al [57], who introduced a groundbreaking welding system that operates on a pneumatic power source. This innovative system is characterized by its compact design, consisting of a fixation table with an anvil serving as the backplate for the sheets to be welded, a rotary pneumatic tool, and an air compressor as the primary power source for driving the rotary pneumatic tool. This departure from traditional electrical power sources represents a significant advancement in FSW technology, offering newfound portability and flexibility to the welding process.

The Al-Sabur et al. system addresses the long-standing challenge of FSW machine portability, opening avenues for applications in diverse environments and scenarios. This shift towards pneumatic power not only reduces the weight and bulkiness associated with traditional electrical systems but also facilitates on-site welding in locations where a stable electric power supply may be challenging to access. The incorporation of a pneumatic power source in FSW machines marks a pivotal step towards overcoming the historical constraints of non-portability, underscoring the importance of exploring alternative energy sources to enhance the versatility and applicability of friction stir welding technology.

Fig. I-16 shows the setup proposed by Al Sabur and al. [57].

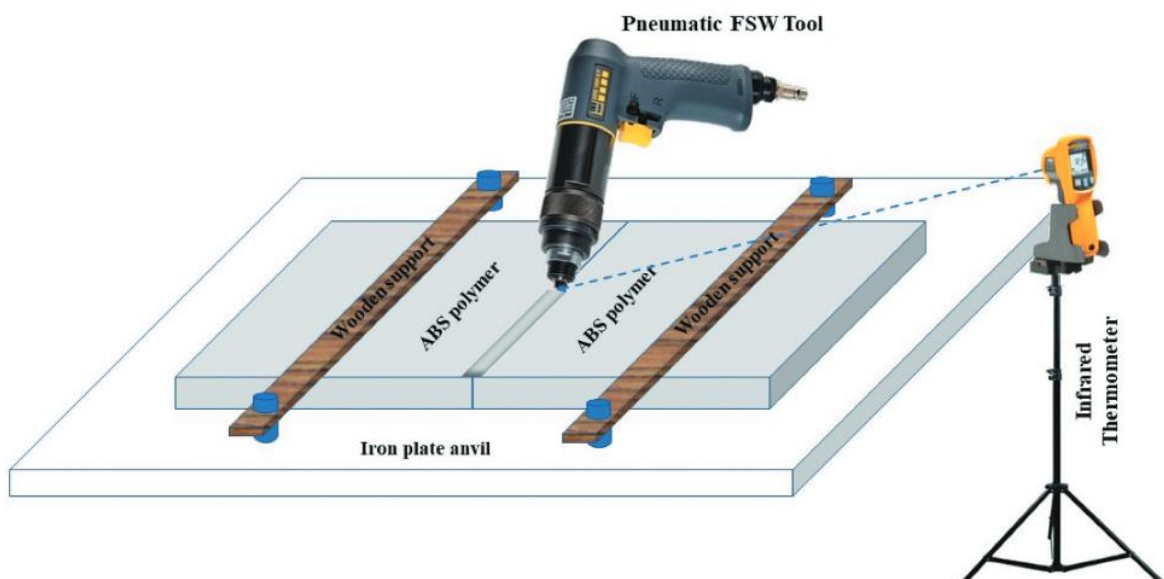


Fig. I-16 - pneumatic FSW setup [57].

I.6.1 potential advantages of a pneumatic source in FSW

The incorporation of a pneumatic power source into friction stir welding (FSW) technology offers a compelling avenue for innovation, unlocking a myriad of potential benefits. Notably, this shift holds the promise of ushering in a new era of more compact FSW equipment. Air motors, ubiquitous in pneumatic systems, exhibit a distinct advantage in size and weight compared to their electric counterparts. This downsizing potential could pave the way for the development of highly portable and efficient FSW machines, introducing greater flexibility and accessibility across a spectrum of applications.

Furthermore, the adoption of pneumatic power introduces a novel dimension of mobility to FSW setups. With the utilization of mobile air compressors, FSW machines gain the ability to operate in diverse locations, presenting a level of versatility often unattainable with traditional electric-powered systems. This newfound mobility proves particularly advantageous in scenarios necessitating on-site welding, where access to a stable power supply is constrained. The transition to pneumatic sources also holds the potential to mitigate risks in hazardous environments by eliminating dependence on electric power, thereby bolstering safety protocols in FSW operations.

Nonetheless, like any pioneering technological advancement, there remain areas that necessitate further exploration and optimization. Al-Sabur et al., trailblazers in the integration of pneumatic power sources, have identified several gaps warranting attention. One critical aspect involves the establishment of clear criteria for selecting pneumatic rotary tools, ensuring their alignment with the specific demands of FSW applications. Another area ripe for improvement is the identification of criteria for selecting an air compressor suitable for FSW operations, taking into account factors such as pressure, volume, and portability.

Additionally, the lack of a well-defined system for fixing or controlling the movement of the rotary tool during welding poses a challenge. The movement was previously ensured manually, introducing considerable instability and inconsistency to the welding operation. Addressing this gap is crucial for attaining precision and control in Friction Stir Welding (FSW) processes, ultimately enhancing the overall efficiency and reliability of the technology. In summary, although the integration of pneumatic power sources into FSW technology holds

immense promise, ongoing research is essential to refine and optimize various aspects, ensuring a comprehensive and effective application of this innovative approach in the field of welding technology.

Moving on to the thesis, it endeavors to fill a pivotal gap in the current understanding of the friction stir welding (FSW) process. The primary goal is to develop a comprehensive numerical model capable of predicting the torque requirements inherent in FSW. The model intricately crafted harvesting the power of machine learning's artificial neural networks by considering various FSW parameters, places particular emphasis on the rotational speed – a user-defined input parameter crucial to the welding process. By integrating rotational speed and torque as input and predicted outcome parameters, respectively, the model facilitates the calculation of the motor power required for a given FSW scenario. This predictive capability becomes instrumental in making well-informed decisions pertaining to the selection of an appropriate pneumatic motor for a specific FSW process.

The inclusion of rotational speed as a key input parameter is pivotal, given its significant role in influencing torque during the FSW process. The numerical model's capacity to account for this parameter, in conjunction with others, provides a holistic understanding of torque requirements, offering a more nuanced and accurate prediction. By translating the predicted torque into motor power requirements, this model contributes significantly to the optimization of the FSW process, aiding in the selection of an optimum pneumatic motor based on the specific demands of the welding operation.

In summation, this thesis endeavors to bridge existing gaps in knowledge by presenting a numerical model that seamlessly integrates various FSW parameters, with a specific focus on rotational speed, to predict torque requirements. The resulting insights empower decision-makers to make informed choices regarding the selection of pneumatic motors, ultimately contributing to the overall efficiency and effectiveness of the FSW process.

I.7. Conclusion

This chapter has systematically explored the principles and potential of friction stir welding (FSW), a unique joining process that utilizes a non-consumable tool to generate frictional heat and plastically deform materials without melting. We have critically examined the core

elements of FSW, including its operational mechanisms, tool configuration, joint design considerations, and its distinct advantages and limitations compared to traditional fusion welding methods.

Furthermore, we have analyzed the influence of crucial FSW parameters on the process and final joint quality. This analysis highlighted the significance of tool rotational speed, travel speed, axial load, and material properties in controlling heat generation, material flow, and ultimately, the strength and integrity of the welded joint.

The exploration then delved into the practical aspect of FSW by reviewing conventional FSW machines and their dedicated power sources. This section focused on their design configurations, operational characteristics, and potential limitations. Notably, the chapter also introduced the emerging concept of pneumatic power sources, recognizing their potential to offer improved energy efficiency and process control in future FSW applications.

In conclusion, this chapter has established a comprehensive foundation for understanding the fundamentals of FSW. By dissecting the process, its parameters, equipment, and potential advancements, we have demystified this transformative technology and equipped readers with the necessary knowledge to navigate its intricacies and leverage its vast potential across diverse industrial applications. However, further research and development are necessary to optimize parameters, expand material compatibility, and explore innovative tool designs to fully unlock the capabilities of this dynamic joining technology.

CHAPTER II

Chapter II - METHODOLOGY

II.1. Introduction

In the previous chapter, we delved into the intricacies of Friction Stir Welding (FSW), elucidating its fundamental principles, machine configurations, and the emerging concept of utilizing pneumatic sources for enhanced efficiency. However, amidst the exploration of FSW's potential, a critical gap was identified, prompting the need for further investigation and intervention, which forms the cornerstone of this thesis.

This chapter marks a pivotal transition towards numerical and parametric methodology, serving as the bedrock for our comprehensive study of the FSW phenomenon. Our approach integrates advanced techniques from the realm of Machine Learning and Deep Learning, namely Artificial Neural Networks (ANN), Random Forest (RF), and Polynomial Regression. These sophisticated methodologies are employed to construct predictive models capable of forecasting torque in FSW, leveraging ten pivotal input parameters that intricately influence the welding process.

Beyond mere prediction, our endeavor extends to a parametric analysis facilitated by the innovative Shapley Additive exPlanations framework. This analytical tool allows for the classification of each variable's significance in shaping the outcomes of our predictive models. Through this elucidation, we gain invaluable insights into the nuanced interplay between input parameters and torque output in FSW.

However, the pursuit of optimization transcends mere prediction and analysis. To unearth an optimum parameter configuration that minimize energy consumption in FSW operations, we employ a metaheuristic algorithm known as the Pelican Optimization Algorithm. This iterative optimization technique emulates the adaptive foraging behavior of pelicans, strategically navigating the expansive search space to identify parameter sets that yield optimum performance.

Central to our methodology is the quest to uncover not only the requisite torque and rotational speed (RS) for welding various materials but also to ascertain an optimum pneumatic

motor or hand tool suited for each material's specific requirements. This endeavor underscores our commitment to bridging theoretical insights with practical implications, thereby facilitating informed decision-making in FSW operations.

In this chapter, we provide a comprehensive elucidation of the methodologies employed in our thesis, laying the groundwork for a systematic exploration of FSW dynamics and the quest for optimized pneumatic welding solutions.

II.2. Background of study methodology

II.2.1 Deep learning

Deep learning, an integral facet of machine learning (ML) methodologies, operates within complex hierarchical structures aimed at discerning intricate data representations [58]. These approaches encompass a spectrum of learning modes, including supervised, semi-supervised, and unsupervised paradigms. In supervised learning, the focus lies on classification tasks, whereas unsupervised learning endeavors to cluster similar features or characteristics [59]. The essence of deep learning lies in its innate capacity to extract features implicitly across multiple layers, signifying the profound "depth" of its network architecture (Fig. II-1). Notably, deep learning algorithms exhibit versatility, seamlessly adapting to both supervised and unsupervised learning scenarios. In unsupervised learning, where unlabeled data typically outweighs labeled data, deep learning emerges as particularly advantageous. By discerning optimal features, deep learning offers a comprehensive end-to-end solution [60] [59] [61].

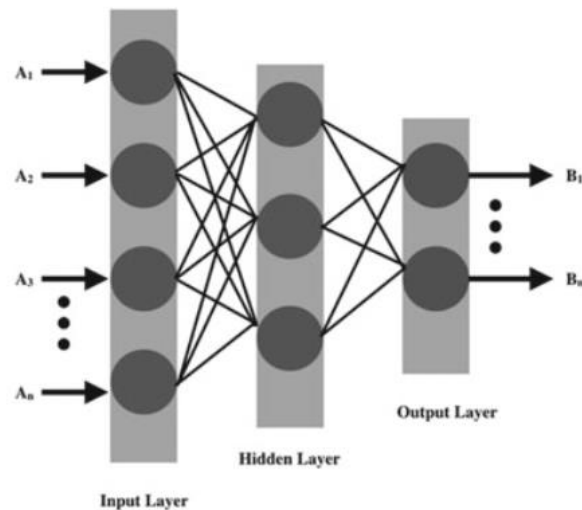


Fig. II-1 - graphical representation of neural networks [187].

II.2.1.1 Classes of deep learning

II.2.1.1.1 Generative Deep Architectures

Generative Deep Architectures represent sophisticated neural network structures aimed at discerning high-order properties within visible or observed data, facilitating pattern analysis and characterization of statistical distributions associated with linked classes and observed data. This architecture can transition into a discriminative framework through the application of Bayes' rule [60].

II.2.1.1.2 Discriminative Deep Architectures

True to their name, Discriminative Deep Architectures directly empower pattern analysis by distinguishing posterior divisions of various classes based solely on observed data. Notably, Convolutional Neural Networks (CNNs) serve as a prime example of this architecture type [60].

II.2.1.1.3 Hybrid Deep Architectures

Hybrid Deep Architectures signify a fusion of generative and discriminative deep architectures, aiming to discriminate effectively while leveraging the strengths of generative architectures through advanced optimization techniques [60].

II.2.1.2 Deep learning techniques:

II.2.1.2.1 Deep Neural Network (DNN)

The Deep Neural Network (DNN) stands as a fundamental example of deep learning algorithms, comprising an artificial neural network (ANN) with numerous input and output layers. Distinguished by its depth derived from multiple internal layers, the DNN enables implicit feature extraction from data, optimizing the conversion of input into output, regardless of linear or nonlinear relationships. Operating as feedforward networks, DNNs transmit data from input to output layers without feedback loops, utilizing vast datasets and training parameters such as learning rate, size, and initial weights [62].

II.2.1.2.2 Convolutional Neural Network (CNN)

Convolutional Neural Networks (CNNs) are another crucial algorithm within deep learning, aligned with the principles of traditional neural networks. Particularly prominent in tasks like speech recognition and computer vision, CNNs exhibit depth and operate as feedforward networks [60].

II.2.1.2.3 Recurrent Neural Networks (RNN)

Recurrent Neural Networks (RNNs) represent a distinctive class where data can flow bidirectionally, finding notable applications in language modeling [60].

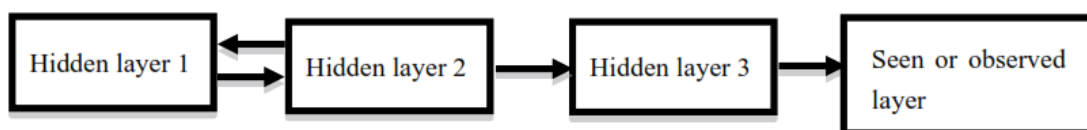


Fig. II-2 - graphical representation of deep belief network [63].

Table II-1 - Difference between machine learning and deep learning [63]

Machine learning	Deep learning
Machine learning algorithms enable the machine to make decisions	Deep neural networks work on the principal of artificial neural networks (ANNs)
ML algorithms work on less amount of data	Deep learning techniques require a large amount of data to learn
In ML, features need to be identified	In DL, the machine learns the features automatically from the given data
The problem solved by machine learning algorithms is divided into small parts, and then, each part is solved individually	Problems in deep learning are solved by neural networks

II.2.1.2.4 Deep Belief Network (DBN)

Deep Belief Network (DBN) stands as a profound component within machine learning (ML), representing a deep neural network comprised of multiple layers featuring hidden units. While connections exist between layers, no direct connections are present between units within each layer. Often referred to as a generative graphical model, DBN is characterized by its composition of unsupervised, simple networks such as auto-encoders or restricted Boltzmann machines (RBMs). Notably, each sub-network's hidden layer serves as the visible layer for the subsequent one [60] [64] (Fig. II-2 and Table II-1).

II.2.1.3 Metaheuristic algorithms: A methodology of search and optimization for parameters

The term "optimization" denotes the process of determining the best values for various system characteristics to complete system design at the lowest possible cost [65] [66]. Real-world applications in artificial intelligence and machine learning are typically unconstrained or discrete [67]. Conventional optimization methods face challenges in finding optimal solutions due to drawbacks like convergence to local optima and an undefined search space [68]. Various stochastic methods have been developed to address these limitations and enhance system performance, minimizing computation costs [69] [70] [71]. Optimization problems span various scientific subjects [72] [73].

Stochastic algorithms, such as metaheuristic algorithms, optimize problems randomly, benefiting from higher avoidance of local optima compared to conventional optimization

algorithms [74] [75]. Metaheuristic algorithms, which guide subordinate heuristics iteratively, combine different concepts intelligently for exploring and exploiting the search space [76]. They are problem-independent algorithms, seeking approximate optimal solutions to complex and nonlinear optimization problems [77].

All metaheuristic algorithms consist of two main components, sharing characteristics like the search process divided into intensification (exploitation) and diversification (exploration) phases. Exploitation involves using local information to generate new, better solutions, often leading to high convergence rates but potentially getting trapped in local optima [78]. In contrast, exploration produces diverse solutions, avoiding local modes and facilitating global-scale search but at the cost of slow convergence and increased computational effort [79].

A proper equilibrium between exploration and exploitation is crucial for an algorithm's performance. Overemphasis on either can result in suboptimal outcomes. To address these challenges, reviews and surveys about metaheuristic algorithms have been selected from the literature [80]. Hybridizing optimization algorithms can overcome issues like convergence speed [80].

In the realms of science and engineering, the solution of numerous optimization tasks poses considerable challenges, prompting a contemporary focus on the application of metaheuristic (MH) algorithms. The spotlight on metaheuristics has intensified in recent years, driven by the profound inspiration drawn from nature. The self-organization property observed in natural systems, such as the collective intelligence emerging from swarms of birds or colonies of insects, serves as a fundamental muse for the development of innovative problem-solving approaches [81].

Nature, with its inherent self-organizing principles, has demonstrated the remarkable ability of swarms or colonies, despite individual entities possessing minimal competence, to achieve intricate and essential activities vital for their survival. This realization has fueled the design and implementation of numerous MH algorithms that emulate and draw inspiration from these natural phenomena. The utilization of metaheuristics, rooted in the collective and adaptive behaviors observed in nature, offers a promising avenue for addressing complex optimization challenges in diverse scientific and engineering domains [81].

II.2.1.4 Working process of metaheuristics

In this section, we delve into the intricate design process and methodology of Metaheuristic Algorithms (MHAs), presenting a comprehensive overview of their general framework. While

articulating the fundamental steps or tasks inherent in MH algorithms poses a considerable challenge, we strive to accomplish this by examining past advancements and envisioning potential future improvements geared towards augmenting their performance. Fig. II-3 provides a visual representation of the general framework employed by MH algorithms, highlighting that, despite employing diverse search methodologies, they largely adhere to a common structure. The essential tasks within MH algorithms are outlined below:

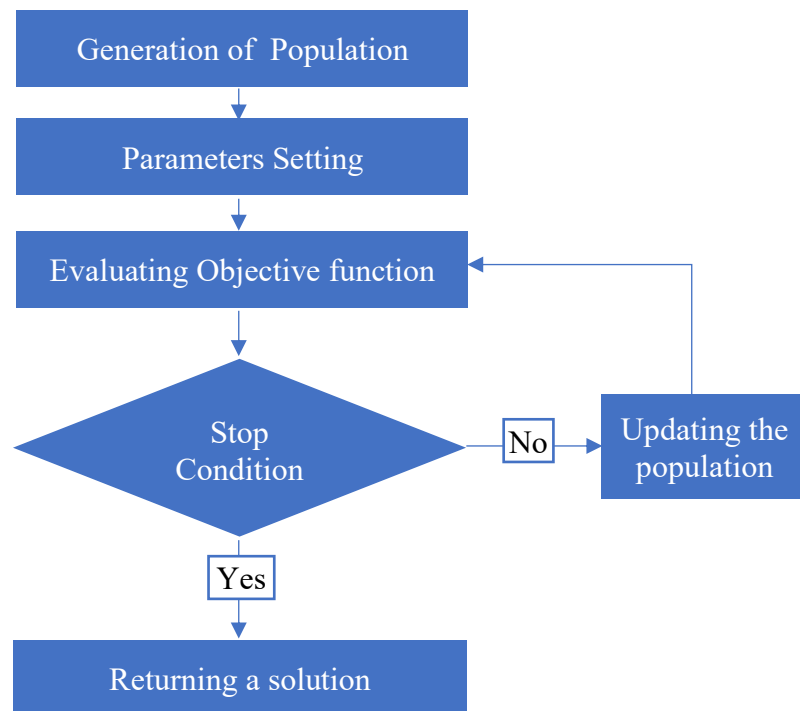


Fig. II-3 - MH algorithms Working process.

II.2.1.4.1 Initialization

The initiation phase, typically executed randomly, significantly influences diversity and convergence in algorithm operation. Recognizing the pivotal role of initialization, researchers explore methods enhancing population diversity to ensure optimal solutions remain unaffected by starting decisions. While uniform distributions are commonly employed, their suitability varies across applications. Alternative initialization techniques, such as chaotic initialization, sequence-based deterministic initialization, opposition-based learning, and Latin hypercube sampling, offer diverse strategies [82].

II.2.1.4.2 Parameter Settings

Initial parameter values exert considerable influence on solution quality, demanding optimal sets for performance metrics evaluation. As most metaheuristic algorithms are parameterized,

the process of determining the best parameter set, known as parameter optimization or tuning, significantly impacts processing time and result quality. Task 2 encompasses critical parameters like the maximum number of iterations, error rate, and population size, emphasizing their importance in achieving optimal outcomes.

II.2.1.4.3 Evaluate Objective Function

In optimization problems, the objective function is represented by test functions, frequently benchmarked in publications to assess metaheuristic algorithm effectiveness. The absence of a standard test suite prompts researchers to use diverse test functions, complicating overall algorithm robustness evaluation. Utilizing a diverse set of functions and sensitivity parameters, such as dimensionality increase, enhances the assessment of newly developed algorithms.

II.2.1.4.4 Stop Conditions

A primary challenge in metaheuristics is the lack of effective termination criteria. Many algorithms terminate after a predefined number of iterations, potentially leading to premature conclusions or unnecessary prolongation. Combining the maximum number of iterations with specified tolerance or error rate remains an effective stopping criterion, aiming for a balance between computational efficiency and solution optimality.

II.2.1.4.5 Update and Move Agents

This task involves two subtasks: update and move. If stop conditions are unmet, the algorithm updates and performs the move task. "Update" refers to the meta-operation enabling algorithms to progress to the next iteration (I+1), improving results. The move subtask, often performed randomly, expands the search space, emphasizing the iterative nature of the update and move agent tasks. The repetition of these tasks continues until the set stop criteria are satisfied.

II.2.1.5 Types of Metaheuristics

In the literature, metaheuristic (MH) algorithms can be classified based on several criteria: population-based versus single-point search, nature-inspired versus non-nature-inspired, static objective versus dynamic objective function, and methods employing memory versus memoryless methods, as well as the utilization of various neighborhoods versus a single neighborhood. Consequently, each algorithm can be categorized into one of the following groups, depending on its source of inspiration:

II.2.1.5.1 Evolutionary-based algorithms (EAs)

Evolutionary-based algorithms (EAs) represent the most prevalent and oldest type of metaheuristic, drawing inspiration from the principle of survival of the fittest observed in natural evolution. EAs initiate the optimization process with randomly generated solutions, which, over time and iterations, undergo improvement in fitness value through the creation of new solutions and the elimination of less fit ones. These algorithms demonstrate effectiveness without relying on specific assumptions about the underlying fitness landscape, often successfully identifying optimal or near-optimal solutions.

II.2.1.5.2 Swarm intelligence-based algorithms (SI)

Swarm Intelligence (SI) Algorithms constitute the most prominent class of metaheuristics, aiming to model the cooperative, adaptive, cognitive, and concerted gregarious behavior observed in natural flocks or communities. These communities encompass various entities such as schools of fish, flocks of birds, herds of mammals, colonies of insects like bees, and diverse flocks of other organism species. Researchers are increasingly drawn to this category of metaheuristics, which competes significantly with Evolutionary-based Algorithms (EAs).

II.2.1.5.3 Natural science-based algorithms (NSAs)

NSAs replicate specific chemical principles or physical processes found in nature, encompassing phenomena like gravity, electrical charges, ion motion, river systems, and more.

II.2.1.5.4 Human-based algorithms (HBAs)

Human-Based Algorithms (HBAs) fall within the realm of human behavior, encompassing non-physical activities such as thinking and associated societal perceptions. Researchers have witnessed a heightened interest in this category of algorithms over the past decade, with this enthusiasm continuing to surge.

Table II-2 presents few of the latest developed metaheuristic algorithms

Table II-2 - A few recent metaheuristic algorithms

Algorithm type	Algorithm	Ref.	Inspiration	Year
Swarm Based Algorithms	Beluga whale optimization (BWO)	[83]	Behaviors of beluga whales	2022
	Pelican Optimization Algorithm (POA)	[84]	Behaviors of Pelicans	2022
	Giant Trevally Optimizer (GTO)	[85]	Hunting strategies of giant trevallies	2022
	Termite life cycle optimizer (TLCO)	[86]	Life cycle of a termite colony	2023
	Nutcracker Optimization Algorithm (NOA)	[87]	Intelligent behaviors of nutcrackers	2023
Natural Science-based algorithms	Special Relativity Search (SRS)	[88]	Particles movement and interaction in an electromagnetic field	2022
	Energy Valley Optimizer (EVO)	[89]	Stability and different modes of particle decay	2023
	Young's Double-Slit Experiment (YDSE) optimizer	[90]	Derived from Young's double-slit experiment	2023
Human-based algorithms	War Strategy Optimization Algorithm (WSO)	[91]	The strategic positioning of military forces during wars	2022

It is important to highlight that several Metaheuristic Algorithms (MHAs) have emerged in recent years, expanding beyond the previously mentioned categories. Some notable examples include:

Sports-Inspired Algorithms: These algorithms draw inspiration from sports, replicating the procedures, regulations, and dynamics of various sports, with a primary focus on football. Examples include the League Championship Algorithm [92], World Cup Optimization [93], and Football Game Algorithm [94].

Music-Based Algorithms: Algorithms in this category find inspiration from music, incorporating musical principles into their design. Examples include Melody Search [95] and Harmony Search [96].

Plant-Based Algorithms: Simulating the intelligence of plants, algorithms in this category mimic plant behaviors. Well-known examples include the Path Planning Algorithm [97], Rooted Tree Optimization Algorithm [98], and the Flower Pollination Algorithm [99].

Mathematics-Based Algorithms: Drawing on the principles of mathematics, algorithms in this class leverage mathematical characteristics. Notable metaheuristics in this category include the Sine Cosine Algorithm [100] and Arithmetic Optimization Algorithm [101].

Water-Behavior Algorithms: Inspired by the intelligent movements of water, algorithms based on water behavior have been developed. Examples include the Water Flow Algorithm [102] and Circular Water Wave Algorithm [103].

II.2.1.6 Advantages and disadvantages of Metaheuristics:

Metaheuristic algorithms (MHAs) have gained prominence in stochastic optimization, showcasing promising performances and addressing various problems. The advantages of MHAs include their ease of implementation, applicability across diverse fields, ability to handle complex problems within reasonable timeframes, flexibility in population size, and the emergence of global behavior from simple individuals at the local level.

II.2.1.6.1 Advantages of Metaheuristics

Metaheuristic algorithms offer several advantages that contribute to their widespread application in various domains:

1. **Ease of Implementation:** Metaheuristics are known for their simplicity in implementation. They provide a practical and straightforward approach, making them accessible even without prior extensive knowledge or ground truth information.
2. **Versatility Across Fields:** MH algorithms demonstrate versatility, proving effective in addressing a wide array of problems across different fields. Their adaptability allows researchers and practitioners to apply them to diverse challenges, ranging from engineering and optimization to business and science.
3. **Efficient Problem Solving:** A significant advantage lies in the ability of metaheuristic algorithms to solve complex problems within reasonable timeframes. This efficiency is

particularly crucial in scenarios where exact algorithms might struggle due to time constraints, providing practical solutions in a timely manner.

4. Flexible Population Size: The flexibility in adjusting the population size is a fundamental aspect of MH algorithms. Unlike some optimization techniques, metaheuristics are not overly dependent on specific population sizes. This adaptability allows for effective control mechanisms, ensuring optimal performance without strict population constraints.

5. Emergence of Global Behavior: One of the intriguing features of metaheuristics is their capacity to generate global behavior through interactions among relatively simple individuals operating independently at the local level. This emergent behavior contributes to the effectiveness of metaheuristic algorithms in finding optimal or near-optimal solutions.

In summary, the advantages of metaheuristics encompass ease of implementation, versatility, efficient problem-solving capabilities, flexibility in population size, and the emergence of global behavior from local interactions. These attributes make metaheuristic algorithms valuable tools for addressing a diverse range of optimization challenges.

II.2.1.6.2 Disadvantages

Challenges in Solving Large-Scale Optimization Problems: When addressing large-scale optimization problems, the evaluation of the fitness function can pose a substantial computational bottleneck, especially when the function's complexity is high. This bottleneck becomes a critical consideration in optimizing the efficiency of metaheuristic algorithms.

Risk of Premature Convergence in Decentralized MH Algorithms: Metaheuristic (MH) algorithms, lacking centralized control, face the inherent risk of becoming stuck or prematurely converging to a local optimum. To overcome this challenge, the development of adaptive mechanisms becomes imperative. These mechanisms ensure a continuous balance between exploration and exploitation within the search space, safeguarding against premature convergence and enhancing the robustness of MH algorithms.

Time-Consuming Nature of MH Algorithms: Metaheuristic algorithms, known for their versatility, tend to be time-consuming techniques. Their efficiency is notably influenced by factors such as the dimensionality of the problem and the required number of iterations. Addressing these considerations becomes crucial, particularly in scenarios where computational resources are constrained or where time efficiency is a critical factor.

Lack of Standardized Structures for Algorithm Comparison: A notable limitation in the field is the absence of uniform structures or templates for well-known algorithms like PSO, FA, and GWA. This absence hinders the systematic comparison of newly introduced algorithms. To address this gap, there is a need for standardized frameworks or templates that facilitate a more comprehensive and transparent evaluation of the relative strengths and weaknesses of different algorithms. This would enable a more informed selection of algorithms based on specific optimization requirements.

II.3. Methodology specifics

II.3.1 Artificial Neural Network

Artificial Neural Networks (ANNs) are a class of machine learning algorithms inspired by the structure and function of biological neural networks in the human brain. In this section, we provide an overview of ANNs, including their architecture, training process, and applications in regression and classification tasks.

II.3.1.1 Architecture of ANNs

ANNs consist of interconnected nodes organized into layers: an input layer, one or more hidden layers, and an output layer [104]. Each node (neuron) in the network processes input data using an activation function, transforming the input into an output signal [104]. The connections between nodes are characterized by weights, which are adjusted during the training process to optimize model performance [104].

II.3.1.2 Training Process

- ANNs are trained using an iterative optimization algorithm, typically gradient descent, to minimize a predefined loss function that measures the difference between predicted and actual outputs. During training, the model updates its weights using backpropagation, a technique that calculates the gradient of the loss function with respect to each weight and adjusts the weights accordingly to reduce prediction errors [105].

II.3.1.3 Regression with Artificial Neural Networks

In regression tasks, ANNs are trained to predict continuous output values based on input features. The output layer typically consists of a single node, and the activation function used in this layer depends on the nature of the prediction task (e.g., linear activation for unbounded predictions or sigmoid activation for bounded predictions) [105].

II.3.1.4 Classification with Artificial Neural Networks

- In classification tasks, ANNs are trained to assign input data to predefined classes or categories. The output layer usually employs a softmax activation function for multiclass classification or a sigmoid activation function for binary classification, producing probability distributions over the classes [105].

II.3.1.5 Advantages of Artificial Neural Networks

- Flexibility: ANNs can model complex, nonlinear relationships between input and output variables, making them suitable for a wide range of tasks. Scalability, ANNs can scale to handle large datasets with thousands or millions of examples, given sufficient computational resources. Feature Learning, ANNs can automatically learn hierarchical representations of features from raw data, reducing the need for manual feature engineering [106].

II.3.2 Random Forest Algorithm

The Random Forest algorithm is a powerful ensemble learning technique commonly used for both classification and regression tasks. It belongs to the family of decision tree-based algorithms and is renowned for its robustness, scalability, and ability to handle high-dimensional datasets with complex interactions. This section provides an in-depth overview of the Random Forest algorithm, covering its key components, working principles, and implementation steps.

II.3.2.1 Decision trees

- At the core of the Random Forest algorithm lie decision trees, which are hierarchical structures comprising nodes representing decision rules based on input features. Each decision

tree recursively partitions the feature space into regions, aiming to minimize impurity or maximize information gain at each split [107].

II.3.2.2 Ensemble Learning

- Random Forest operates on the principle of ensemble learning, where multiple decision trees are trained independently on random subsets of the training data. Each decision tree learns a different aspect of the data, capturing unique patterns and relationships [107].

II.3.2.3 Random Feature Selection

- During the construction of each decision tree, a random subset of input features is selected at each split point. This randomness introduces diversity among the trees, reducing the risk of overfitting and enhancing the model's generalization performance [107].

II.3.2.4 Bootstrapping

- Random Forest employs bootstrapping, a resampling technique where multiple bootstrap samples (random subsets of the training data with replacement) are generated. Each decision tree is trained on a different bootstrap sample, ensuring diversity in the training process [107].

II.3.2.5 Aggregation

- Once all decision trees are trained, predictions are made by aggregating the individual predictions of each tree. For regression tasks, the final prediction is typically the mean or median of the predictions from all trees in the forest. For classification tasks, the majority class prediction (for binary classification) or the class with the highest probability (for multiclass classification) is considered [107].

II.3.2.6 Hyperparameters

- Random Forest offers several hyperparameters that can be tuned to optimize model performance, including the number of trees in the forest (`n_estimators`), the maximum depth of each tree (`max_depth`), the minimum number of samples required to split a node

(`min_samples_split`), and the maximum number of features considered for splitting (`max_features`) [107].

II.3.2.7 Out-of-Bag (OOB) Error

- Random Forest utilizes the out-of-bag (OOB) error estimate as an internal validation metric. During training, each decision tree is evaluated on the data points not included in its corresponding bootstrap sample. The OOB error is then computed as the average error across all trees, providing an unbiased estimate of the model's performance [108].

II.3.2.8 Feature Importance

- Random Forest calculates feature importance scores based on how much each feature contributes to reducing impurity or increasing information gain across all decision trees. These scores can be used to identify the most influential features in predicting the target variable.

II.3.3 Polynomial regression

Polynomial regression is a type of linear regression model that extends the relationship between the independent variable x and the dependent variable y by incorporating polynomial terms. This section provides a detailed overview of polynomial regression, including its underlying principles, advantages, limitations, and implementation steps.

II.3.3.1 Polynomial Regression Model

- Polynomial regression assumes that the relationship between the independent variable x and the dependent variable y follows a polynomial function of degree n , given by:

$$y = \beta_0 + \beta_1x + \beta_2x^2 + \dots + \beta_nx^n + \varepsilon \quad (\text{II-1})$$

$\beta_0, \beta_1, \beta_2, \dots, \beta_n$ are the coefficients of the polynomial terms, and ε represents the error term.

II.3.3.2 Working Principle

- Polynomial regression fits a curve (polynomial function) to the data points by minimizing the sum of squared differences between the observed and predicted values. The goal is to find the optimal coefficients that best describe the relationship between x and y .

II.3.3.3 Advantages

Flexibility, Polynomial regression can capture nonlinear relationships between variables, making it suitable for modeling complex data patterns. Interpretability, The coefficients of polynomial terms provide insights into the direction and magnitude of the relationship between x and y . Ease of Implementation, Polynomial regression can be implemented using standard linear regression techniques, requiring minimal additional preprocessing.

II.3.3.4 Limitations

Overfitting, As the degree of the polynomial increases, the model may become overly complex and prone to overfitting, especially with limited data. Extrapolation, Polynomial regression may not generalize well outside the range of the observed data, leading to unreliable predictions in extrapolated regions.

II.3.3.5 Hyperparameters

- The main hyperparameter in polynomial regression is the degree of the polynomial n . Higher degrees allow the model to capture more complex relationships but increase the risk of overfitting.

II.3.4 Shapley Additive Explanations (SHAP): Understanding Model Predictions

II.3.4.1 Overview of SHAP

SHAP is an interpreting model based on game theory [109] and local explanations [110]; it offers a means to estimate the contribution of each feature. Assuming an ANN model where a group N (with n features) is used to predict an output (N). In SHAP, the contribution of each feature (ϕ_i is the contribution of feature i) on the model output $v(N)$ is allocated based on their marginal

contribution [111]. Based on several axioms to help allocate the contribution of each feature, shapely values are determined through:

$$\varphi_i = \sum_{S \subseteq N \setminus \{i\}} \frac{|S|! (n - |S| - 1)!}{n!} [v(S \cup \{i\}) - v(S)] \quad (\text{II-2})$$

A linear function of binary features g is defined based on the following additive feature attribution method:

$$g(z') = \varphi_0 + \sum_{i=1}^M \varphi_i z'_i \quad (\text{II-3})$$

Where $z' \in M$, equals 1 when a feature is observed; otherwise, it equals 0, and M is the number of input features [112].

II.3.4.2 Working Principle

SHAP values quantify the marginal contribution of each feature to the difference between the actual prediction and the expected prediction (baseline). By considering all possible combinations of features and their permutations, SHAP values ensure fairness and consistency in attributing credit to each feature [113].

II.3.4.3 Interpretability

Positive SHAP values indicate features that contribute to increasing the model's prediction, while negative values suggest features that push the prediction towards lower values. The magnitude of SHAP values reflects the relative importance of each feature, allowing for a nuanced understanding of feature impact [113].

II.3.4.4 Advantages

Individual Explanations: SHAP provides interpretable explanations for each prediction, enabling users to understand the model's decision-making process on a case-by-case basis.

Global Insights, Aggregating SHAP values across multiple predictions reveals overarching trends and patterns in feature importance, offering valuable insights into model behavior. Model-Agnostic, SHAP is compatible with a wide range of machine learning models, including tree-based models, linear models, neural networks, and more [113].

II.3.5 Pelican Optimization Algorithm (POA): Harnessing Nature's Wisdom for Optimization

The Pelican Optimization Algorithm (POA) is a metaheuristic optimization algorithm inspired by the foraging behavior of pelicans. In this section, we delve into the key concepts, working principles, and applications of the POA in solving optimization problems.

II.3.5.1 Concept and Inspiration

The POA draws inspiration from the foraging behavior of pelicans, which exhibit efficient hunting strategies to locate prey in a vast and dynamic environment [84]. Pelicans employ a combination of exploration and exploitation strategies to search for food, adapting their movements based on environmental cues and the availability of resources. Fig. II-4 Shows the flowchart of the POA.

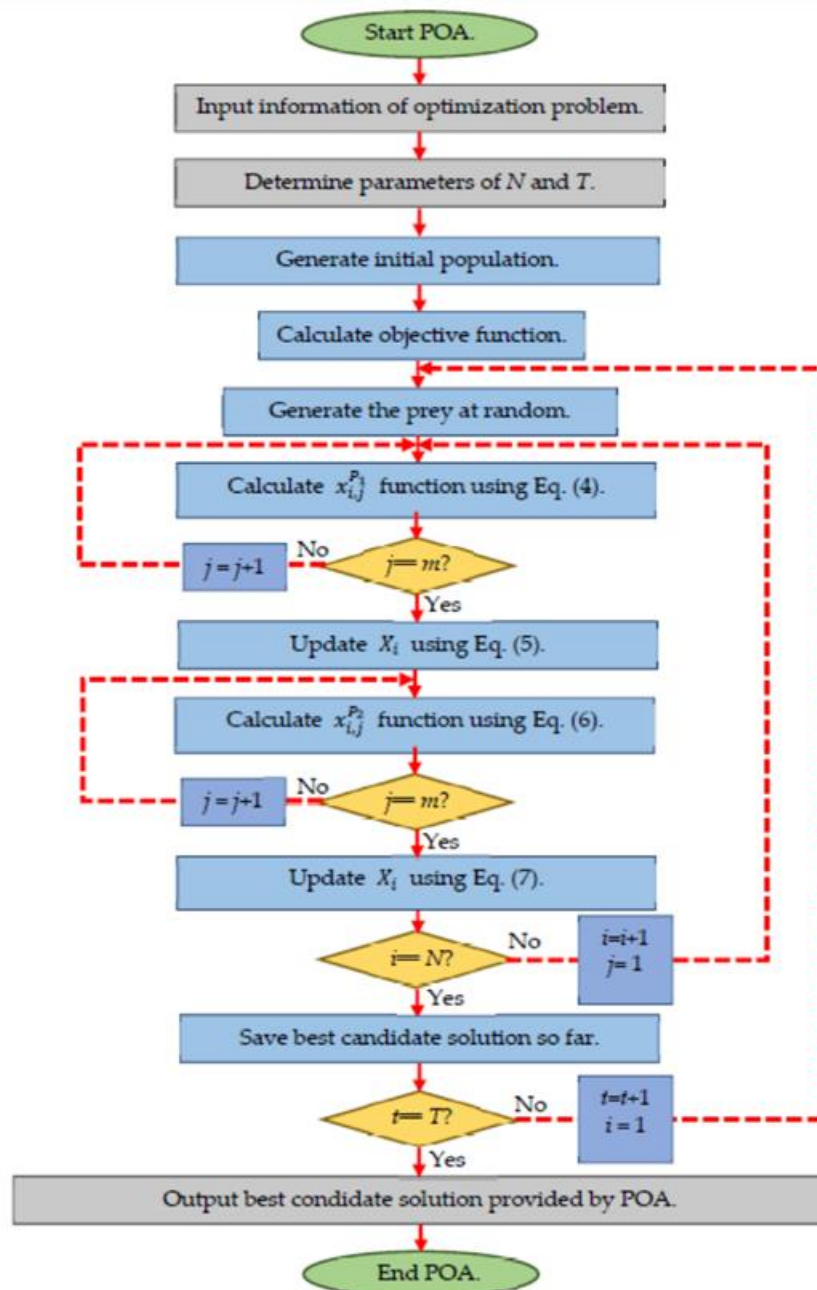


Fig. II-4 – Flowchart of Pelican Optimization Algorithm [84]

II.3.5.2 Working Principles

- The POA simulates the foraging behavior of pelicans through a population-based optimization approach. The algorithm maintains a population of candidate solutions (pelicans)

that traverse the search space to find optimal solutions. Pelicans explore the search space through random movements and exploit promising regions based on the quality of solutions encountered [84].

II.3.5.3 Exploration Phase

- During the exploration phase, pelicans exhibit random movements across the search space, aiming to discover new regions with potentially better solutions. Pelicans explore the search space using stochastic methods such as random walks or perturbations to avoid getting trapped in local optima [84].

II.3.5.4 Exploitation Phase

- In the exploitation phase, pelicans focus on refining their search around promising regions identified during exploration. Pelicans adjust their movements based on the quality of solutions encountered, gravitating towards regions with higher fitness values [84].

II.3.5.5 Adaptive Behavior

- The POA incorporates adaptive mechanisms to balance exploration and exploitation throughout the optimization process. Pelicans dynamically adjust their exploration and exploitation rates based on the convergence behavior of the algorithm and the diversity of solutions in the population [84].

II.3.5.6 Applications of the Pelican Optimization Algorithm

- The POA has been successfully applied to a wide range of optimization problems, including engineering design [114], scheduling, financial portfolio optimization, and image processing. Its ability to efficiently explore complex search spaces and identify high-quality solutions makes it particularly well-suited for optimization tasks with nonlinear, multimodal, or high-dimensional objective functions [84].

II.3.5.7 Advantages of the Pelican Optimization Algorithm

- Versatility: The POA can be adapted to different optimization problems by customizing its parameters and operators [115] [116] [117].

- Robustness: The algorithm's population-based approach and adaptive behavior enable it to handle noisy or uncertain objective functions.

- Efficiency: The POA often converges to near-optimal solutions with relatively few iterations, making it computationally efficient for large-scale optimization tasks.

II.4. Some applications of Machine Learning, Deep Learning, and metaheuristics in FSW

Table II-3 provides a comprehensive overview of the multifaceted applications of Machine learning, deep learning, and metaheuristic algorithms. This meticulously organized table delineates various research papers, offering insights into the year of publication, the materials subjected to welding, the input parameters considered, the resultant output findings, and the accuracy achieved through the methodologies employed. The breadth of applications showcased in this table underscores the versatility of these methodologies, spanning across diverse domains such as modeling, prediction, and optimization of parameters. Through these methodologies, researchers have explored and addressed a myriad of challenges, thereby advancing the efficacy and precision of welding processes in various industrial and academic contexts.

Table II-3 - Some of the Deep learning & metaheuristics used with FSW technology [118]

No	Ref	Implementation	Inputs	Outputs	Material type	Target	Accuracy rate (%)	Applied method/s
1	[119]	Similar	Plastic strain, strain rate, and temperature	Microstructure	AA6082 T6	Modeling prediction	0.72	ANN
2	[120]	Similar	Weld speed, tool rotation speed	Tensile strength, yield strength, elongation, hardness, hardness of heat affected zone	Hot rolled aluminim	Modeling prediction	98	ANN
3	[121]	Similar	Plastic strain, strain rate, and temperature	Microstructure	AA7075-T6	Modeling prediction	Less %50 than analytical method	ANN
4	[122]		Rotational speed, penetration depth, dwell time	Max. tensile force, plunging load, process time	AA6061-T6	Modeling prediction optimization	N/A	ANN GA
5	[123]	Similar	Tool rotational speed, welding speed	Ultimate tensile strength, yield stress, percentage elongation, hardness (HAZ), hardness (weld mat)	AA1080	Modeling prediction optimization	99	ANN GA
6	[124]		Rotational speed and welding speed	Residual stress	N/A	Optimization	N/A	NSGA-II
7	[125]	Similar	Plastic strain, strain rate, and temperature	Microstructure, microhardness	Ti-6Al-4V	Modeling prediction	N/A	ANN
8	[126]	Similar	Tool type, tool probe diameter and shoulder flat surfaces	Weld strength, weld cross-section area, average grain size of weld and average grain size of TMAZ	Al alloy	Modeling prediction	0,76(ANN) 0,923(FL)	ANN fuzzy logic
9	[127]	Dissimilar	Rotational and traverse speeds	Tensile strength	Al-Mg and CuZn34	Modeling prediction	97	ANN

10	[128]		CSRR and contact gap conductance parameters a and b	CSRR and contact gap conductance parameters a and b	AA7449	Modeling prediction	N/A	ANN
11	[129]	Dissimilar	Rotational speed, traverse speed	Tensile shear force, hardness	AA7075-O and AA5083-O	Modeling prediction optimization	98	ANN PSO
12	[130]	Similar	Rotational speed, feed rate, longitudinal position and thickness percentage	Microhardness	AZ31 magnesium	Modeling prediction	96	ANN
13	[131]	Similar	Acoustic emission signals	Tool profile, tool rotation speed, travel speed, tensile strength	AA1050H24	Signal processing prediction	99	Wavelet ANN
14	[132]	Similar	Number of passes, tool rotation speed, tool traverse speed, addition of nanosized Al ₂ O ₃ powder	Microhardness	Mild steel	Modeling prediction	N/A	ANN
15	[133]	Dissimilar	Rotational speed, translational speed, axial load, tool geometry	Tensile strength	AA6061 and AZ61	Modeling prediction	100	ANN
16	[134]	Similar	Rotational speed of the tool, welding speed, axial force, shoulder diameter, pin diameter, tool hardness	Yield strength, tensile strength, notch-tensile strength and hardness of welding zone	AA 7075-T6	Modeling prediction	0.99	ANN
17	[135]	Dissimilar	Tool plunge rate, Tool rotation speed, preheating time	Plunging forces, torques, temperatures, shear resistance	Polycarbonate sheets	Modeling prediction	95	ANN
18	[136]	Similar	Pin diameter and shoulder diameter	Heat-affected zone, thermal and strain values on weld zone	AA5083	Modeling prediction	98	ANN
19	[137]	Similar	Tool rotational speed, welding speed	Tensile strength, hardness and elongation	Al Alloy	Prediction optimization	97	Fuzzy ABC ICA
20	[138]	Similar	Base metal, tapered cylindrical pin, triangular pin	Microhardness	AA6061	Modeling prediction	84.79	ANN

21	[139]	Similar	Rotational speed, translational speed, maximum temperature and the slope of the heating curve, p (mm)	Microhardness and ultimate tensile strength	AA5754	Modeling prediction	96	ANN
22	[140]	Dissimilar	Tool pin profile, rotational speed, welding speed and axial force	Tensile strength	AA6351-AA5083	Modeling prediction	95	ANN
23	[141]	Dissimilar	Tool rotational speed, welding speed, shoulder diameter and pin diameter	Tensile strength, microhardness and grain size	AA5083-O-AA6063-T6	Modeling prediction optimization	98	ANN GA
24	[142]	Similar	Spindle speed, plunge force, welding speed and empirical force	Ultimate tensile strength	AA2219-T87	Modeling prediction	93	ANN ANFIS
25	[143]	Similar	Rotational speed, translational speed, shoulder diameter	Intergranular corrosion susceptibility	AA5083	Modeling prediction	N/A	ANN
26	[144]	Similar/Dissimilar	Material type, tool traverse speed, tool rotation speed	Tensile strength	A17075-O and A17075-T6	Modeling prediction	97	ANN
27	[145]	Similar	Dispersion, asymmetry and excess	Tensile strength	AA1100	Modeling prediction	3,08 0,53(AAP E)	ANN SVM
28	[146]	Dissimilar	Tool rotational speed, tool traverse speed and axial force	Tensile Strength, yield strength, elongation	AA6061-T6 and AA6351-T6	Prediction optimization	97	ABC
29	[147]	Similar	Process parameters and extracted signal features	Tensile strength, yield strength	AA1100	Signal processing prediction	94	Wavelet ANN
30	[148]	Similar	Reinforcing particles type, rotational speed, traverse speed	Axial force, hardness, ultimate tensile strength	A356 cast alloy	Modeling optimization	N/A	ANN NSGA-II
31	[149]	Similar	Rotational speed, traverse speed	Silicon particle size, hardness, axial force, tensile strength	A356 cast alloy	Modeling optimization	N/A	ANN NSGA-II
32	[150]	Similar	Tools, tool rotation, tilt angle, welding speed	Tensile strength, impact strength	AA6082-T6	Modeling prediction optimization	N/A	ANN GRA

33	[151]	Similar	Plunge depth, tool rotational speed, welding speed, tool geometry, shoulder diameter, pin diameter, tool pin length and dwell time	Ultimate tensile strength, yield stress, percentage elongation, bending angle and hardness	AA1100	Modeling prediction optimization	93	ANN GA DE
34	[152]	Similar	Tool rotational speed, tool travel speed and tool tilt angle	Tensile strength, microhardness and corrosion resistance	AA2219	Modeling prediction optimization	99	ANN GA
35	[153]	Similar	Feed rate, EFI, rotational speed	Welding quality	AA-2219-T87	Prediction filtering optimization	100	kNN fuzzy-kNN ABC
36	[154]	Similar	Tool rotation speed, the plunge depth, and the stirring time	Lap-shear fracture load	High-density polyethylene (HDPE)	Modeling prediction	99.01	ANN
37	[155]	Similar	Tool rotation speed, welding speed, shoulder diameter and pin diameter	Tensile strength	AA1100	Modeling prediction	99	ANN
38	[156]	Similar	Tool rotation speed, welding speed, shoulder diameter and pin diameter	Tensile strength	AA1100	Modeling prediction	%-28 max. error	ANN
39	[157]	Dissimilar	Tool rotational speed, welding speed, axial force and the tool pin profile	Wear rate	AA6061 T6-AA5083-0	Modeling prediction	95	ANN
40	[158]	Dissimilar	Governing parameter, measurement datas	Tensile strength	AA6061-T651	Modeling prediction	100	SVM
41	[159]	Similar	Rotational speed, welding speed, rotational speed to welding speed ratio and processing time	Vertical force	AZ31	Modeling prediction	0,9918 0,9449 (R)	ANN SVM
42	[160]	Similar	Pin profile, tool angle, rotational speed, weld speed	Horizontal force, vertical force, grain size, temperature, tensile strength, hardness, joint thickness, elongation	AA1100	Modeling optimization	N/A	ANN NSGA-II

43	[161]	Similar	Rotational speed, groove width, traverse speed, type of ceramic particle	Wear rate	AA6082	Modeling prediction	95	ANN
44	[162]	Similar	Forces and accelerations in three spatial directions, spindle torque, and temperatures for tool shoulder and tool probe	Welding quality	EN AW-6082 T6	Modeling prediction	99.1	ANN
45	[163]	Similar	Rotational speed, welding speed	Tensile strength	AA6061-T6	Modeling prediction	N/A	ANN
46	[164]	Similar	Tool parameters	Ultimate tensile strength, yield stress, percentage elongation, bending angle and hardness	AA1100	Modeling prediction optimization	99	ANN PSO GA DE
47	[165]	Dissimilar	Rotating velocity, welding speed, Zn interlayer thickness, ultrasound power	Tensile shear load	AA7075-T6 AZ31BMg	Modeling prediction optimization	90	ANN GWOA
48	[166]	Similar	Shoulder diameter, rotational speed, traverse speed	Ultimate tensile strength, elongation, impact strength	AA6082-T6	Modeling Prediction optimization	95	ANN NSGA-II FFO PSO

II.5. Conclusion

In conclusion, the methodology chapter serves as the linchpin of our research endeavor, delineating a systematic framework for the comprehensive study of Friction Stir Welding (FSW) dynamics and the integration of pneumatic sources for enhanced operational efficiency. Through the amalgamation of advanced techniques from the realms of Machine Learning, Deep Learning, and Metaheuristic Optimization, our methodology embodies a multifaceted approach aimed at unraveling the intricacies of FSW processes.

The utilization of Artificial Neural Networks (ANN), Random Forest (RF), and Polynomial Regression techniques enables us to construct predictive models capable of forecasting torque in FSW, leveraging a comprehensive set of input parameters. These models lay the foundation for informed decision-making and process optimization, empowering practitioners to anticipate and mitigate potential challenges in FSW operations.

Furthermore, the application of the Shapley Additive exPlanations framework enriches our understanding of the underlying factors influencing torque output in FSW. By elucidating the relative importance of each input parameter, this analytical tool provides valuable insights into the complex interplay between process variables and welding outcomes.

However, the true essence of our methodology lies in its pursuit of optimization. Through the Pelican Optimization Algorithm, we navigate the vast parameter space inherent in FSW operations, systematically identifying parameter sets that minimize energy consumption while maximizing welding efficiency. This iterative optimization process mirrors the adaptive foraging behavior of pelicans, ensuring the exploration of diverse solution spaces and the identification of optimal configurations tailored to specific material requirements.

In essence, the methodology chapter lays the groundwork for a comprehensive exploration of FSW dynamics and the integration of pneumatic sources, underscoring our commitment to bridging theoretical insights with practical applications. By leveraging cutting-edge techniques and innovative methodologies, our research endeavors to propel FSW technology into new frontiers, unlocking unprecedented efficiency, precision, and operational excellence in material joining processes.

CHAPTER III

Chapter III - Modeling and parametric importance Analysis of torque in FSW

III.1. Introduction

This chapter delves deeply into the development of artificial neural network (ANN), random forest (RF), and polynomial regression (PR) models aimed at predicting torque during friction stir welding (FSW), particularly for a variety of materials, the majority of which are aluminum alloys.

The predictive capability of these models hinges on ten carefully selected input parameters: AS TS, RS TS, L0, R1, R2, R3, L1, Alpha, WS, and RS. Parametric studies are conducted to assess and rank the importance of each parameter in terms of its impact on torque predictability within the developed models. Performance evaluation metrics such as mean squared error (MSE), mean absolute error (MAE), and mean absolute percentage error (MAPE) are utilized for comparative analysis.

III.2. Materials and Methods

III.2.1 Experimental studies

The current study was built based on data from 287 experiments conducted in 21 previous studies for aluminum alloys, as shown in Table 1. The study included the most used categories in FSW studies, which are AA1xxx, AA2xxx, AA5xxx, AA6xxx, and AA7xxx alloys with different heat treatment ranges.

Notably, the data pool exhibited a mixed nature, with numeric data complemented by values extracted from graphical representations. The dataset contains experiments on similar and dissimilar plates. All pins are either cylindrical or conical in shape. A type of correlation was used to overcome the lack of pin length in several studies. A distinctive feature of the dataset was the replacement of pin-related attributes. The dataset's summary statistics in Table 2 offer insights into the dataset's distribution and central tendencies, where T is torque, RS is the rotation speed of the tool, and WS is velocity. R1, R2, and R3 are the radius of the shoulder, pin base, and pin tip, respectively. L0 is plate thickness, L1 is the tool's pin length, and Alpha

represents the tilt angle. The AS TS and RS TS are the tensile strengths of the advancing and retreating plate sides, respectively.

Table III-1 - Welding configurations of the examined studies [167]

SID	Advancing side	Retreating Side	Plate thickness (mm)	Source
1	A356 (Al-7Si-0.3Mg)	A356 (Al-7Si-0.3Mg)	6.4	[31]
2	AA6061-T6	AA6061-T6	6	[168]
3	AA2024-T3	AA2024-T3	6	[169]
4	AA5052-H34	AA5052-H34	5	[35]
5	AA2024-T3	AA2024-T3	9.5	[170]
6	AA5083-130 HV	AA6082-T6	3	[171]
7	AA5083-130 HV	AA6082-T6	3	[171]
8	AA6061-T6	AA6061-T6	6	[172]
9	AA6061-T651	AA6061-T651	32	[173]
10	AA6061-T651	AA6061-T651	25	[173]
11	AA7050-T7451	AA7050-T7451	6.35	[30]
12	AA6061-T6	AA5083-H111	3	[174]
13	AA5052-H34	AA5052-H34	5	[175]
14	AA5754	AA5754	2	[176]
15	AA1100-H14	AA1100-H14	8	[177]
16	AA7039-T6	AA7039-T6	9.5	[178]
17	AA7039-T6	AA7039-T6	9.5	[178]
18	AA7039-T6	AA7039-T6	6.3	[178]
19	AA2219-T87	AA2219-T87	9.5	[29]
20	AA2219-T87	AA2219-T87	8.3	[29]
21	AA2219-T87	AA2219-T87	9.5	[29]
22	AA2524-T351	AA2524-T351	6.4	[28]
23	AA2024-T4	AA2024-T4	5.9	[34]
24	AA7075-T6	AA7075-T6	3.5	[179]
25	AA6092/17.5 SiCp-T6 composite	AA6092/17.5 SiCp-T6 composite	6	[180]
26	AA6061-T6	AA6061-T6	4.7	[181]

III.2.2 Methodology

III.2.2.1 ANN model

The neural network model, with its architecture illustrated in Fig. III-1 was designed and trained to predict torque values based on a comprehensive set of input features. The model architecture is constructed using Python scripts and libraries like TensorFlow and Keras. The

model comprises multiple layers. Standardization of the feature set was implemented using StandardScaler to ensure consistent scaling across variables.

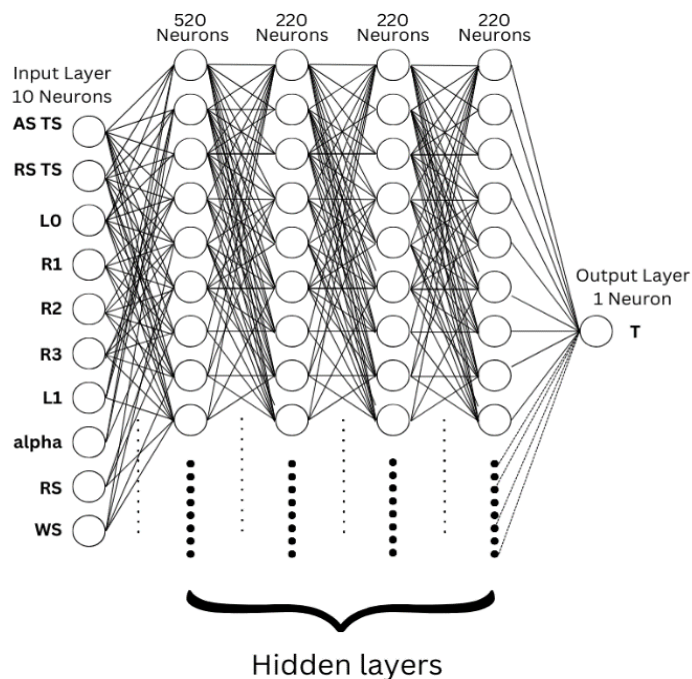


Fig. III-1 - Architecture of the ANN model [167]

There is a first dense layer with 520 neurons and a rectified linear unit (ReLU) activation function in the neural network architecture. After that, three hidden layers were added, and each one had 220 neurons activated by ReLU. Empirical findings during model development served as a guide for choosing these layer sizes, with a focus on balancing model complexity and generalization performance. The output layer consists of a single neuron responsible for predicting torque values.

For optimization, the Adam optimizer was employed. The loss function chosen was mean squared error (MSE), aligning with the objective of minimizing the difference between predicted and actual torque values. During training, the model was subjected to 700 epochs with a batch size of 276. Early experimentation revealed that a validation split of 20% yielded optimal results, enabling the model to generalize effectively while avoiding overfitting.

A Python script was employed to partition it into training, validation, and test sets. Specifically, the data was divided into feature variables (X) and a target variable (y). The training and validation data, constituting 70% of the dataset, were separated from the test data (30%) using the `train_test_split` function, with a random state of 70 to ensure reproducibility. The statistics of the experimental data used for training, testing, and validating the ANN model are shown in Table III-2.

Table III-2 - Statistics of the dataset used in this study [167]

modal parameters	mean	std	min	25%	50%	75%	max
AS TS	371.05	130.68	133.96	262.00	326.00	492.00	567.00
RS TS	370.58	131.00	133.96	262.00	326.00	492.00	567.00
L0	10.82	9.44	2.00	5.00	6.40	9.50	32.00
R1	10.12	3.09	5.00	7.50	10.00	12.70	17.50
R2	4.03	1.61	1.50	3.00	3.55	6.00	6.25
R3	3.48	1.73	1.25	2.00	3.00	5.00	6.25
L1	7.56	4.64	1.20	4.00	6.00	9.35	15.90
alpha	1.25	1.19	0.00	0.00	2.00	2.50	3.00
WS	184.51	263.67	28.00	76.20	102.00	202.92	1800.00
RS	646.28	500.47	52.41	265.00	549.73	900.00	2800.00
T	88.09	96.15	6.18	14.87	48.56	105.92	340.49

III.2.2.2 Random Forest Algorithm

The operation commenced with the collection of experimental data stored in a CSV file. The dataset contains information on various parameters such as the radius of the shoulder (R1), pin base (R2), pin tip (R3), tool's pin length (L1), tensile strengths of advancing (AS TS) and retreating (RS TS) plate sides, plate thickness (L0), tilt angle (alpha), rotation speed of the tool (RS), and velocity (WS). The target variable considered for regression analysis is torque (T). Data was loaded into a pandas DataFrame for further processing.

The independent variables (features) essential for constructing the Random Forest model were identified as R1, R2, R3, L1, AS TS, RS TS, L0, alpha, WS, and RS. The target variable, T, was specified as the torque.

The dataset was split into training and testing sets using the `'train_test_split'` function from the scikit-learn library. Approximately 70% of the data was allocated to the training set, with the remaining 30% reserved for testing.

A Random Forest Regressor was instantiated with specific hyperparameters: 10000 estimators, a maximum depth of 10, and a random state of 70 for reproducibility. The model was trained

using the training data (X_{train} , y_{train}) on all the dataset to create a global model. Afterwards a local model was created for each of the 26 experimental setups (see Table III-1) individually.

The SHAP library was employed to interpret the output of the Random Forest model. SHAP values were calculated for each observation in the dataset to understand the contribution of individual features to the model's predictions. A SHAP summary plot was generated to provide a visual representation of feature importance.

Predictions were made on the test set using the trained Random Forest model, and various regression metrics were calculated, including Mean Squared Error (MSE), Mean Absolute Error (MAE), and R-squared (R^2) score. These metrics serve as indicators of the model's performance in predicting torque values.

To enhance interpretability, a scatter plot comparing actual torque values to predicted values was generated. Additionally, a diagonal line representing perfect predictions was overlaid on the plot.

III.2.2.3 Polynomial Regression

Python's machine learning library "sklearn" was used to find a polynomial equation that fits our dataset. The dataset was split into training and testing data X and Y, respectively, then systematically varied the degree of the polynomial from 1st to 5th degree and captured the performance of each of the polynomials through multiple metrics (R square, mean square error, mean absolute percentage error, mean absolute error, and sum square error) for later comparisons with the other two models.

The comprehensive methodology, spanning data preprocessing, modeling, exploration, optimization, and visualization, was meticulously executed using the Python programming language. Key libraries, including pandas, scikit-learn, joblib, matplotlib, and shap, were instrumental in realizing the entire process. The code implementation occurred within a Jupyter Notebook environment, facilitating seamless experimentation and thorough analysis.

III.3. Results and discussion

III.3.1 ANN model

The architecture and training parameters that were chosen for the current model helped to rapidly reach a low loss of value, as shown in Fig. III-2. The training was stopped after 700 epochs when it reached a meager loss value and avoided overfitting. The trained model also showed impressive predictive capability, as illustrated in Fig. III-3, where the predicted values are relatively accurate.

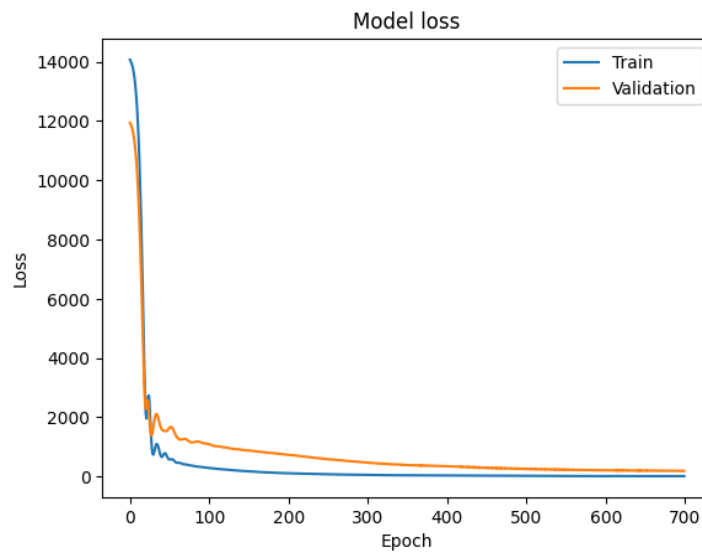


Fig. III-2 - Predicted values of torque loss for training and validation datasets [167]

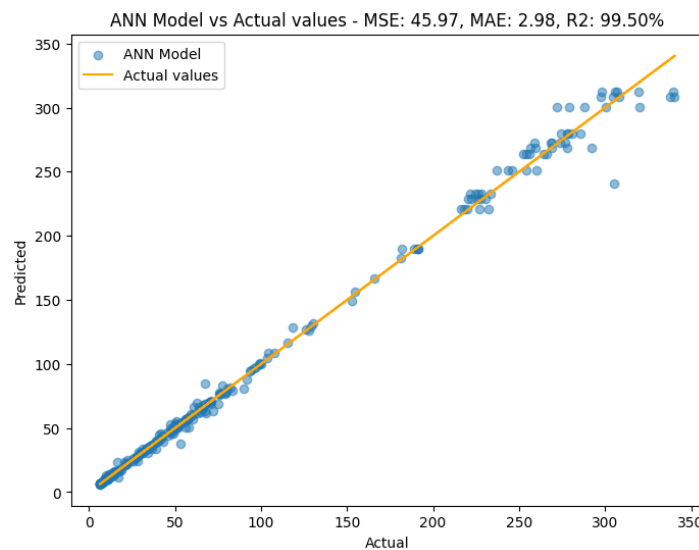


Fig. III-3 – ANN Predicted and experimental torque comparison.

Several criteria were employed to assess the accuracy of the predictive model. The resulting R-squared of 99.50% can be referred to as the variability in torque requirements, which can be effectively attributed to the input parameters. This result underscores the model's robust explanatory capacity. The limited values of MAE = 2.98 indicated that the predicted torque does not deviate from the experimental sets. Moreover, the MAPE of 3.85% reflects its reliability in estimating torque requirements with a high degree of fidelity. Finally, the RMSE of 6.78 shows the precision of the predictions.

III.3.2 Random Forest Algorithm

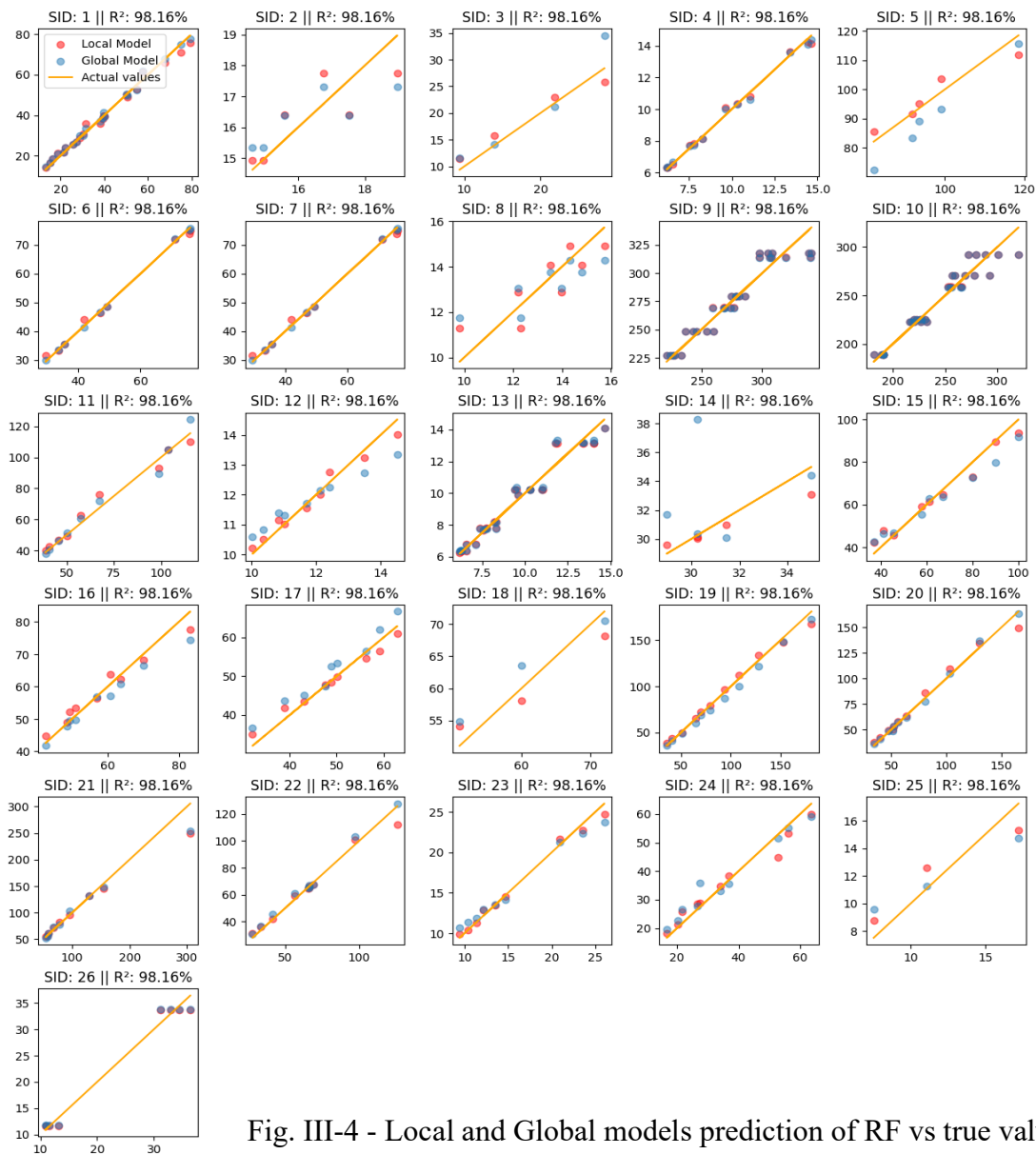


Fig. III-4 - Local and Global models prediction of RF vs true values

Fig. III-4 offers a detailed juxtaposition of the predicted values derived from both the global and local models against the actual experimental results across various experimental configurations. Generally, there is a remarkable consistency between the predictions of the local and global models, suggesting a robust predictive capability across most scenarios. However, a notable deviation is observed for SID 13, where the predictions diverge noticeably. Similarly, for SID 2 and 14, the models demonstrate a degree of variance from the experimental values, highlighting instances where the predictability is less precise. Nevertheless, for the majority of cases, the models exhibit a commendable level of predictability, reaffirming their efficacy in forecasting torque outcomes. In the other hand Fig. III-5 shows the overall comparison between the predictivity of the global RF model and the experimental values, where it shows great fit and correlation except for the higher range of torque values approximately above 250 N.m where it RF shows a little distortion in values.

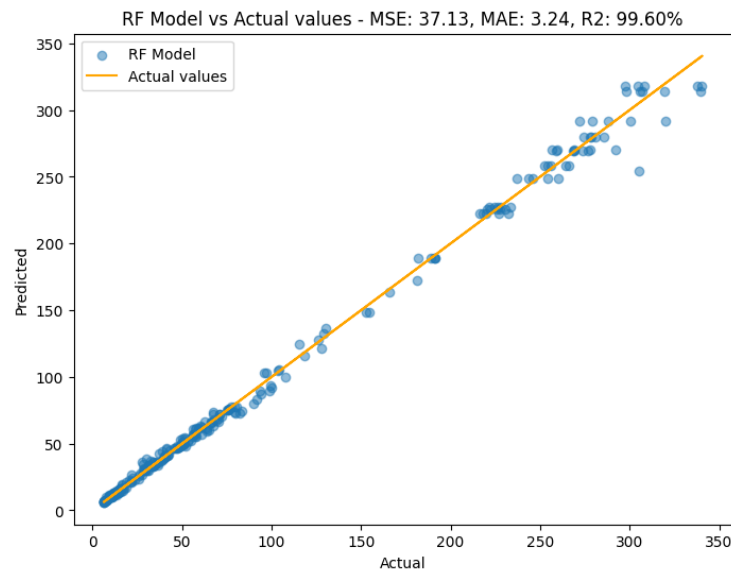


Fig. III-5 - RF Predicted and experimental torque comparison.

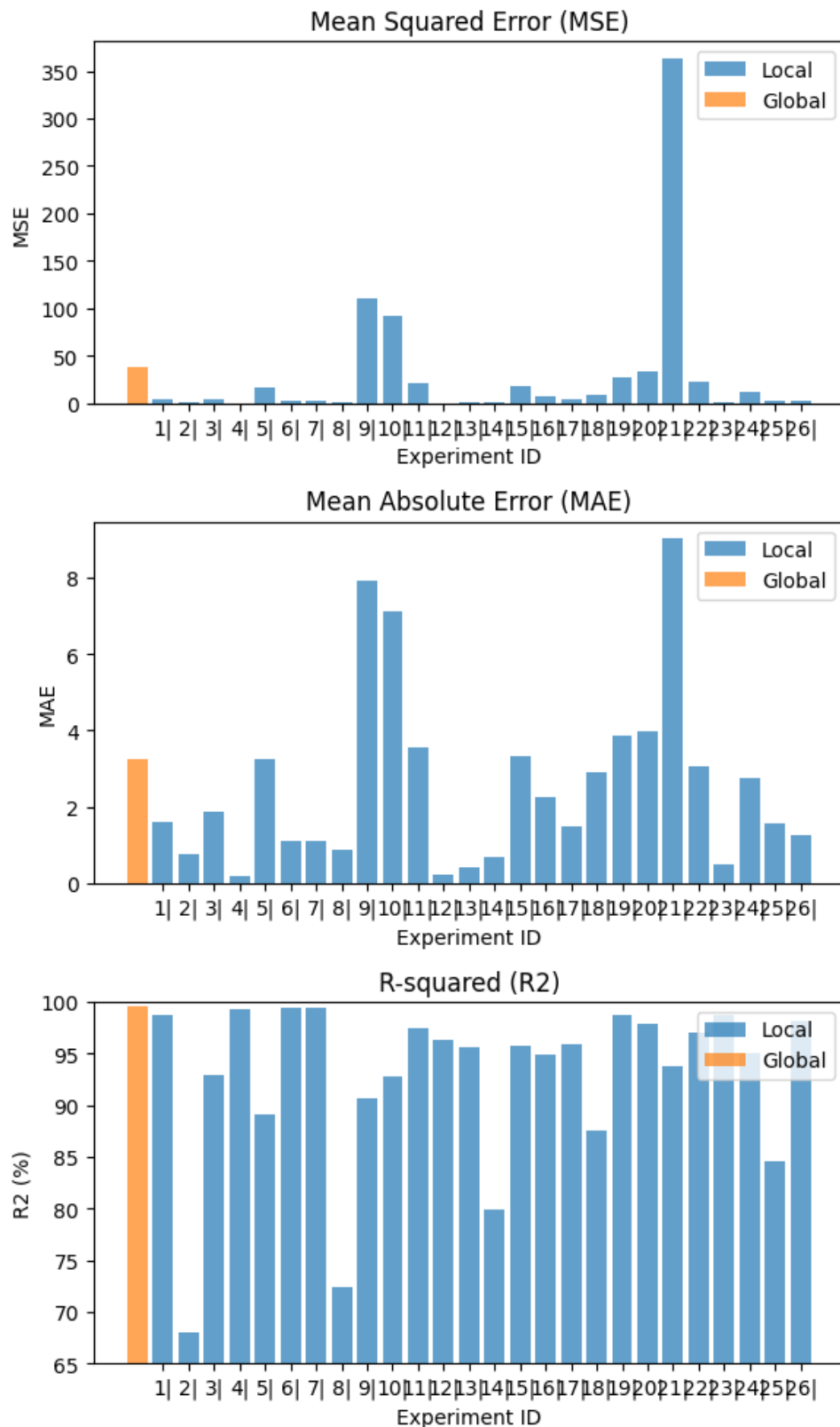


Fig. III-6 - Metrics of the RF models (Global and Local)

Various criteria were utilized to evaluate the accuracy of the predictive models. The R-squared value, boasting an impressive 99.60%, signifies the substantial variability in torque requirements that can be effectively explained by the input parameters. This result underscores the robust explanatory power of the model, indicating its ability to capture and account for the complexities inherent in the torque prediction process.

Furthermore, the limited values of Mean Absolute Error (MAE) at 3.25 indicate minimal deviation between the predicted torque values and the corresponding experimental data sets. This suggests that the predictive models consistently provide accurate estimations of torque requirements across different scenarios, reinforcing their reliability and precision.

Moreover, the Mean Absolute Percentage Error (MAPE) of 4.54% highlights the high degree of fidelity in the model's predictions, indicating a relatively small average percentage deviation from the actual torque values. This underscores the model's capability to provide reliable and consistent estimations of torque requirements, essential for optimizing friction stir welding processes.

Finally, the Root Mean Square Error (RMSE) value of 6.15 further accentuates the precision of the predictions, indicating the average magnitude of the residuals between predicted and observed torque values. This metric reinforces the overall accuracy and effectiveness of the predictive models in capturing the intricacies of torque prediction in friction stir welding processes.

III.3.3 Polynomial regression

Fig. III-7 provides valuable insights into the discrepancy between the overarching polynomial regression model and its localized counterparts. It illustrates a substantial variance between the predictions generated by the global model and those derived from individual local models, emphasizing notable divergences across various experimental setups. However, it's noteworthy that despite this disparity, instances of alignment between the global and local models are observed, particularly evident in scenarios such as SID 1.

Moreover, referring to Fig. III-8, a comprehensive overview of the global model's performance is presented, highlighting its efficacy in capturing the underlying trends of the dataset. Notably,

the scatter plot depicted in Fig. III-8 reveals a cohesive distribution of predicted values in relation to their experimental counterparts, underscoring the overall robustness of the global model's predictive capabilities. This indicates that while discrepancies exist between the global and local models, the global model still serves as a reliable predictor, showcasing its adaptability and generalizability across various experimental conditions.

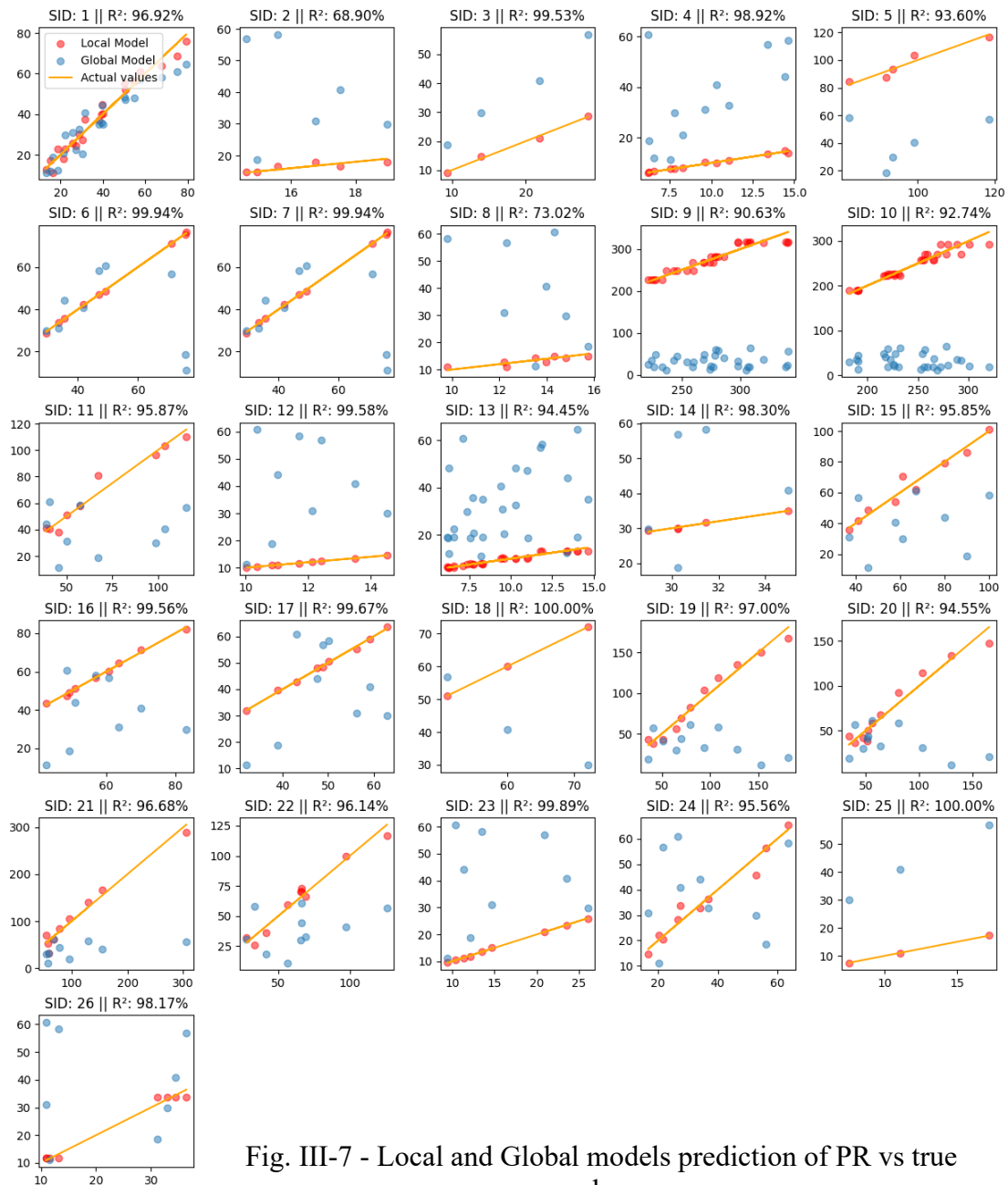


Fig. III-7 - Local and Global models prediction of PR vs true values

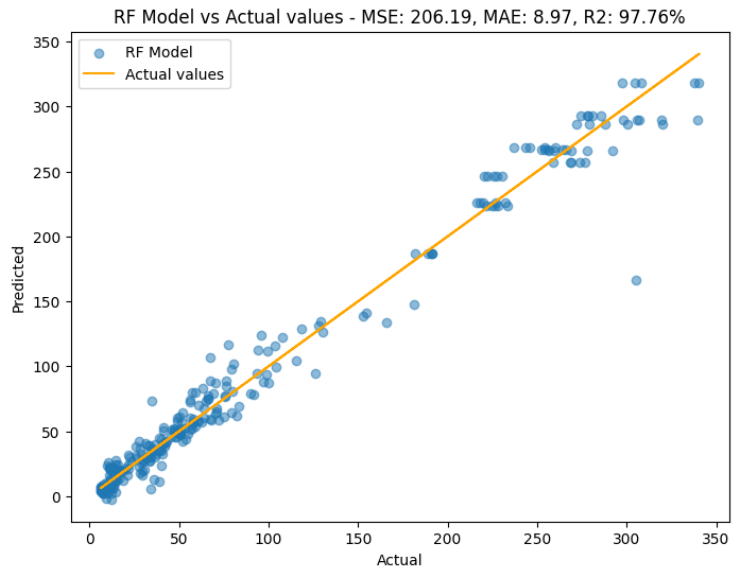


Fig. III-8 - PR Predicted and experimental torque comparison.

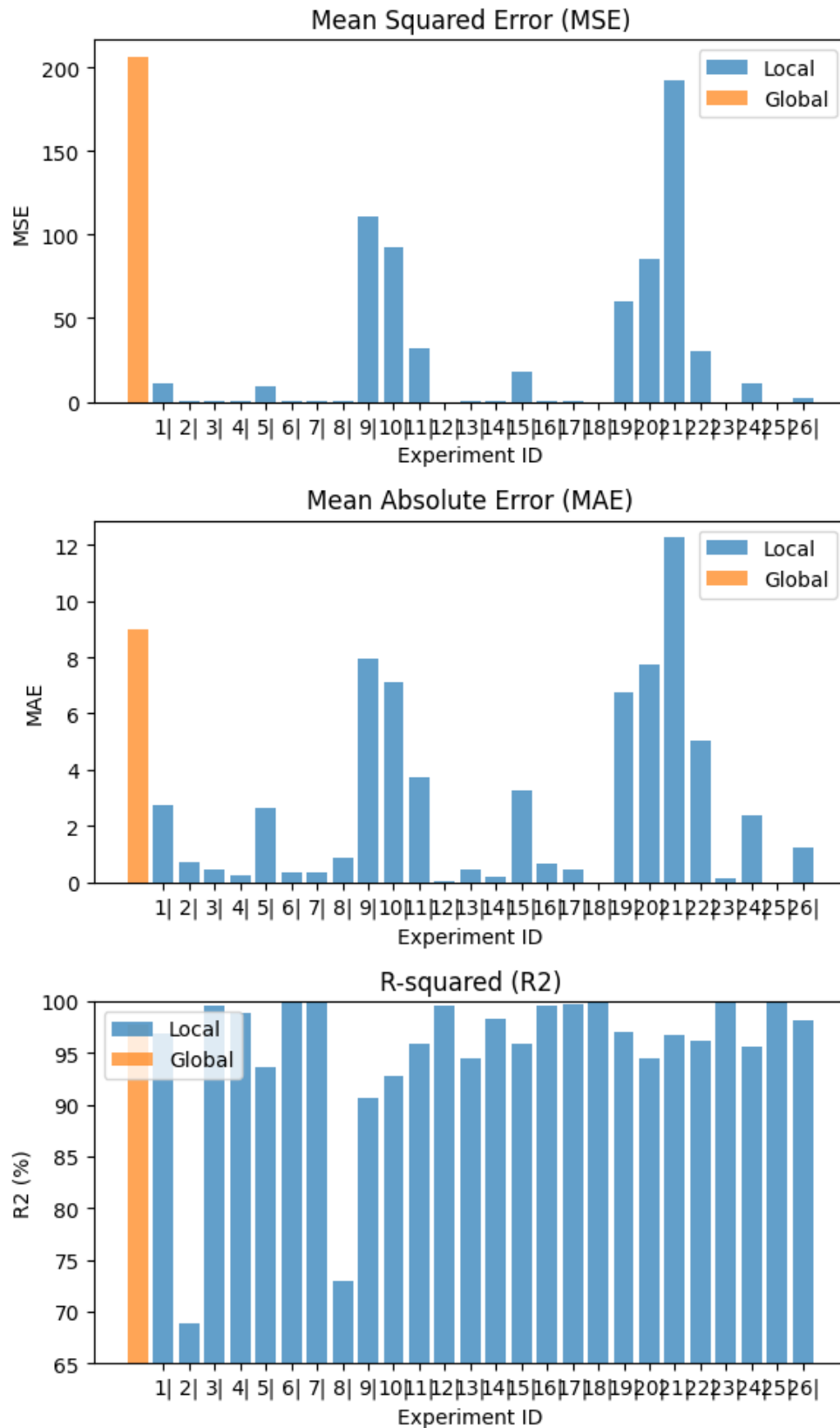


Fig. III-9 - Metrics of the PR models (Global and Local)

As stated in Table III-3, The comparisons show that the current ANN model performed better than the polynomial regression on testing data however RF model shows better results than both other models. Collectively, these metrics explain the outstanding performance of the three models in predicting torque.

Table III-3: Comparing results of polynomial regression, ANN model, and the RF model

	ANN model	RF Model	Polynomial Regression
MSE	45.97	37.13	206.19
R2	0.995	0.996	0.978
MAE	2.98	3.24	8.97
MAPE	3.85%	4.54%	21.24%
RMSE	6.78	6.09	14.36
SSE	13192.49	10656.92	59175.34

III.3.4 Artificial Shapley Additive exPlanations (SHAP)

For the Random Forest (RF) model, the mean absolute SHAP values indicate the relative importance of each input parameter in predicting torque. Notably, the parameter "RS" stands out with the highest average impact of 30.97, suggesting that variations in this parameter significantly influence torque predictions. Similarly, parameters like "R2" and "R3" exhibit considerable impacts of 16.89 and 12.70, respectively, highlighting their importance in the RF model's decision-making process. On the other hand, parameters such as "AS TS" and "RS TS" demonstrate relatively low impacts, indicating their limited influence on torque predictions within the RF model.

Conversely, for the Artificial Neural Network (ANN) model, the mean absolute SHAP values present a different pattern of parameter importance. Here, the parameter "RS" again emerges as highly impactful, with an average impact of 43.61, reinforcing its significance in determining torque values. Interestingly, parameters like "alpha" and "R3" also exhibit notable impacts, suggesting their substantial roles in the ANN's predictive capabilities. Conversely, parameters like "L1" and "AS TS" demonstrate comparatively lower impacts in the ANN model, indicating their relatively lesser influence on torque predictions within this framework.

Collectively, these mean absolute SHAP values provide valuable insights into the parameter importance for each model. While both models prioritize certain parameters such as "RS," they also differ in their emphasis on other parameters, reflecting their unique approaches to torque prediction. Understanding these nuances can inform parameter selection strategies and enhance model interpretability and performance in real-world applications.

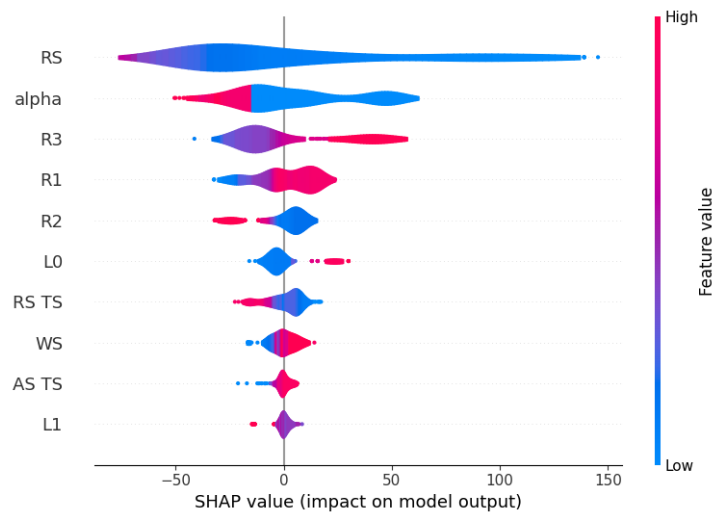


Fig. III-11 - SHAP values for the predictive ANN torque

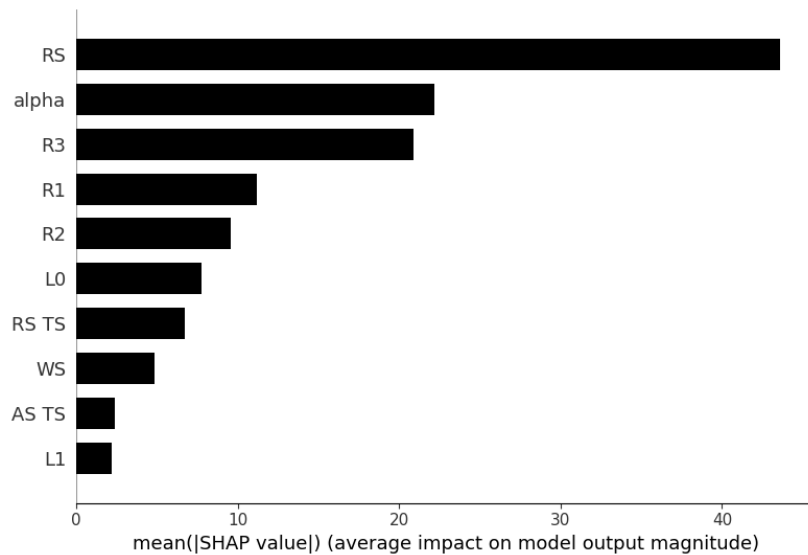


Fig. III-10 - mean absolute SHAP values for ANN.

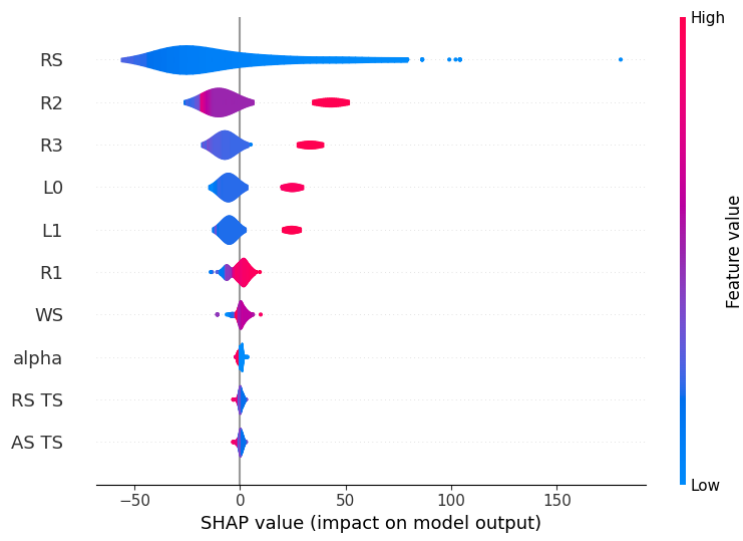


Fig. III-12 - SHAP values for the predictive RF torque model

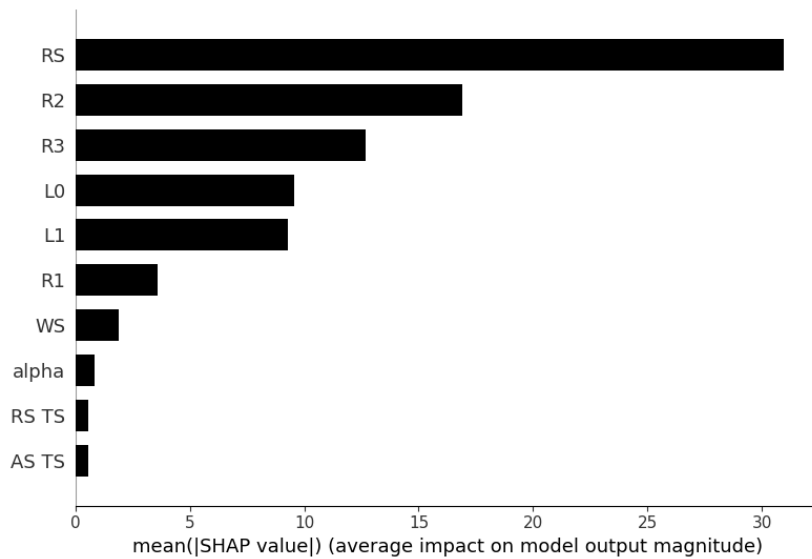


Fig. III-13 - mean absolute SHAP values for RF

Table III-4 - Absolute mean SHAP values for the impact of each parametes on the model's output

Parameters	ANN	RF
RS	43.61	30.97
WS	4.86	1.88
alpha	22.16	0.83
R1	11.22	3.59
R2	9.58	16.89
R3	20.91	12.70
L1	2.21	9.29
AS TS	2.42	0.54
RS TS	6.73	0.54
L0	7.76	9.58

The Random Forest (RF) model, known for its ensemble learning technique, showcases remarkable predictive performance across various metrics. With a Mean Absolute Percentage Error (MAPE) of 4.54% and a Root Mean Squared Error (RMSE) of 6.09, the RF model demonstrates exceptional accuracy and precision in forecasting torque values. Moreover, its impressive R^2 Score of 0.996 indicates a robust ability to explain the variance in the target variable, further reinforcing its reliability.

In contrast, the Polynomial Regression (PR) model, despite its simplicity, lags behind in predictive accuracy and precision. Its relatively high MAPE of 21.24% and RMSE of 14.36 reveal substantial discrepancies between predicted and actual values, suggesting limitations in capturing the underlying patterns in the data. While the PR model may offer interpretability, its performance metrics underscore its challenges in accurately modeling the torque requirements.

Meanwhile, the Artificial Neural Network (ANN) model demonstrates competitive performance, boasting a MAPE of 3.85% and an RMSE of 6.78. These values, although slightly inferior to the RF model, still reflect the ANN's proficiency in predicting torque values with high accuracy and precision. Furthermore, the ANN's R^2 Score of 0.995 signifies strong explanatory power, indicating its capacity to capture the complex relationships within the dataset.

Overall, while the RF model emerges as the top performer in terms of predictive accuracy and precision, the ANN model closely follows suit, underscoring its effectiveness in torque prediction. Conversely, the PR model's comparatively higher error metrics highlight its limitations in capturing the nuanced dynamics of torque data. These insights illuminate the strengths and weaknesses of each model, enabling informed decision-making in selecting the most suitable approach for torque prediction tasks.

III.4. Conclusion

This investigation into the predictive modeling of torque in friction stir welding (FSW) processes has yielded insightful findings regarding the performance of artificial neural network (ANN), random forest (RF), and polynomial regression (PR) models. Leveraging a dataset encompassing ten crucial input parameters, we meticulously evaluated the predictive capabilities of each model across diverse experimental setups.

The artificial neural network (ANN) model exhibited impressive performance metrics, with a mean absolute percentage error (MAPE) of 3.85% and a root mean squared error (RMSE) of 6.78, indicative of its high accuracy and precision in torque prediction. Furthermore, its robust explanatory power, exemplified by an R-squared (R^2) score of 0.995, underscores its efficacy in capturing the intricate relationships within the dataset.

Similarly, the random forest (RF) model emerged as a standout performer, boasting exceptional accuracy and precision with a MAPE of 4.54% and an RMSE of 6.09. Its ability to elucidate the variance in torque values, coupled with low error metrics, highlights its robustness in forecasting torque requirements across a range of experimental conditions.

Conversely, the polynomial regression (PR) model, while offering interpretability, demonstrated limitations in predictive accuracy and precision. With a relatively higher MAPE of 21.24% and an RMSE of 14.36, it struggled to capture the underlying patterns in the data, thereby hindering its effectiveness in accurately modeling torque requirements.

Our comprehensive analysis provides valuable insights for practitioners and researchers in the FSW domain. By understanding the nuanced dynamics of torque prediction, informed decisions can be made in selecting the most suitable model for specific applications.

Furthermore, the utilization of advanced machine learning techniques such as ANN and RF holds promise for enhancing process optimization and efficiency in FSW operations.

Moving forward, further research efforts could focus on refining and fine-tuning the developed models, exploring additional input parameters, and investigating the integration of advanced optimization algorithms to enhance predictive accuracy and efficiency. By continually advancing predictive modeling techniques, we can pave the way for innovation and excellence in the field of friction stir welding.

CHAPTER IV

Chapter IV - A hybrid Artificial intelligence approach for Tool and Motor Selection in a Pneumatic FSW setup

IV.1. Introduction

In the preceding chapter, we delved into the development and validation of various machine learning models using empirical data. Building upon this foundation, this chapter introduces a novel hybrid approach that integrates the power of metaheuristic algorithms, specifically the Pelican Optimization Algorithm (POA), with the previously established machine learning models. This fusion aims to optimize the FSW process by leveraging the predictive capabilities of machine learning models within the objective function of the POA. The overarching goal is to minimize power consumption while iteratively searching for the most optimal solution.

The results obtained from the POA yield a comprehensive set of values encompassing tool geometry, welding speed (WS), rotational speed (RS), torque, and power requirements for welding each of the input materials. To ensure the robustness of the approach, a diverse set of commonly used materials in FSW have been meticulously selected as our sample for optimization and search.

Ultimately, the outcomes derived from the hybridization of the POA with machine learning models, specifically pertaining to torque, rotational speed, and power, will play a pivotal role in informing decision-making processes regarding the selection of a pneumatic motor for the FSW process across the sampled materials. This demonstration of effectiveness underscores the significance of our approach in addressing the research gap concerning the identification of a suitable pneumatic motor (or rotary hand tool) for pneumatic portable FSW applications.

IV.2. Materials and Methods

IV.2.1 Materials

The sample materials selected for this study are extracted from the dataset since these materials are the commonly used materials with FSW. The welding plates are of similar and dissimilar types, each plate is represented in our modeling by its thickness and base tensile strength. Table III-1 has the list of the chosen materials for our welding configuration.

IV.2.2 Methodology

IV.2.2.1 Population initialization

The population initialization process was meticulously crafted to ensure randomness and reflect the inherent relationships between key parameters in FSW process. Each parameter's initial value were randomly selected from intervals defined by the minimum and maximum experimental values stated in Table 13, ensuring a diverse and representative starting point for the optimization process.

However, for parameters R2, R3, and L1, a more nuanced approach was employed to accurately capture their interdependencies with other parameters. Specifically, R2 and L1 were represented as ratios relative to their associated parameters, R1 and L0, respectively. For instance, R2 was expressed as the ratio $R2/R1$, leveraging the inherent relationship where R2 is always less than or equal to R1. Similarly, L1 was characterized by the ratio $L1/L0$, acknowledging the dependence of pin length on plate thickness.

Moreover, the parameter R3 was defined by the ratio $R3/R2$, acknowledging the proportional relationship between the top radius of the pin and its bottom radius due to its tapered conical shape. This tailored approach ensured that the initial population was not only randomly generated but also appropriately scaled and reflective of the intricate relationships between these critical parameters in the FSW process. By incorporating these considerations, we laid a solid foundation for the subsequent optimization process, enabling more effective exploration of the parameter space and ultimately enhancing the quality of the optimization outcomes. The intervals for the parameters are as follows:

- R1: Values ranging from 5.0 to 17.5, incremented by 0.5.
- R2: Values ranging from 17% of R1 to 67% of R1, incremented by 2%.
- R3: Values ranging from 42% of R2 to 100% of R2, incremented by 2%.
- L1: Values ranging from 50% of L0 to 100% of L0, incremented by 2%.
- alpha: Values ranging from 0.0 to 3.0, incremented by 0.5.
- WS: Values ranging from 28.0 to 1800.0, incremented by 10.0.
- RS: Values ranging from 52.41 to 2800.0, incremented by 10.0.

IV.2.2.2 Objective function

The objective function seeks to minimize power consumption within FSW process and is defined as the product of rotational speed by the torque predicted from the machine learning model (IV-1). This objective function underscores the central objective of the research: to optimize FSW parameters to achieve superior weld quality and operational efficiency, while also pinpointing the tool geometry suitable for low-power FSW.

$$P_{pred} = T_{pred} \cdot RS \cdot \frac{2\pi}{60} \quad (IV-1)$$

IV.2.2.3 Values update

To update the position of the agents, the algorithm employs techniques derived from the Pelican Optimization Algorithm framework. Specifically, the position update equations are formulated to balance exploration and exploitation, ensuring a comprehensive exploration of the solution space while also exploiting promising regions. Both the exploration and exploitation phases update equations involve stochastic mechanisms that introduce randomness into the search process, enabling the algorithm to escape local optima and discover globally optimal solutions. Through these equations, the algorithm iteratively refines the positions of the agents, gradually converging towards optimal solutions. This exploration phase plays a crucial role in the effectiveness of the optimization algorithm, allowing it to efficiently explore the solution space and identify regions with the potential for further improvement.

IV.2.2.3.1 Exploration phase:

Since the values of the parameters are derived from a prechosen set of values, our equations for updating the position of the agents represents a random method to pick a value from the prechosen ones instead of generating new ones. Equation (IV-2) shows the value updating method.

$$Pos_{exploration} = round \left(Pos_{old} + rand \cdot (Pos_{prey} - rand_2 \cdot Pos_{old}) \right) \% n \quad (IV-2)$$

$Pos_{exploration}$: the position of the value on the values vector.

$rand$: is a random real number between 0 and 1.

$rand_2$ is a random number of the set $\{1, 2\}$.

Pos_{old} : is the old position of the agent.

Pos_{prey} : is the position of the prey.

n : The number of values in the vector of values.

IV.2.2.3.2 Exploitation Phase:

In this phase each parameter is updated using the following equation:

$$Pos_{exploitation} = round(Pos_{old} + r \cdot \left(1 - \frac{i}{i_{max}}\right) \cdot (2 \cdot rand \cdot Pos_{old}) \% n \quad (IV-3)$$

$Pos_{exploration}$: the new position of the value on the values vector.

$rand$: is a real number generated randomly between 0 and 1.

Pos_{old} : old position of Pelican.

r : One of the POA parameters, in this case we consider it 0.5.

IV.3. Results and discussion

IV.3.1 POA-ANN

Fig. IV-1 depicts the iterative progression of power value prediction, While the ANN-POA hybrid model demonstrates encouraging advancements in optimizing power consumption, occasional instances of generating unrealistic predictions, such as negative values for power and torque, raise concerns regarding its reliability in certain scenarios.

The emergence of negative power and torque values suggests potential limitations or anomalies within the optimization process. These discrepancies may arise from inaccuracies in data representation, deficiencies in model training, or inherent complexities within the dynamics of the FSW system that the model may struggle to adequately address.

Despite intermittent inconsistencies, the ANN-POA hybrid model effectively achieves reductions in power consumption across successive iterations. Its capacity to identify optimization opportunities and methodically diminish power requirements represents a significant stride toward enhancing efficiency and sustainability in FSW operations.

Nevertheless, rectifying the issue of unrealistic predictions necessitates further exploration and refinement of the model. Strategies such as fine-tuning optimization algorithm parameters, augmenting data preprocessing methodologies, and implementing additional constraints or validation checks to prevent negative predictions could bolster the reliability and robustness of the ANN-POA hybrid model.

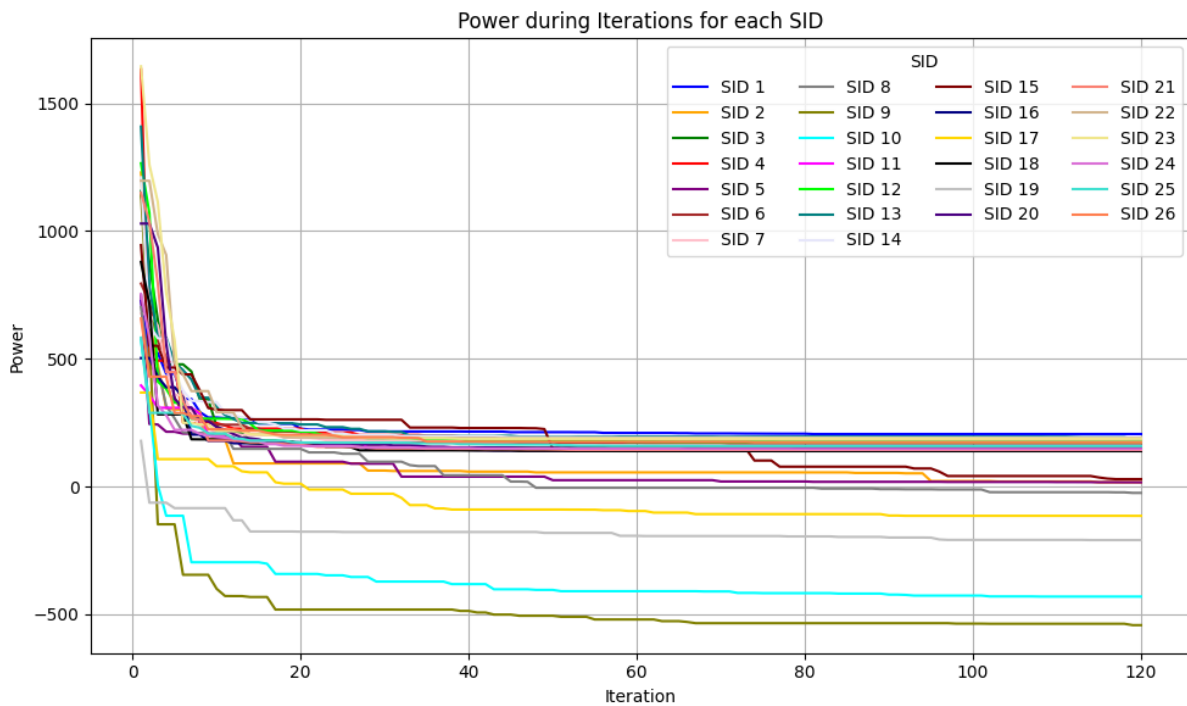


Fig. IV-1 - Power level during the iterations of the ANN-POA model

IV.3.2 POA-RF

Fig. IV-2 illustrates the progressive reduction in predicted power values across successive iterations. This evolution is indicative of the promising capability of the hybrid model, combining Random Forest (RF) with the Pelican optimization algorithm (POA), to systematically decrease power consumption. Such a trend is significant as it foreshadows the

potential for developing lighter pneumatic equipment tailored specifically for friction stir welding (FSW) operations.

The steady decline in predicted power consumption implies the model's adeptness at identifying and optimizing key parameters influencing energy usage during FSW. By leveraging the collective power of RF's predictive prowess and POA's optimization algorithms, the hybrid model effectively navigates the complex landscape of FSW dynamics, pinpointing opportunities for efficiency enhancement.

The implications of this trend extend beyond mere reduction in power consumption. Lighter pneumatic equipment translates to enhanced maneuverability and agility during FSW operations, contributing to overall process efficiency and productivity. Additionally, decreased power requirements signify potential cost savings and environmental benefits, aligning with sustainable manufacturing practices.

Moreover, the ability of the hybrid model to consistently drive down power consumption underscores its versatility and adaptability across varying operational scenarios. This adaptiveness ensures that the model remains relevant and effective in addressing evolving challenges and requirements within the FSW domain.

IV.3.3 Pneumatic motor selection

Given the fundamental characteristics of pneumatic motors, namely torque, rotational speed, and power, we can tailor our selection of pneumatic motors or rotary hand tools to suit each welding scenario. Power estimation can be approximated using the equation below [31]:

$$Q_{FS} = P_{Tool} = M\omega + F_x v \approx M\omega \quad (IV-4)$$

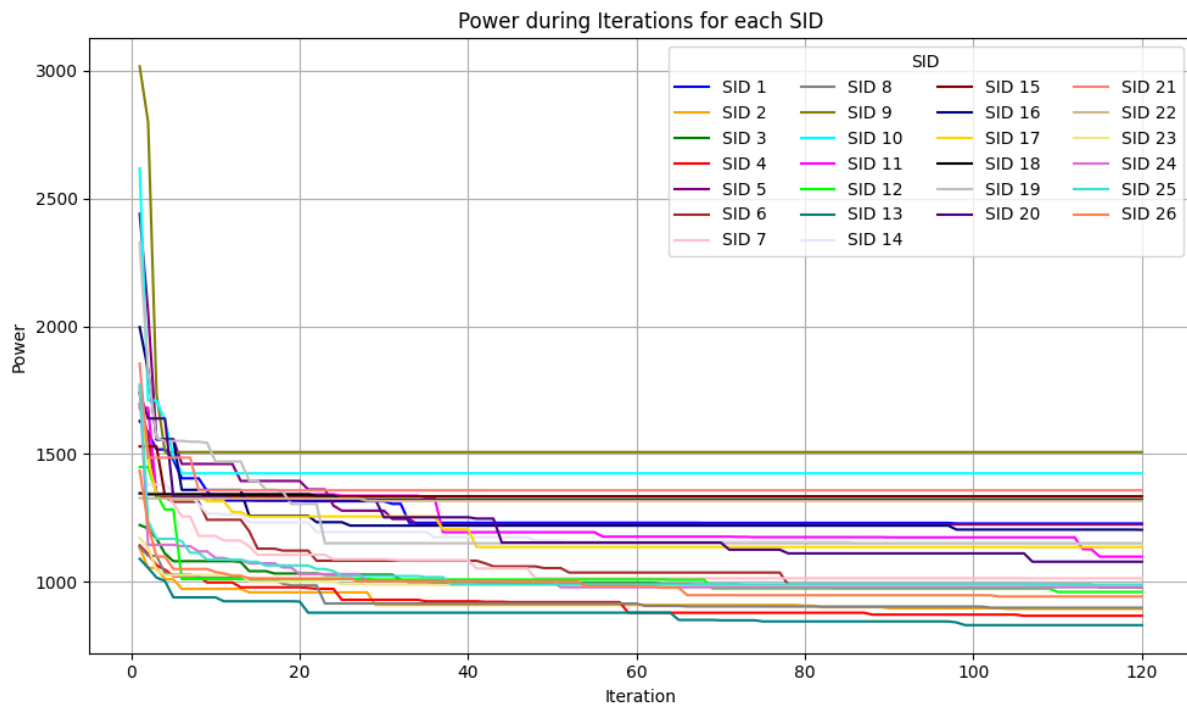


Fig. IV-2 - Power level during iterations of RF-POA

In light of the underperformance of polynomial regression and the occasional occurrence of unrealistic values with the ANN model, a strategic decision has been made to place our reliance on the RF-POA approach for the final outcomes. The values attained by RF-POA, as detailed in Table IV-2, offer a comprehensive reference for users of pneumatic FSW setups or machines. This dataset serves as an invaluable resource, guiding users in the selection of optimal motors or rotary hand tools and FSW equipment tailored to their specific welding requirements, accounting for material compositions and thicknesses. Furthermore, our study extends invaluable recommendations concerning the ideal parameter levels, including welding speed (WS), tilt angle, and rotational speeds, custom-fitted to meet the demands of each unique application.

Yet, the significance of our research extends beyond mere data aggregation. It marks the culmination of a robust hybrid machine learning model, blending the predictive prowess of Random Forest (RF) algorithms with the sophisticated optimization capabilities of the Pelican optimization algorithm. This synergistic fusion not only ensures accurate predictions but also enables efficient parameter optimization, elevating welding performance and productivity.

Table IV-1 - ANN-POA Optimal parameters for selection of pneumatic FSW motor (hand tool) and FSW tool geometry

SID	Tool geometry				Process Parameters		Motor characteristics		
	R1	R2	R3	Pin Length	Tilt Angle	WS	RS	Torque	$\approx P_{Tool}$
1	5.00	3.35	1.41	5.50	2.00	580.00	52.41	37.47	205.63
2	5.00	1.55	1.46	6.00	1.50	610.00	2800.00	0.06	17.20
3	5.00	3.35	1.41	6.00	2.50	28.00	52.41	27.46	150.71
4	5.00	3.35	1.41	5.00	2.00	540.00	52.41	33.61	184.46
5	5.00	0.85	0.75	9.50	2.00	250.00	2560.00	0.06	16.74
6	5.00	3.35	1.41	3.00	1.50	690.00	52.41	30.86	169.38
7	5.00	3.35	1.41	3.00	1.00	160.00	52.41	32.75	179.73
8	5.00	1.25	0.93	6.00	1.50	590.00	2800.00	-0.08	-24.64
9	5.00	0.85	0.48	23.04	3.00	780.00	2800.00	-1.85	-542.20
10	5.00	2.25	0.95	24.50	3.00	670.00	2800.00	-1.47	-430.46
11	5.00	3.35	1.41	5.46	2.50	28.00	52.41	25.68	140.96
12	5.00	3.35	1.41	3.00	1.00	800.00	52.41	31.77	174.36
13	5.00	2.85	1.25	3.50	1.50	790.00	52.41	34.25	187.95
14	5.00	3.35	1.41	2.00	1.00	900.00	52.41	34.85	191.24
15	5.00	2.25	2.07	8.00	2.50	50.00	2800.00	0.10	29.17
16	5.00	3.35	1.41	6.46	3.00	28.00	52.41	25.55	140.22
17	5.00	0.85	0.46	9.50	1.50	540.00	2750.00	-0.40	-114.56
18	5.00	3.35	1.41	6.05	2.50	28.00	52.41	25.31	138.93
19	5.00	0.85	0.43	9.50	2.50	550.00	2800.00	-0.71	-209.29
20	5.00	3.35	1.41	5.98	2.50	28.00	52.41	27.42	150.48
21	5.00	3.35	1.41	6.27	3.00	28.00	52.41	26.20	143.81
22	5.00	1.65	0.69	3.20	0.50	28.00	52.41	34.55	189.60
23	5.00	1.75	0.74	2.95	0.50	28.00	52.41	34.13	187.31
24	5.00	3.35	1.41	3.50	2.00	28.00	52.41	26.76	146.86
25	5.00	3.35	1.41	5.88	2.00	28.00	52.41	28.96	158.93
26	5.00	3.35	1.41	3.29	1.00	790.00	52.41	31.60	173.42

Table IV-2 - RF-POA Optimum parameters for selection of pneumatic FSW motor (hand tool) and FSW tool geometry

SID	Tool geometry				Process Parameters		Motor characteristics		
	R1	R2	R3	Pin Length	Tilt Angle	WS	RS	Torque	$\approx P_{Tool}$
1	5.50	2.20	2.07	3.71	0.50	28.00	710.00	16.52	1228.01

2	5.00	2.20	2.11	3.84	0.00	100.00	600.00	14.23	893.89
3	5.00	2.10	2.10	4.20	0.50	50.00	710.00	13.26	985.73
4	5.00	2.20	1.80	3.60	0.50	130.00	600.00	13.79	866.72
5	5.00	1.50	1.50	4.75	2.00	28.00	330.00	35.43	1224.28
6	5.00	2.20	2.11	2.88	0.00	80.00	600.00	15.56	977.69
7	5.50	1.54	1.14	3.00	0.50	50.00	600.00	16.13	1013.53
8	5.00	2.20	2.11	3.72	0.00	100.00	600.00	14.30	898.50
9	6.00	1.68	0.84	24.96	1.00	210.00	52.41	274.67	1507.50
10	6.50	1.69	1.62	12.50	0.00	210.00	52.41	259.52	1424.33
11	5.00	3.30	2.64	4.19	2.00	40.00	330.00	31.78	1098.14
12	5.50	2.09	2.09	3.00	0.00	660.00	600.00	15.28	960.14
13	5.00	2.20	1.80	3.80	0.00	110.00	600.00	13.21	830.20
14	5.00	2.20	2.07	2.00	0.00	100.00	600.00	18.29	1148.99
15	7.00	2.38	1.43	4.48	1.00	140.00	52.41	243.17	1334.60
16	5.00	1.10	0.62	5.13	2.00	40.00	330.00	34.82	1203.23
17	6.50	2.86	2.17	5.51	3.00	30.00	330.00	32.87	1136.00
18	5.50	0.99	0.53	3.40	0.50	40.00	710.00	17.78	1321.92
19	5.50	3.19	2.17	4.75	1.50	30.00	330.00	33.30	1150.70
20	5.00	2.50	2.20	4.15	2.00	40.00	330.00	31.21	1078.38
21	7.50	1.50	1.44	4.75	0.50	150.00	52.41	247.39	1357.75
22	5.50	1.10	0.51	3.20	0.50	40.00	710.00	17.71	1316.92
23	5.00	2.10	1.93	3.78	0.50	30.00	710.00	13.23	983.81
24	5.50	2.20	1.94	3.36	0.50	50.00	600.00	15.57	978.35
25	5.00	2.20	1.94	3.60	0.00	50.00	710.00	13.30	988.69
26	5.00	2.10	1.97	3.85	0.00	300.00	600.00	15.00	942.17

IV.4. Conclusion

This chapter has introduced a novel hybrid approach for tool and motor selection in pneumatic Friction Stir Welding (FSW) setups, integrating metaheuristic algorithms with machine learning models to optimize power consumption. Through meticulous methodology and rigorous exploration, we have demonstrated the potential of this approach to drive innovation and sustainability in pneumatic FSW technology.

The results of our hybridization efforts, particularly with the POA-RF model, have shown promising advancements in reducing power consumption, paving the way for lighter pneumatic equipment tailored for FSW operations. However, occasional inconsistencies observed with

the ANN-POA hybrid model underscore the need for ongoing refinement and validation to ensure reliability and effectiveness.

Looking ahead, future research endeavors will focus on addressing these challenges while exploring additional optimization strategies and incorporating more comprehensive datasets. By continuously refining our approach and embracing innovation, we can unlock the full potential of pneumatic FSW technology, driving efficiency, productivity, and sustainability in manufacturing processes.

Furthermore, the development of software integrating our model will streamline its practical application, enhancing its predictive capacities and positioning it as an indispensable asset in the field. By leveraging the collective power of machine learning and optimization algorithms, we can propel the pneumatic FSW industry forward, ushering in a new era of excellence and advancement.

This chapter marks a significant step forward in the quest to optimize FSW processes, laying the groundwork for future innovations and discoveries. With dedication, collaboration, and a commitment to excellence, we can revolutionize pneumatic FSW technology and shape the future of manufacturing.

GENERAL CONCLUSION

GENERAL CONCLUSION

This thesis culminates in a comprehensive exploration of friction stir welding (FSW) processes, with a primary focus on optimizing efficiency and minimizing power consumption through the integration of pneumatic sources. Structured across four chapters, the study navigates through theoretical foundations, methodological frameworks, predictive modeling endeavors, and innovative optimization techniques, ultimately offering insights and solutions that propel FSW technology into new frontiers.

The journey begins with an in-depth examination of FSW fundamentals, emphasizing the transformative potential of pneumatic sources in enhancing portability and energy efficiency. This foundational understanding sets the stage for subsequent investigations into predictive modeling and optimization strategies tailored for pneumatic FSW applications.

In the methodology chapter, a multifaceted approach emerges, integrating advanced machine learning techniques such as artificial neural networks (ANN) and random forest (RF) algorithms with innovative optimization algorithms like the Pelican Optimization Algorithm (POA). This synergistic fusion enables the development of predictive models capable of forecasting torque and power consumption in FSW operations, while the POA facilitates the identification of optimum parameter configurations that minimize energy consumption and enhance efficiency.

The validation of these models in the predictive modeling chapter underscores their efficacy and reliability, with impressive performance metrics and robust explanatory power. However, occasional inconsistencies observed with certain hybrid models necessitate ongoing refinement and validation efforts to ensure their reliability and effectiveness in real-world applications.

In the final chapter, a novel hybrid approach emerges, leveraging metaheuristic algorithms with machine learning models to optimize power consumption and streamline tool and motor selection in pneumatic FSW setups. The outcomes of this hybridization effort demonstrate promising advancements in reducing power consumption, while also addressing the critical need for portability in welding operations. By integrating pneumatic sources, the thesis not

only contributes to efficiency and sustainability but also enhances flexibility and mobility in modern welding applications.

Looking ahead, future research endeavors will focus on addressing remaining challenges, refining optimization strategies, and embracing innovation to unlock the full potential of pneumatic FSW technology. The development of software integrating predictive models will further enhance their practical application, positioning them as indispensable assets in the field of manufacturing.

In essence, this thesis marks a significant milestone in the quest to optimize FSW processes, offering a holistic framework that combines theoretical insights with practical solutions. By embracing interdisciplinary approaches and fostering collaboration, we can revolutionize pneumatic FSW technology and shape the future of welding in manufacturing.

REFERENCES

REFERENCES

- [1] J. P. Davim, Ed., *Welding Technology*. in Materials Forming, Machining and Tribology. Cham: Springer International Publishing, 2021. doi: 10.1007/978-3-030-63986-0.
- [2] R. Mishra and Y. Ma, "Friction stir welding and processing," *Material Science and Engineering R*, vol. 50, pp. 1–78, 2005.
- [3] A. Halfpenny, "A practical discussion on fatigue," in *Managing Durability*, 2008.
- [4] A. Bachmann, M. Roehler, S. J. Pieczona, M. Kessler, and M. F. Zaeh, "Torque-based adaptive temperature control in friction stir welding: a feasibility study," *Production Engineering*, vol. 12, no. 3–4, pp. 391–403, 2018, doi: 10.1007/s11740-018-0798-z.
- [5] L. Trueba, G. Heredia, D. Rybicki, and L. Johannes, "Effect of tool shoulder features on defects and tensile properties of friction stir welded aluminum 6061-T6," *J Mater Process Technol*, vol. 219, pp. 271–277, 2015.
- [6] M. Hiten and M. Shalin, "A Review Paper on: Friction Stir Welding (FSW)," *International Journal of Advanced Research in Engineering Science & Management*, pp. 1–13, 2017.
- [7] F. Shahid, "Mechanical and Microstructural Analysis of Dissimilar," vol. 25, no. October, pp. 6–14, 2015.
- [8] A. Farias, G. F. Batalha, E. F. Prados, R. Magnabosco, and S. Delijaicov, "Tool wear evaluations in friction stir processing of commercial titanium Ti-6Al-4V," *Wear*, vol. 302, no. 1–2, pp. 1327–1333, 2013.
- [9] Y. N. Zhang, X. Cao, S. Larose, and P. Wanjara, "Review of tools for friction stir welding and processing," *Can. Metall. Q.*, vol. 51, no. 3, pp. 250–261, 2012.
- [10] S. K. Selvam and T. P. Pillai, "Analysis of heavy alloy tool in friction stir welding," *Int. J. ChemTech Res.*, vol. 5, no. 3, pp. 1346–1358, 2013.
- [11] K. Chiteka, "Friction Stir Welding/Processing Tool Materials and Selection," vol. 2, no. 11, pp. 8–18, 2013.
- [12] R. Rai, A. De, H. Bhadeshia, and T. DebRoy, "Review: friction stir welding tools," *Sci. Technol. Weld. Join.*, vol. 16, no. 4, pp. 325–342, 2011.
- [13] X. He, F. Gu, and A. Ball, "Progress in Materials Science A review of numerical analysis of friction stir welding," *Prog. Mater. Sci.*, vol. 65, pp. 1–66, 2014.
- [14] M. Mehta, G. M. Reddy, A. V Rao, and A. De, "Numerical modeling of friction stir welding using the tools with polygonal pins," *Def. Technol.*, vol. 11, no. 3, pp. 229–236, 2015.
- [15] M. H. Tolephih, K. M. Mashloosh, and Z. Waheed, "Comparative Study of the Mechanical Properties of (FS) and MIG Welded Joint in (AA7020-T6) Aluminum Alloy," *Al-Khwarizmi Eng. J.*, vol. 7, no. 2, pp. 22–35, 2011.
- [16] H. Liu, K. Nakata, N. Yamamoto, and J. Liao, "Grain Orientation and Texture Evolution in Pure Titanium Lap Joint Produced by Friction Stir Welding," vol. 51, no. 11, pp. 2063–2068, 2010.
- [17] Y. Gao, T. Tsumura, and K. Nakata, "Dissimilar welding of titanium alloys to steels," *Trans. JWRI*, vol. 41, no. 2, pp. 7–12, 2012.
- [18] "Joining of CP-Ti to 304 stainless steel using friction stir welding technique," *Mater.Des.*, vol. 31, no. 10, pp. 4800–4807, 2010.
- [19] K. Ishida, Y. Gao, K. Nagatsuka, M. Takahashi, and K. Nakata, "Microstructures and mechanical properties of friction stir welded lap joints of commercially pure titanium and 304 stainless steel," *J. Alloys Compd.*, vol. 630, pp. 172–177, 2015.
- [20] M. S. Sidhu and S. S. Chatha, "Friction Stir Welding—Process and its Variables : A Review," *Int. J. Emerg. Technol. Adv. Eng.*, vol. 2, no. 12, pp. 275–279, 2012.
- [21] S. S. Sengar and J. Kumar, "A study of recent trends in friction stir welding," *Int. J. Emerg. Technol. Adv. Eng.*, vol. 2, no. 12, pp. 646–649, 2012.
- [22] S. Pervaiz, A. Rashid, I. Deiab, and M. Nicolescu, "Influence of Tool Materials on Machinability of Titanium- and Nickel-Based Alloys: A Review," *Mater. Manuf. Process.*, vol. 29, no. 3, pp. 219–252, 2014.
- [23] K. S. C. H. Muralimohan, "Properties of Friction Welding Titanium-stainless Steel Joints with a Nickel Interlayer," *Procedia Mater. Sci.*, vol. 5, pp. 1120–1129, 2014.
- [24] M. P. Meshram, B. K. Kodli, and S. R. Dey, "Friction Stir Welding of Austenitic Stainless Steel by PCBN Tool and its Joint Analyses," *Procedia Mater. Sci.*, vol. 6, no. Icmpe, pp. 135–139, 2014.

- [25] M. Khandkar, J. Khan, and A. Reynolds, "Prediction of temperature distribution and thermal history during friction stir welding: input torque based model," *Sci Technol Weld Join*, vol. 8, no. 3, pp. 165–174, 2003, [Online]. Available: <http://dx.doi.org/10.1179/136217103225010943>
- [26] H. Schmidt, J. Hattel, and J. Wert, "An analytical model for the heat generation in friction stir welding," *Modell Simul Mater Sci Eng*, vol. 12, no. 1, pp. 143–157, 2004, [Online]. Available: <http://dx.doi.org/10.1088/0965-0393/12/1/013>
- [27] J. W. Pew, T. W. Nelson, and C. D. Sorensen, "Torque based weld power model for friction stir welding," *Sci Technol Weld Join*, vol. 12, no. 4, pp. 341–347, 2007, [Online]. Available: <http://dx.doi.org/10.1179/174329307X197601>
- [28] J. Yan, M. Sutton, and A. Reynolds, "Process–structure–property relationships for nugget and heat affected zone regions of AA2524-T351 friction stir welds," *Sci Technol Weld Join*, vol. 10, no. 6, pp. 725–736, 2005, [Online]. Available: <http://dx.doi.org/10.1179/174329305X68778>
- [29] T. Long, W. Tang, and A. Reynolds, "Process response parameter relationships in aluminium alloy friction stir welds," *Sci Technol Weld Join*, vol. 12, no. 4, pp. 311–317, 2007, [Online]. Available: <http://dx.doi.org/10.1179/174329307X197566>
- [30] P. Upadhyay and A. P. Reynolds, "Effects of thermal boundary conditions in friction stir welded AA7050-T7 sheets," *Mater Sci Eng A*, vol. 527, no. 6, pp. 1537–1543, 2010, [Online]. Available: <http://dx.doi.org/10.1016/j.msea.2009.10.039>
- [31] S. Cui, Z. W. Chen, and J. D. Robson, "A model relating tool torque and its associated power and specific energy to rotation and forward speeds during friction stir welding/processing," *Int J Mach Tools Manuf*, vol. 50, no. 12, pp. 1023–1030, 2010, [Online]. Available: <http://dx.doi.org/10.1016/j.ijmachtools.2010.09.005>
- [32] C. Leitao, R. Louro, and D. M. Rodrigues, "Using torque sensitivity analysis in accessing friction stir welding/processing conditions," *J Mater Process Technol*, vol. 212, no. 10, pp. 2051–2057, 2012, [Online]. Available: <http://dx.doi.org/10.1016/j.jmatprotec.2012.05.009>
- [33] R. Kumar, K. Singh, and S. Pandey, "Process forces and heat input as function of process parameters in AA5083 friction stir welds," *Trans Nonferrous Met Soc China*, vol. 22, no. 2, pp. 288–298, 2012, [Online]. Available: [http://dx.doi.org/10.1016/S1003-6326\(11\)61173-4](http://dx.doi.org/10.1016/S1003-6326(11)61173-4)
- [34] H. Su, C. S. Wu, A. Pittner, and M. Rethmeier, "Simultaneous measurement of tool torque, traverse force and axial force in friction stir welding," *J Manuf Proc*, vol. 15, no. 4, pp. 495–500, 2013, [Online]. Available: <http://dx.doi.org/10.1016/j.jmapro.2013.09.001>
- [35] K. J. Quintana Cuellar and J. L. L. Silveira, "Analysis of torque in friction stir welding of aluminum alloy 5052 by inverse problem method," *J. Manuf. Sci. Eng.*, vol. 139, no. 4, p. 41017, 2017.
- [36] A. Arora, R. Nandan, A. Reynolds, and P. DebRoy, "Torque, power requirement and stir zone geometry in friction stir welding through modeling and experiments," *Scr Mater*, vol. 60, no. 1, pp. 13–16, 2009, [Online]. Available: <http://dx.doi.org/10.1016/j.scriptamat.2008.08.015>
- [37] Z. Zhang and H. W. Zhang, "Solid mechanics-Based Eulerian model of friction stir welding," *Int J Adv Manuf Technol*, vol. 72, no. 9, pp. 1647–1653, 2014, [Online]. Available: <http://dx.doi.org/10.1007/s00170-014-5789-4>
- [38] W. R. Longhurst, A. M. Strauss, G. E. Cook, and P. A. Fleming, "Torque control of friction stir welding for manufacturing and automation," *Int. J. Adv. Manuf. Technol.*, vol. 51, pp. 905–913, 2010, [Online]. Available: <http://dx.doi.org/10.1007/s00170-010-2678-3>
- [39] W. R. Longhurst, A. M. Strauss, and G. E. Cook, "Enabling automation of friction stir welding: the modulation of weld seam input energy by traverse speed force control," *J. Dyn. Syst. Meas. Control.*, vol. 132, no. 041002, 2010, [Online]. Available: <http://dx.doi.org/10.1115/1.4001795>
- [40] Y. Okawa, M. Taniguchi, H. Sugii, and Y. Marutani, "Development of 5-axis friction stir welding system," in *SICE-ICASE Int. Jt. Conf.*, 2006, pp. 1266–1269. [Online]. Available: <http://dx.doi.org/10.1109/SICE.2006.315435>
- [41] C. B. Smith, "Robotic friction stir welding using a standard industrial robot," in *2nd Frict. Stir Weld. Int. Symp.*, Gothenburg, Sweden, 2000.
- [42] M. Soron and I. Kalaykov, "A robot prototype for friction stir welding," in *2006 IEEE Conf. Robot. Autom. Mechatronics*, 2006, pp. 1–5. [Online]. Available: <http://dx.doi.org/10.1109/RAMECH.2006.252646>
- [43] N. Mendes, P. Neto, M. A. Simão, A. Loureiro, and J. N. Pires, "A novel friction stir welding robotic platform: welding polymeric materials," *Int. J. Adv. Manuf. Technol.*, 2014, [Online]. Available: <http://dx.doi.org/10.1007/s00170-014-6024-z>
- [44] T. Minton and D. J. Mynors, "Utilisation of engineering workshop equipment for friction stir welding," *J. Mater. Process. Technol.*, vol. 177, pp. 336–339, 2006, [Online]. Available: <http://dx.doi.org/10.1016/j.jmatprotec.2006.03.227>

- [45] W. R. Longhurst, A. M. Strauss, G. E. Cook, C. D. Cox, C. E. Hendricks, and B. T. Gibson, "Investigation of force-controlled friction stir welding for manufacturing and automation," *Proc. Inst. Mech. Eng. B J. Eng. Manuf.*, vol. 224, pp. 937–949, 2010, [Online]. Available: <http://dx.doi.org/10.1243/09544054JEM1709>
- [46] B. J. De, "Robotic Friction Stir Welding for Flexible Production," Lund University, 2012.
- [47] R. J. Steel, S. M. Packer, R. D. Fleck, S. Sanderson, and C. Tucker, "Proceedings of the 1st International Joint Symposium on Joining and Welding," in *Proc. 1st Int. Jt. Symp. Join. Weld.*, Elsevier, 2013, pp. 125–127. [Online]. Available: <http://dx.doi.org/10.1533/978-1-78242-164-1.125>
- [48] N. Ku, S. Ha, and M.-I. Roh, "Design of controller for mobile robot in welding process of shipbuilding engineering," *J. Comput. Des. Eng.*, vol. 1, pp. 243–255, 2014, [Online]. Available: <http://dx.doi.org/10.1016/j.jcde.2014.07.002>
- [49] O. Marcotte and L. Vanden-Abeelee, "2d and 3d friction stir welding with articulated robot arm," in *8th Int. Symp. Frict. Stir Weld.*, 2010, pp. 778–797.
- [50] X. Zhao, P. Kalya, R. G. Landers, and K. Krishnamurthy, "Design and implementation of a nonlinear axial force controller for friction stir welding processes," in *2007 Am. Control conf.*, 2007, pp. 5553–5558. [Online]. Available: <http://dx.doi.org/10.1109/ACC.2007.4282731>
- [51] E. F. Shultz, A. Fehrenbacher, F. E. Pfefferkorn, M. R. Zinn, and N. J. Ferrier, "Shared control of robotic friction stir welding in the presence of imperfect joint fit-up," *J. Manuf. Process.*, vol. 15, pp. 25–33, 2013, [Online]. Available: <http://dx.doi.org/10.1016/j.jmapro.2012.07.002>
- [52] P. Wanjara, B. Monsarrat, and S. Larose, "Gap tolerance allowance and robotic operational window for friction stir butt welding of AA6061," *J. Mater. Process. Technol.*, vol. 213, pp. 631–640, 2013, [Online]. Available: <http://dx.doi.org/10.1016/j.jmatprotec.2012.10.010>
- [53] J. F. Hinrichs, C. B. Smith, B. F. Orsini, R. J. DeGeorge, B. J. Smale, and P. C. Ruehl, "Friction stir welding for the 21st century automotive industry," in *Fifth Int. Conf. Frict. Stir Weld.*, 2004, pp. 1–13.
- [54] N. Mendes, P. Neto, A. Loureiro, and A. P. Moreira, "Machines and control systems for friction stir welding: A review," *Mater Des*, vol. 90, pp. 256–265, 2016, [Online]. Available: <https://doi.org/10.1016/j.matdes.2015.10.124>
- [55] L. M. Marzoli, A. V. Strombeck, J. F. Dos Santos, C. Gambaro, and L. M. Volpone, "Friction stir welding of an AA6061/Al2O3/20p reinforced alloy," *Compos. Sci. Technol.*, vol. 66, pp. 363–371, 2006, [Online]. Available: <http://dx.doi.org/10.1016/j.compscitech.2005.04.048>
- [56] J. Shi, Y. Wang, G. Zhang, and H. Ding, "Optimal design of 3-DOF PKM module for friction stir welding," *Int. J. Adv. Manuf. Technol.*, vol. 66, pp. 1879–1889, 2012, [Online]. Available: <http://dx.doi.org/10.1007/s00170-012-4467-7>
- [57] R. Al-Sabur, M. Serier, and A. N. Siddiquee, "Analysis and construction of a pneumatic-powered portable friction stir welding tool for polymer joining," *Advances in Materials and Processing Technologies*, pp. 1–15, Jan. 2023, doi: 10.1080/2374068X.2023.2173769.
- [58] Y. LeCun, Y. Bengio, and G. Hinton, "Deep learning," *Nature*, vol. 521, no. 7553, p. 436, 2015.
- [59] L. Deng and D. Yu, "Deep learning: methods and applications," *Foundations and Trends in Signal Processing*, vol. 7, no. 3–4, pp. 197–387, 2014.
- [60] L. Deng, "Three classes of deep learning architectures and their applications: a tutorial survey," *APSIPA Trans Signal Inf Process*, 2012.
- [61] J. Schmidhuber, "Deep learning in neural networks: an overview," *Neural Netw.*, vol. 61, pp. 85–117, 2015, doi: 10.1016/j.neunet.2014.09.003.
- [62] N. Bhatia and M. C. Rana, "Deep learning techniques and its various algorithms and techniques," *Int. J. Eng. Innov. Res.*, vol. 4, no. 5, 2015.
- [63] D. Dhall, R. Kaur, and M. Juneja, "Machine learning: a review of the algorithms and its applications," *Proceedings of ICRIC 2019: Recent Innovations in Computing*, pp. 47–63, 2020.
- [64] R. Kaur, M. Juneja, and A. K. Mandal, "A comprehensive review of denoising techniques for abdominal CT images," *Multimedia Tools Appl.*, vol. 77, no. 17, pp. 22735–22770, 2018.
- [65] H. Sadeeq and A. M. Abdulazeez, "Hardware implementation of firefly optimization algorithm using FPGA," in *ICOASE 2018 – Int. Conf. Adv. Sci. Eng.*, 2018, pp. 30–35. [Online]. Available: <https://doi.org/10.1109/ICOASE.2018.8548822>
- [66] S. M. Almufti, R. B. Marqas, P. S. Othman, and A. B. Sallow, "Single-based and population-based metaheuristics for solving np-hard problems," *Iraqi J. Sci.*, vol. 62, no. 5, pp. 1710–1720, 2021, [Online]. Available: <https://doi.org/10.24996/ijsc.2021.62.5.34>
- [67] H. S. Yahia and A. S. Mohammed, "Path planning optimization in unmanned aerial vehicles using meta-heuristic algorithms: A systematic review," *Environ. Monit. Assess.*, vol. 195, no. 1, 2023, [Online]. Available: <https://doi.org/10.1007/s10661-022-10590-y>

- [68] A. S. Issa, Y. H. Ali, and T. A. Rashid, "An efficient hybrid classification approach for COVID-19 based on Harris Hawks optimization and Salp Swarm optimization," *Int. J. online Biomed. Eng.*, vol. 18, no. 13, pp. 113–130, 2022, [Online]. Available: <https://doi.org/10.3991/ijoe>.
- [69] H. T. Sadeeq and A. M. Abdulazeez, "Improved Northern Goshawk Optimization Algorithm for Global Optimization," in *2022 4th International Conference on Advanced Science and Engineering (ICOASE)*, IEEE, Sep. 2022, pp. 89–94. doi: 10.1109/ICOASE56293.2022.10075576.
- [70] H. Sadeeq, A. Abdulazeez, N. Kako, and A. Abraham, "A Novel Hybrid Bird Mating Optimizer with Differential Evolution for Engineering Design Optimization Problems," in *Lect. Notes Data Eng. Commun. Technol.*, vol. 5, 2018, pp. 522–534. doi: 10.1007/978-3-319-59427-9_55.
- [71] H. T. Sadeeq, A. M. Abdulazeez, N. A. Kako, D. A. Zebari, and D. Q. Zeebaree, "A New Hybrid Method for Global Optimization Based on the Bird Mating Optimizer and the Differential Evolution," in *2021 7th International Engineering Conference "Research & Innovation amid Global Pandemic" (IEC)*, IEEE, Feb. 2021, pp. 54–60. doi: 10.1109/IEC52205.2021.9476147.
- [72] B. M. Abed and W. M. Jasim, "Multi Objective Optimization Algorithms for Mobile Robot Path Planning: A Survey," *International Journal of Online and Biomedical Engineering (iJOE)*, vol. 18, no. 15, pp. 160–177, Dec. 2022, doi: 10.3991/ijoe.v18i15.34397.
- [73] S. Kochhar and R. Garg, "Spectrum Sensing for Cognitive Radio Using Genetic Algorithm," *International Journal of Online Engineering (iJOE)*, vol. 14, no. 09, p. 190, Sep. 2018, doi: 10.3991/ijoe.v14i09.9064.
- [74] A. S. Eesa, A. M. Abdulazeez, and Z. Orman, "Cuttlefish algorithm – A novel bio-inspired," *Int. J. Sci. Eng. Res.*, vol. 4, no. 9, pp. 1978–1986, 2013.
- [75] A. S. Eesa, A. Mohsin, A. Brifcani, and Z. Orman, "A new tool for global optimization problems- Cuttlefish algorithm," 2014.
- [76] C. Blum and A. Roli, "Metaheuristics in combinatorial optimization: Overview and conceptual comparison," *ACM Comput. Surv.*, vol. 35, no. 3, pp. 268–308, 2003, doi: 10.1145/937503.937505.
- [77] X.-S. Yang, *Nature-inspired metaheuristic algorithms*. 2010.
- [78] J. Xu and J. Zhang, "Exploration-exploitation tradeoffs in metaheuristics: Survey and analysis," in *Proc. 33rd Chinese Control Conf. CCC 2014*, 2014, pp. 8633–8638. doi: 10.1109/ChiCC.2014.6896450.
- [79] K. Hussain, M. N. M. Salleh, S. Cheng, and Y. Shi, "On the exploration and exploitation in popular swarm-based metaheuristic algorithms," *Neural Comput Appl*, vol. 31, no. 11, pp. 7665–7683, Nov. 2019, doi: 10.1007/s00521-018-3592-0.
- [80] A. Darwish, "Bio-inspired computing: Algorithms review, deep analysis, and the scope of applications," *Future Computing and Informatics Journal*, vol. 3, no. 2, pp. 231–246, Dec. 2018, doi: 10.1016/j.fcij.2018.06.001.
- [81] H. T. Sadeeq and A. M. Abdulazeez, "Metaheuristics: A Review of Algorithms," *International Journal of Online and Biomedical Engineering (iJOE)*, vol. 19, no. 09, pp. 142–164, Jul. 2023, doi: 10.3991/ijoe.v19i09.39683.
- [82] Q. Li, Y. Bai, and W. Gao, "Improved Initialization Method for Metaheuristic Algorithms: A Novel Search Space View," *IEEE Access*, vol. 9, pp. 121366–121384, 2021, doi: 10.1109/ACCESS.2021.3073480.
- [83] C. Zhong, G. Li, and Z. Meng, "Beluga whale optimization: A novel nature-inspired metaheuristic algorithm," *Knowl Based Syst*, vol. 251, p. 109215, Sep. 2022, doi: 10.1016/j.knosys.2022.109215.
- [84] P. Trojovský and M. Dehghani, "Pelican Optimization Algorithm: A Novel Nature-Inspired Algorithm for Engineering Applications," *Sensors*, vol. 22, no. 3, p. 855, Jan. 2022, doi: 10.3390/s22030855.
- [85] H. T. Sadeeq and A. M. Abdulazeez, "Giant Trevally Optimizer (GTO): A Novel Metaheuristic Algorithm for Global Optimization and Challenging Engineering Problems," *IEEE Access*, vol. 10, pp. 121615–121640, 2022, doi: 10.1109/ACCESS.2022.3223388.
- [86] H.-L. Minh, T. Sang-To, G. Theraulaz, M. Abdel Wahab, and T. Cuong-Le, "Termite life cycle optimizer," *Expert Syst Appl*, vol. 213, p. 119211, Mar. 2023, doi: 10.1016/j.eswa.2022.119211.
- [87] M. Abdel-Basset, R. Mohamed, M. Jameel, and M. Abouhawwash, "Nutcracker optimizer: A novel nature-inspired metaheuristic algorithm for global optimization and engineering design problems," *Knowl Based Syst*, vol. 262, p. 110248, Feb. 2023, doi: 10.1016/j.knosys.2022.110248.
- [88] V. Goodarzimehr, S. Shojaee, S. Hamzehei-Javaran, and S. Talatahari, "Special Relativity Search: A novel metaheuristic method based on special relativity physics," *Knowl Based Syst*, vol. 257, p. 109484, Dec. 2022, doi: 10.1016/j.knosys.2022.109484.
- [89] M. Azizi, U. Aickelin, H. A. Khorshidi, and M. Baghalzadeh Shishehgharkhaneh, "Energy valley optimizer: a novel metaheuristic algorithm for global and engineering optimization," *Sci Rep*, vol. 13, no. 1, p. 226, Jan. 2023, doi: 10.1038/s41598-022-27344-y.

- [90] M. Abdel-Basset, D. El-Shahat, M. Jameel, and M. Abouhawwash, "Young's double-slit experiment optimizer : A novel metaheuristic optimization algorithm for global and constraint optimization problems," *Comput Methods Appl Mech Eng*, vol. 403, p. 115652, Jan. 2023, doi: 10.1016/j.cma.2022.115652.
- [91] Tummala. S. L. V. Ayyarao *et al.*, "War Strategy Optimization Algorithm: A New Effective Metaheuristic Algorithm for Global Optimization," *IEEE Access*, vol. 10, pp. 25073–25105, 2022, doi: 10.1109/ACCESS.2022.3153493.
- [92] A. Husseinzadeh Kashan, "League Championship Algorithm (LCA): An algorithm for global optimization inspired by sport championships," *Appl Soft Comput*, vol. 16, pp. 171–200, Mar. 2014, doi: 10.1016/j.asoc.2013.12.005.
- [93] N. Razmjoo, M. Khalilpour, and M. Ramezani, "A new meta-heuristic optimization algorithm inspired by FIFA World Cup Competitions: Theory and its application in PID designing for AVR system," *J. Control. Autom. Electr. Syst.*, vol. 27, no. 4, pp. 419–440, 2016, doi: 10.1007/s40313-016-0242-6.
- [94] E. Fadakar and M. Ebrahimi, "A new metaheuristic football game inspired algorithm," in *2016 1st Conference on Swarm Intelligence and Evolutionary Computation (CSIEC)*, 2016, pp. 6–11. doi: 10.1109/CSIEC.2016.7482120.
- [95] S. M. Ashrafi and A. B. Dariane, "Performance evaluation of an improved harmony search algorithm for numerical optimization: Melody search (MS)," *Eng. Appl. Artif. Intell.*, vol. 26, no. 4, pp. 1301–1321, 2013, doi: 10.1016/j.engappai.2012.08.005.
- [96] A. Rezoug and D. Boughaci, "A self-adaptive harmony search combined with a stochastic local search for the 0-1 multidimensional knapsack problem," *Int. J. Bio-Inspired Comput.*, vol. 8, pp. 234–239, 2016, doi: 10.1504/IJBIC.2016.078641.
- [97] Y. Zhou, Y. Wang, X. Chen, L. Zhang, and K. Wu, "A novel path planning algorithm based on plant growth mechanism," *Soft Comput.*, vol. 21, 2017, doi: 10.1007/s00500-016-2045-x.
- [98] Y. Bekakra, Y. Labbi, D. Ben Attous, and O. P. Malik, "Rooted Tree Optimization Algorithm to Improve DTC Response of DFIM," *Journal of Electrical Engineering & Technology*, vol. 16, no. 5, pp. 2463–2483, Sep. 2021, doi: 10.1007/s42835-021-00796-4.
- [99] X.-S. Yang, "Flower Pollination Algorithm for Global Optimization," in *Lect. Notes Comput. Sci.*, vol. 7445 LNCS, 2012, pp. 240–249. doi: 10.1007/978-3-642-32894-7_27.
- [100] S. Mirjalili, "SCA: A sine cosine algorithm for solving optimization problems," *Knowledge-Based Syst.*, vol. 96, pp. 120–133, 2016, doi: 10.1016/j.knsys.2015.12.022.
- [101] L. Abualigah, A. Diabat, S. Mirjalili, M. Abd Elaziz, and A. H. Gandomi, "The Arithmetic Optimization Algorithm," *Comput Methods Appl Mech Eng*, vol. 376, p. 113609, Apr. 2021, doi: 10.1016/j.cma.2020.113609.
- [102] A. A. Kamarudin, Z. A. Othman, and H. M. Sarim, "Water flow algorithm decision support tool for travelling salesman problem," *AIP Conf. Proc.*, vol. 1761, no. 1, p. 20054, Aug. 2016, doi: 10.1063/1.4960894.
- [103] M. E. Colak and A. Varol, "A novel intelligent optimization algorithm inspired from circular water waves," *Elektron. ir Elektrotehnika*, vol. 21, no. 5, pp. 3–6, 2015, doi: 10.5755/j01.eee.21.5.13316.
- [104] Y. chen Wu and J. wen Feng, "Development and Application of Artificial Neural Network," *Wirel Pers Commun*, vol. 102, no. 2, pp. 1645–1656, Sep. 2018, doi: 10.1007/s11277-017-5224-x.
- [105] Z. Zhang, "Artificial Neural Network," *Multivariate Time Series Analysis in Climate and Environmental Research*, pp. 1–35, 2017, doi: 10.1007/978-3-319-67340-0_1.
- [106] G. Papazafeiropoulos, "Stepwise Regression for Increasing the Predictive Accuracy of Artificial Neural Networks: Applications in Benchmark and Advanced Problems," *Modelling*, vol. 5, no. 1, pp. 153–179, Jan. 2024, doi: 10.3390/modelling5010009.
- [107] G. Biau and E. Scornet, "A random forest guided tour," *TEST*, vol. 25, no. 2, pp. 197–227, Jun. 2016, doi: 10.1007/s11749-016-0481-7.
- [108] I. Krupkin and J. Hardin, "Prediction Error Estimation in Random Forests," *arXiv preprint arXiv:2309.00736*, 2023.
- [109] E. Štrumbelj and I. Kononenko, "Explaining prediction models and individual predictions with feature contributions," *Knowl Inf Syst*, vol. 41, pp. 647–665, 2014.
- [110] M. T. Ribeiro, S. Singh, and C. Guestrin, "Why should I trust you? Explaining the predictions of any classifier," in *Proceedings of*, 2016, pp. 1135–1144.
- [111] Y. J. Levy and E. Solan, "Stochastic games," in *Complex Social and Behavioral Systems: Game Theory and Agent-Based Models*, 2020, pp. 229–250.
- [112] S. M. Lundberg and S.-I. Lee, "A unified approach to interpreting model predictions," *Adv Neural Inf Process Syst*, vol. 30, 2017.

- [113] G. Van den Broeck, A. Lykov, M. Schleich, and D. Suci, "On the Tractability of SHAP Explanations," *Journal of Artificial Intelligence Research*, vol. 74, pp. 851–886, Jun. 2022, doi: 10.1613/jair.1.13283.
- [114] Y. R. Naidu, "Multi-objective Pelican Optimization Algorithm for Engineering Design Problems," in *International Conference on Distributed Computing and Intelligent Technology*, Springer Nature Switzerland, 2023.
- [115] N. Premkumar and R. Santhosh, "Pelican optimization algorithm with blockchain for secure load balancing in fog computing," *Multimed Tools Appl.*, pp. 1–23, 2023.
- [116] Z. Wang and others, "Enhanced pelican optimization algorithm for cluster head selection in heterogeneous wireless sensor networks," *Sensors*, vol. 23, no. 18, p. 7711, 2023.
- [117] N. Alamir and others, "Developing hybrid demand response technique for energy management in microgrid based on pelican optimization algorithm," *Electric Power Systems Research*, vol. 214, p. 108905, 2023.
- [118] B. Eren, M. A. Guvenc, and S. Mistikoglu, "Artificial intelligence applications for friction stir welding: A review," *Metals and Materials International*, vol. 27, pp. 193–219, 2021.
- [119] L. Fratini and G. Buffa, "Continuous dynamic recrystallization phenomena modelling in friction stir welding of aluminium alloys: a neural-network-based approach," *Proc. Inst. Mech. Eng. B J. Eng. Manuf.*, vol. 221, pp. 857–864, 2007, doi: 10.1243/09544054JEM674.
- [120] H. Okuyucu, A. Kurt, and E. Arcaklioglu, "Artificial neural network application to the friction stir welding of aluminum plates," *Mater. Des.*, vol. 28, pp. 78–84, 2007, doi: 10.1016/j.matdes.2005.06.003.
- [121] L. Fratini and G. Buffa, "Metallurgical phenomena modeling in friction stir welding of aluminium alloys: analytical versus neural network based approaches," *J. Eng. Mater. Technol. Trans. ASME*, vol. 130, pp. 310011–310016, 2008, doi: 10.1115/1.2931142.
- [122] H. Atharifar, "Optimum parameters design for friction stir spot welding using a genetically optimized neural network system," *Proc. Inst. Mech. Eng. B J. Eng. Manuf.*, vol. 224, pp. 403–418, 2010, doi: 10.1243/09544054JEM1467.
- [123] I. N. Tansel, M. Demetgul, H. Okuyucu, and A. Yapici, "Optimizations of friction stir welding of aluminum alloy by using genetically optimized neural network," *Int. J. Adv. Manuf. Technol.*, vol. 48, pp. 95–101, 2010, doi: 10.1007/s00170-009-2266-6.
- [124] C. C. Tutum and J. H. Hattel, "A multi-objective optimization application in Friction Stir Welding: Considering thermo-mechanical aspects," in *IEEE Congress on Evolutionary Computation*, 2010. doi: 10.1109/cec.2010.5586482.
- [125] G. Buffa, L. Fratini, and F. Micari, "Mechanical and microstructural properties prediction by artificial neural networks in FSW processes of dual phase titanium alloys," *J. Manuf. Process.*, vol. 14, pp. 289–296, 2012, doi: 10.1016/j.jmapro.2011.10.007.
- [126] H. K. Mohanty, M. M. Mahapatra, and P. Kumar, "Predicting the effects of tool geometries on friction stirred aluminium welds using artificial neural networks and fuzzy logic techniques," *Int. J. Manuf. Res.*, vol. 8, pp. 296–312, 2013, doi: 10.1504/IJMR.2013.055245.
- [127] M. H. Shojaeefard, M. Akbari, M. Tahani, and F. Farhani, "Sensitivity analysis of the artificial neural network outputs in friction stir lap joining of aluminum to brass," *Adv. Mater. Sci. Eng.*, 2013, doi: 10.1155/2013/574914.
- [128] H. Wang, P. A. Colegrove, and J. dos Santos, "Hybrid modelling of 7449-T7 aluminium alloy friction stir welded joints," *Sci. Technol. Weld. Join.*, vol. 18, pp. 147–153, 2013, doi: 10.1179/1362171812Y.0000000078.
- [129] M. H. Shojaeefard, R. A. Behnagh, M. Akbari, and others, "Modelling and pareto optimization of mechanical properties of friction stir welded AA7075/AA5083 butt joints using neural network and particle swarm algorithm," *Mater. Des.*, vol. 44, pp. 190–198, 2013, doi: 10.1016/j.matdes.2012.07.025.
- [130] B. M. Darras, I. M. Deiab, and A. Naser, "Prediction of friction stir processed AZ31 magnesium alloy micro-hardness using artificial neural networks," *Adv. Mater. Res.*, vol. 1043, pp. 91–95, 2014, doi: 10.4028/www.scientific.net/AMR.1043.91.
- [131] E. Jiménez-Macías, A. Sánchez-Roca, H. Carvajal-Fals, and others, "Wavelets application in prediction of friction stir welding parameters of alloy joints from vibroacoustic ANN-based model," *Abstr. Appl. Anal.*, 2014, doi: 10.1155/2014/728564.
- [132] A. Ghasemi-Kahrizsangi, S. F. Kashani-Bozorg, M. Moshref-Javadi, and M. Sharififar, "Friction stir processing of mild steel/Al₂O₃ nanocomposite: modeling and experimental studies," *Metallogr. Microstruct. Anal.*, vol. 4, pp. 122–130, 2015, doi: 10.1007/s13632-015-0193-5.
- [133] D. Raguraman, D. Muruganandam, N. Senthilkumar, and L. A. Kumaraswami Dhas, "Tensile strength prediction on different FSW tools using ANN and regression equations," *Int. J. Appl. Eng. Res.*, vol. 10, pp. 545–551, 2015.

- [134] E. Maleki, "Artificial neural networks application for modeling of friction stir welding effects on mechanical properties of 7075-T6 aluminum alloy," *IOP Conf. Ser. Mater. Sci. Eng.*, vol. 103, no. 1, p. 12034, 2015, doi: 10.1088/1757-899X/103/1/012034.
- [135] A. Paoletti, F. Lambiase, and A. Di Ilio, "Optimization of friction stir welding of thermoplastics," *Procedia CIRP*, vol. 33, pp. 562–567, 2015, doi: 10.1016/j.procir.2015.06.078.
- [136] M. H. Shojaeefard, A. Khalkhali, M. Akbari, and P. Asadi, "Investigation of friction stir welding tool parameters using FEM and neural network," *Proc. Inst. Mech. Eng. L J. Mater. Des. Appl.*, vol. 229, pp. 209–217, 2015, doi: 10.1177/1464420713509075.
- [137] R. Teimouri and H. Baseri, "Forward and backward predictions of the friction stir welding parameters using fuzzy-artificial bee colony-imperialist competitive algorithm systems," *J. Intell. Manuf.*, vol. 26, pp. 307–319, 2015, doi: 10.1007/s10845-013-0784-4.
- [138] V. M. Dehabadi, S. Ghorbanpour, and G. Azimi, "Application of artificial neural network to predict Vickers microhardness of AA6061 friction stir welded sheets," *J. Cent. South Univ.*, vol. 23, pp. 2146–2155, 2016, doi: 10.1007/s11771-016-3271-1.
- [139] L. A. C. De Filippis, L. M. Serio, F. Facchini, and others, "Prediction of the vickers microhardness and ultimate tensile strength of aa5754 h111 friction stir welding butt joints using artificial neural network," *Materials*, 2016, doi: 10.3390/ma9110915.
- [140] R. Palanivel, R. F. Laubscher, I. Dinaharan, and N. Murugan, "Tensile strength prediction of dissimilar friction stir-welded AA6351-AA5083 using artificial neural network technique," *J. Braz. Soc. Mech. Sci. Eng.*, vol. 38, pp. 1647–1657, 2016, doi: 10.1007/s40430-015-0483-5.
- [141] S. K. Gupta, K. Pandey, and R. Kumar, "Artificial intelligence-based modelling and multi-objective optimization of friction stir welding of dissimilar AA5083-O and AA6063-T6 aluminium alloys," *Proceedings of the Institution of Mechanical Engineers, Part L: Journal of Materials: Design and Applications*, vol. 232, no. 4, pp. 333–342, Apr. 2018, doi: 10.1177/1464420715627293.
- [142] M. W. Dewan, D. J. Huggett, T. W. Liao, and others, "Prediction of tensile strength of friction stir weld joints with adaptive neuro-fuzzy inference system (ANFIS) and neural network," *Mater. Des.*, vol. 92, pp. 288–299, 2016, doi: 10.1016/j.matdes.2015.12.005.
- [143] R. Harikeasha, M. S. Srinivasan, R. Vignesh, and R. Padmanaban, "ANN model for predicting the intergranular corrosion susceptibility of friction stir processed aluminium alloy AA5083," in *2017 2nd International Conference on Communication and Electronics Systems (ICCES)*, 2017, pp. 716–720.
- [144] F. Sonmez, H. Basak, and S. Baday, "The mechanical strength of aluminum alloys which are joined with friction stir welding modelling with artificial neural networks," *IEEE*, 2017, doi: 10.1109/idap.2017.8090325.
- [145] B. Das, S. Pal, and S. Bag, "Weld quality prediction in friction stir welding using wavelet analysis," *Int. J. Adv. Manuf. Technol.*, vol. 89, pp. 711–725, 2017, doi: 10.1007/s00170-016-9140-0.
- [146] R. S. S. Prasanth and K. Hans Raj, "Determination of Optimal Process Parameters of Friction Stir Welding to Join Dissimilar Aluminum Alloys Using Artificial Bee Colony Algorithm," *Transactions of the Indian Institute of Metals*, vol. 71, no. 2, pp. 453–462, Feb. 2018, doi: 10.1007/s12666-017-1176-9.
- [147] B. Das, S. Pal, and S. Bag, "Torque based defect detection and weld quality modelling in friction stir welding process," *J. Manuf. Process.*, vol. 27, pp. 8–17, 2017, doi: 10.1016/j.jmapro.2017.03.012.
- [148] M. Akbari, M. H. Shojaeefard, P. Asadi, and A. Khalkhali, "Hybrid multi-objective optimization of microstructural and mechanical properties of B4C/A356 composites fabricated by FSP using TOPSIS and modified NSGA-II," *Trans. Nonferrous Met. Soc. China (Engl. Ed.)*, vol. 27, pp. 2317–2333, 2017, doi: 10.1016/S1003-6326(17)60258-9.
- [149] M. Akbari, P. Asadi, P. Zolghadr, and A. Khalkhali, "Multicriteria optimization of mechanical properties of aluminum composites reinforced with different reinforcing particles type," *Proceedings of the Institution of Mechanical Engineers, Part E: Journal of Process Mechanical Engineering*, vol. 232, no. 3, pp. 323–337, Jun. 2018, doi: 10.1177/0954408917704994.
- [150] K. N. Wakchaure, A. G. Thakur, V. Gadakh, and A. Kumar, "Multi-objective optimization of friction stir welding of aluminium alloy 6082-T6 using hybrid Taguchi–Grey relation analysis–ANN method," *Mater. Today Proc.*, vol. 5, pp. 7150–7159, 2018, doi: 10.1016/j.matpr.2017.11.380.
- [151] N. F. Alkayem, B. Parida, and S. Pal, "Optimization of friction stir welding process parameters using soft computing techniques," *Soft. Comput.*, vol. 21, pp. 7083–7098, 2017, doi: 10.1007/s00500-016-2251-6.
- [152] K. Kamal Babu, K. Panneerselvam, P. Sathiyaa, and others, "Parameter optimization of friction stir welding of cryorolled AA2219 alloy using artificial neural network modeling with genetic algorithm," *Int. J. Adv. Manuf. Technol.*, vol. 94, pp. 3117–3129, 2018, doi: 10.1007/s00170-017-0897-6.

- [153] D. J. Huggett, T. W. Liao, M. A. Wahab, and A. Okeil, "Prediction of friction stir weld quality without and with signal features," *Int. J. Adv. Manuf. Technol.*, vol. 95, pp. 1989–2003, 2018, doi: 10.1007/s00170-017-1403-x.
- [154] M. Kurtulmuş and A. Kiraz, "Artificial neural network modelling for polyethylene FSSW parameters," *Sci. Iran.*, vol. 25, pp. 1266–1271, 2018, doi: 10.24200/sci.2018.50030.1473.
- [155] R. V. Vignesh and R. Padmanaban, "Comparison of ANN training algorithms for predicting the tensile strength of friction stir welded aluminium alloy AA1100," *Int. J. Veh. Struct. Syst.*, vol. 10, pp. 98–102, 2018, doi: 10.4273/ijvss.10.2.05.
- [156] R. V. Vignesh and R. Padmanaban, "Artificial neural network model for predicting the tensile strength of friction stir welded aluminium alloy AA1100," *Mater. Today Proc.*, vol. 5, pp. 16716–16723, 2018, doi: 10.1016/j.matpr.2018.06.035.
- [157] R. Raja, "Wear rate prediction of friction stir welded dissimilar aluminum alloy by ANN," *Int. J. Mech. Prod. Eng. Res. Dev.*, vol. 8, pp. 887–892, 2018, doi: 10.24247/ijmperdjun201893.
- [158] A. W. Armansyah and J. Saedon, "Development of prediction system model for mechanical property in friction stir welding using support vector machine (SVM)," *J. Mech. Eng.*, vol. 5, pp. 216–225, 2018.
- [159] A. D'Orazio, A. Forcellese, and M. Simoncini, "Prediction of the vertical force during FSW of AZ31 magnesium alloy sheets using an artificial neural network-based model," *Neural Comput Appl*, vol. 31, no. 11, pp. 7211–7226, Nov. 2019, doi: 10.1007/s00521-018-3562-6.
- [160] A. Khalkhali, S. Ebrahimi-Nejad, and N. G. Malek, "Comprehensive optimization of friction stir weld parameters of lap joint AA1100 plates using artificial neural networks and modified NSGA-II," *Mater. Res. Express*, 2018, doi: 10.1088/2053-1591/aac6f6.
- [161] I. Dinaharan, R. Palanivel, N. Murugan, and R. F. Laubscher, "Predicting the wear rate of AA6082 aluminum surface composites produced by friction stir processing via artificial neural network," *Multidiscipline Modeling in Materials and Structures*, vol. 16, no. 2, pp. 409–423, Sep. 2019, doi: 10.1108/MMMS-05-2019-0102.
- [162] R. Hartl, B. Praehofer, and M. Zaeh, "Prediction of the surface quality of friction stir welds by the analysis of process data using Artificial Neural Networks," *Proceedings of the Institution of Mechanical Engineers, Part L: Journal of Materials: Design and Applications*, vol. 234, no. 5, pp. 732–751, May 2020, doi: 10.1177/1464420719899685.
- [163] M. Vangalapati, K. Balaji, and A. Gopichand, "ANN Modeling and Analysis of Friction Welded AA6061 Aluminum Alloy," *Mater Today Proc*, vol. 18, pp. 3357–3364, 2019, doi: 10.1016/j.matpr.2019.07.258.
- [164] N. F. Alkayem, B. Parida, and S. Pal, "Optimization of friction stir welding process using NSGA-II and DEMO," *Neural Comput Appl*, vol. 31, no. S2, pp. 947–956, Feb. 2019, doi: 10.1007/s00521-017-3059-8.
- [165] Q. Song, Z. Ren, S. Ji, S. Niu, W. Qi, and M. Chen, "Improving the Mechanical Property of Dissimilar Al/Mg Zn-Added Ultrasound-Assisted Friction Stir Lap Welding Joint by Back Propagation Neural Network–Gray Wolf Optimization Algorithm," *Adv Eng Mater*, vol. 21, no. 12, pp. 1–8, Dec. 2019, doi: 10.1002/adem.201900973.
- [166] M. A. Wahid, S. Masood, Z. A. Khan, A. N. Siddiquee, I. A. Badruddin, and A. Algahtani, "A simulation-based study on the effect of underwater friction stir welding process parameters using different evolutionary optimization algorithms," *Proc Inst Mech Eng C J Mech Eng Sci*, vol. 234, no. 2, pp. 643–657, Jan. 2020, doi: 10.1177/0954406219883904.
- [167] S. E. Belalia and others, "Parametric Analysis for Torque Prediction in Friction Stir Welding Using Machine Learning and Shapley Additive Explanations," *Journal of Computational Applied Mechanics*, vol. 55, no. 1, pp. 113–124, 2024, doi: 10.22059/JCAMECH.2024.370055.924.
- [168] A. Banik, S. Mridha, and V. et al. Dey, "An experimental investigation of torque and force generation for varying tool tilt angles and their effects on microstructure and mechanical properties: Friction stir welding of AA 6061-T6," *J. Manuf. Processes*, vol. 31, pp. 395–404, 2018.
- [169] L. Shi, C. S. Wu, and Z. Sun, "An integrated model for analysing the effects of ultrasonic vibration on tool torque and thermal processes in friction stir welding," *Sci. Technol. Weld. Join.*, vol. 23, no. 5, pp. 365–379, 2018.
- [170] J. W. Pew, T. W. Nelson, and C. D. Sorensen, "Development of a torque-based weld power model for friction stir welding," *Friction Stir Weld. Process. IV*, pp. 73–82, 2007.
- [171] M. J. Peel, A. Steuwer, and M. et al. Preuss, "Dissimilar friction stir welds in AA5083-AA6082. Part I: Process parameter effects on thermal history and weld properties," *Metall. Mater. Trans. A*, vol. 37, pp. 2183–2193, 2006.

- [172] A. Banik, J. Deb Barma, and S. C. Saha, "Effect of threaded pin tool for friction stir welding of AA6061-T6 at varying traverse speeds: torque and force analysis," *Iranian Journal of Science and Technology, Transactions of Mechanical Engineering*, vol. 44, pp. 749–764, 2020.
- [173] M. Reza-E-Rabby and A. P. Reynolds, "Effect of tool pin thread forms on friction stir weldability of different aluminum alloys," *Procedia Eng.*, vol. 90, pp. 637–642, 2014.
- [174] H. Jia, H. Zhang, and X. et al. Li, "Evaluation of axial force, tool torque and weld quality of friction stir welded dissimilar 6061/5083 aluminum alloys," *CIRP J Manuf Sci Technol*, vol. 37, pp. 267–277, 2022.
- [175] K. J. Quintana and J. L. L. Silveira, "Mechanistic models and experimental analysis for the torque in FSW considering the tool geometry and the process velocities," *J Manuf Process*, vol. 30, pp. 406–417, 2017.
- [176] M. I. Costa, C. Leitão, and D. M. Rodrigues, "Parametric study of friction stir welding induced distortion in thin aluminium alloy plates: A coupled numerical and experimental analysis," *Thin-Walled Structures*, vol. 134, pp. 268–276, 2019.
- [177] J. W. Qian, X. Liu, and Y. H. et al. Xu, "Periodic variation of torque and its relations to interfacial sticking and slipping during friction stir welding," *Science and Technology of welding and Joining*, vol. 17, no. 4, pp. 338–341, 2012.
- [178] V. Buchibabu, G. M. Reddy, and A. De, "Probing torque, traverse force and tool durability in friction stir welding of aluminum alloys," *J Mater Process Technol*, vol. 241, pp. 86–92, 2017.
- [179] M. Mehta, A. Arora, and D. T. De, "Tool geometry for friction stir welding—optimum shoulder diameter," *Metall Mater Trans A*, vol. 42, no. 9, pp. 2716–2722, 2011, [Online]. Available: <http://dx.doi.org/10.1007/s11661-011-0672-5>
- [180] U. Acharya, B. S. Roy, and S. C. Saha, "Torque and force perspectives on particle size and its effect on mechanical property of friction stir welded AA6092/17.5 SiCp-T6 composite joints," *J Manuf Process*, vol. 38, pp. 113–121, 2019.
- [181] C. Jonckheere and others, "Torque, temperature and hardening precipitation evolution in dissimilar friction stir welds between 6061-T6 and 2014-T6 aluminum alloys," *J Mater Process Technol*, vol. 213, no. 6, pp. 826–837, 2013.
- [182] Z. Zhu, M. Wang, H. Zhang, X. Zhang, T. Yu, and Z. Wu, "A Finite Element Model to Simulate Defect Formation during Friction Stir Welding," *Metals (Basel)*, vol. 7, no. 7, p. 256, 2017, doi: 10.3390/met7070256.
- [183] S. Bocchi, G. D'Urso, C. Giardini, and G. Maccarini, "Effects of Cooling Conditions on Microstructure and Mechanical Properties of Friction Stir Welded Butt Joints of Different Aluminum Alloys," *Applied Sciences*, vol. 9, no. 23, p. 5069, Nov. 2019, doi: 10.3390/app9235069.
- [184] D. Kumar Rajak, D. D. Pagar, P. L. Menezes, and A. Eyvazian, "Friction-based welding processes: friction welding and friction stir welding," *Journal of Adhesion Science and Technology*, vol. 34, no. 24. Taylor and Francis Ltd., pp. 2613–2637, Dec. 16, 2020. doi: 10.1080/01694243.2020.1780716.
- [185] S. Bharti *et al.*, "A Review of Recent Developments in Friction Stir Welding for Various Industrial Applications," *Journal of Marine Science and Engineering*, vol. 12, no. 1. Multidisciplinary Digital Publishing Institute (MDPI), Jan. 01, 2024. doi: 10.3390/jmse12010071.
- [186] J. De Backer, A.-K. Christiansson, J. Oqueka, and G. Bolmsjö, "Investigation of path compensation methods for robotic friction stir welding," *Ind. Robot Int. J.*, vol. 39, pp. 601–608, 2012, [Online]. Available: <http://dx.doi.org/10.1108/01439911211268813>
- [187] A. Dey, "Machine learning algorithms: a review," *Int. J. Comput. Sci. Inf. Technol.*, vol. 7, no. 3, pp. 1174–1179, 2016.